Title
Characterizing Previously Unknown Levels of Genotoxicity Found in Lymphocyte-Mediated Pathogeneses

Author
Malkin, Daniel

Publication Date
2016

Peer reviewed|Thesis/dissertation

UNIVERSITY OF CALIFORNIA

Los Angeles

Characterizing Previously Unknown Levels of Genotoxicity Found in Lymphocyte-Mediated Pathogeneses

A dissertation submitted in partial satisfaction of the requirements for the degree Doctor of Philosophy in Molecular Toxicology

by

Daniel Jacob Malkin

2016

ABSTRACT OF THE DISSERTATION

Characterizing Previously Unknown Levels of Genotoxicity Found in Lymphocyte-Mediated Pathogeneses

by

Daniel Jacob Malkin

Doctor of Philosophy in Molecular Toxicology

University of California, Los Angles, 2016

Professor Robert H. Schiestl, Chair

The genome is constantly subjected to DNA damaging events from the environment in the form of radiation, chemicals, and pollution. Endogenous production of reactive oxygen species also contributes to DNA damage. Conversely, programmed DNA breaks are essential for healthy lymphocyte development during V(D)J and class switch recombination. Dysregulation or mutation of genes involved in the DNA damage and repair pathways can exacerbate environmental insults, impede proper lymphocyte development, and promote cellular transformation. Interleukin-13 (IL-13), Activation-induced cytidine deaminase (AID), Myocyte-specific enhancer factor 2c (Mef2c), and Tumor protein p53 (p53) are all necessary for proper immune function in lymphocytes. There is evidence that these genes are implicated in either establishing or repairing DNA breaks and therefore dysregulation of these genes could lead to

increased levels of oncogenic mutations. IL-13 may increase levels of DNA damage indirectly by inducing inflammation and increasing levels of reactive oxygen species. AID is known to elicit mutations by deamination of cytosine which in turn promotes DNA breaks. Mef2c enhances DNA repair machinery in developing B cells and p53 promotes DNA repair through cell cycle arrest. Using several transgenic mouse models, we have altered the expression of these genes to better establish the solitary role each one has on genomic stability. We found that overexpression of IL-13 in the lungs of CC10-rtTA-IL13 transgenic mice is sufficient to induce genotoxicity in not only the lungs but also circulating blood cells. In a genome-wide translocation sequencing study, we have exposed mechanisms which promote AID -dependent translocation mutations occurring in stimulated B cells. In a third study we have found that Mef2C is an important regulator for the repair of DNA double strand breaks occurring during V(D)J recombination in B cells. Finally, we found that conditional knockout of p53 in mature B cells induces clonal but non-recurrent translocations. Our findings highlight the influence of these genes on genomic stability and the risk of developing oncogenic malignancies.

The dissertation of Daniel Jacob Malkin is approved.

Patrick Allard

Robert P. Gunsalus

Oliver Hankinson

Robert H. Schiestl, Committee Chair

University of California, Los Angeles

2016

Table of Contents

Acknowledgments

Chapter 2 includes an article reprinted from Mutation Research/Fundamental and Molecular Mechanisms of Mutagenesis 769, 100-107, entitled “IL-13 overexpression in mouse lungs triggers systemic genotoxicity in peripheral blood,” Copyright (2014), with permission from Elsevier. Co-authors are Aaron M. Chapman, Jessica Camacho, and Robert H. Schiestl. I designed research, performed research, analyzed data, and wrote the paper in equal contribution with Aaron Chapman.

Chapter 3 includes an article reprinted from Cell, Vol 147 Issue 1 by Roberto Chiarle, Yu Zhang, Richard L. Frock, Susanna M. Lewis, Benoit Molinie, Yu-Jui Ho, Danienne R. Myers, Vivian W. Choi, Mara Compagno, Daniel J. Malkin, Donna Neuberg, Stefano Monti, Cosmas C. Giallourakis, Monica Gostissa, Frederick W. Alt, entitled “Genome-wide Translocation Sequencing Reveals Mechanisms of Chromosome Breaks and Rearrangements in B cells,” Pages 107-119, Copyright (2011), with permission from Elsevier. I assisted in the performance of B cell Isolations, retroviral infections, PCRs, and in vitro I-SceI digestion of PCR amplified genomic fragments.

Chapter 4 is a version of a paper that has been submitted to Nature Immunology. The article is titled “Mef2C Protects Bone Marrow B Lymphopoiesis by Enhancing DNA Repair and V(D)J Recombination,” by Wenyuan Wang, Amelie Montel-Hagen, Tonis Org, Edo Israely, Daniel Malkin, Robert H. Schiestl, Hanna K.A Mikkola. The manuscript is reprinted here with permission from Doctor Wenyuan Wang who designed research and composed the manuscript. I assisted in the performance and analysis of comet and gamma-H2AX genotoxicity assays presented.

Chapter 5 includes an article reprinted from Proceedings of the National Academy of Sciences 110(8) 2934-2939, by Monica Gostissa, Julia M. Bianco, Daniel J. Malkin, Jeffery L. Kutok, Scott J. Rodig, Herbert C. Morse III, Craig H. Bassing, and Frederick W. Alt, entitled "Conditional inactivation of p53 in mature B cells promotes generation of nongerminal center-derived B-cell lymphomas," Copyright (2013), with permission. M.G., C.H.B., and F.W.A. designed research. I contributed by performing research along with M.G., J.M.B, and J.L.K.

Research reported in Chapter 2 and 4 of this publication was supported in part by the National Institute of Environmental Health Sciences of the National Institutes of Health Under Award Number T32ESOJ5457. The content is solely the responsibility of the authors and does not necessarily represent the official views of the national Institutes of Health

Vita

Education

McGill University, Montreal, Quebec

B.Sc. Awarded May 2009

Major- Physiology

Minor-Neuroscience

Research Experience

University of California, Los Angeles

Graduate Student Researcher, Schiestl Lab (June 2012 – Present)

Characterizing genotoxicity in multifactorial immune mediated diseases.

Immune Disease Institute at Boston Children's Hospital in Boston Massachusetts

Research Technician, Alt lab (*August 2009- July* 2011)

Determining how the organization of chromosomes within the nucleus determines programed and spontaneous gene rearrangement in mice.

Selected Teaching Experience

University of California, Los Angeles

Teaching assistant for MCDB 104AL (Winter 2014): Research Immersion Laboratory in Developmental Biology, Dr. Pei Yun Lee.

Teaching assistant for MIMG 101 (Winter 2015): Introductory Microbiology, Dr. Peter Bradley & Dr. Robert Gunsalus

Teaching assistant for ENV HLT C140 (Spring 2016): Fundamentals of Toxicology, Dr. Michael Collins

Financial Support

University of California National Institute of Environmental Health science of the National Institute of Health Training Grant in Molecular Toxicology **(2013-2016)**

Selected Publications

1. Aaron M. Chapman*, Daniel J. Malkin*, Jessica Camacho, Robert H. Schiestl IL-13 Overexpression in Mouse Lungs Triggers Systemic Genotoxicity in Peripheral Blood. Mutation Research 2014 Nov;769:100-7. *Equal Contribution
2. Monica Gostissa , Julia M Bianco , Daniel J Malkin , Jeffery L Kutok , Scott J. Rodig , Herbert C Morse III , Craig H Bassing , Frederick W. Alt Conditional inactivation of p53 in mature B cells promotes generation of non-germinal center-derived B cell Lymphomas. Proc Natl Acad Sci USA. 2013 Feb 19;110(8):2934-9
3. Chiarle R*, Zhang Y*, Frock RL*, Lewis SM*, Molinie B, Ho YJ, Myers DR, Choi VW, Compagno M, Malkin DJ, Neuberg D, Monti S, Giallourakis CC, Gostissa M, Alt FW. Genome-wide translocation sequencing reveals mechanisms of chromosome breaks and rearrangements in B cells. Cell. 2011 Sep 30; 147(1):107-19. *Equal Contribution
4. Wang W, Montel-Hagen A, Malkin D, Schiestl R, Mikkola H Mef2C Protects B Lymphoid Progenitor Homeostasis by Enhancing DNA Repair and V(D)J Recombination (Abstract) 2014 International Society for Experimental Hematology (ISEH) annual conference. Monreal, Canada

Chapter 1 Introduction to DNA damage and repair

Introduction

The genetic instructions encoded within DNA direct virtually all biological processes. When a DNA molecule is altered, the resulting damage or mutation may lead to oncogenic transformation [1]. The integrity of DNA is therefore critical for healthy cellular maintenance. Cells have to maintain replication fidelity in large part by repairing the DNA damage caused by exogenous and endogenous insults. The DNA response and repair pathways possess the critical role of protecting the cell from injury and deleterious genetic mutations [2]. Nevertheless, these pathways are not flawless [3]. Increased levels of genotoxic abuse will inevitably result in higher levels of mutation and consequently an increased risk of developing cancers [1].

Endogenous and exogenous DNA damaging agents will determine the type of DNA lesion and accordingly the method of DNA repair [4][5]. DNA double-strand breaks are caused largely by exogenous sources like ionizing radiation and chemotherapeutic drugs [6]. However programmed cellular events such as recombination constitute an endogenous source of double strand breaks [7]. B and T lymphocytes are unique in that they recombine Variable, Diverse, and Joining gene segments which encode the multitudinous antibodies capable of recognizing virtually all of the antigens which will be presented over the lifetime of the organism [8]. This process requires the formation of programed double strand break and repair. Additionally, a B lymphocyte may undergo class switch recombination after stimulation to change its effector function [9]. This endogenous process also requires the induction of double strand breaks. Double strand breaks whether they are created by exogenous or endogenous means are repaired largely by non-homologous end joining which does not require a homologous template [10]. In the event of a double strand break, histone variant H2AX is phosphorylated on serine 139 by

ataxia telengiactasia mutated (ATM) forming gamma-H2AX [11]. The phosphorylated histone allows DNA to become relaxed at the site of the break creating space for other non-homologous end joining repair proteins [12][13]. Gamma-H2AX is used as a biomarker for double strand breaks since gamma-H2AX foci form quickly and in a 1:1 manner [14]. Ku70/80 heterodimer forms a complex with DNA-PKcs binding to double strand breaks assisting in end bridging and forming a docking site for other non-homologous end joining factors. During the ligation step, DNA ligase IV and its cofactor XRCC4 carry out the ligation of the two ends [15][33] (Figure1).

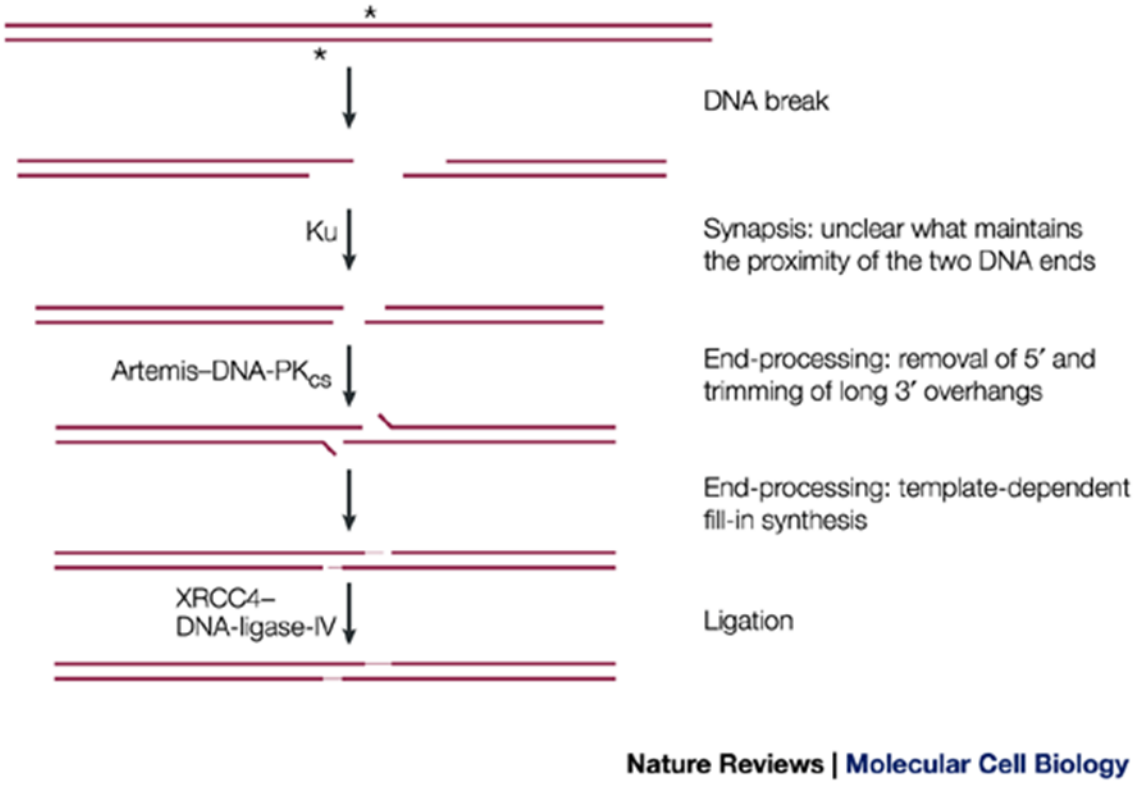

Nature Reviews Molecular Cell Biology **4**, 712-720 (September 2003)

Figure 1

During VDJ recombination, RAG nuclease proteins cleave DNA at recombination signal sequences to create DSBs with hairpin caps which are then opened by Artemis. The two broken ends are then joined by non-homologous end joining factors [16]. During class switch

recombination, heavy chain constant regions are exchanged to alter B-cell effector function. Activation-induced cytidine deaminase (AID) targets switch regions upstream of one of the immunoglobulin heavy chain genes and causes deamination of cytidine residues to uridine [9]. The nucleotide mismatches signal excision promoting double strand breaks. The breaks are again fused using non-homologous end joining factors resulting in a substituted immunoglobulin heavy chain gene [17].

Oxidative stress encompasses a major source of DNA damage. Oxidative damage in the cell is caused by an increase in reactive oxygen species relative to endogenous antioxidant defense mechanisms [18]. Reactive oxygen species derive from both exogenous and endogenous sources. Ionizing radiation, x-rays, cigarette smoke, and environmental pollutants are examples of exogenous sources of oxidative damage [19], but most reactive oxygen species are derived from endogenous sources as by-products of metabolic reactions [20]. Superoxide radicals are produced in roughly 2% of oxidative phosphorylation reactions where oxygen molecules are not completely reduced to produce water ($O_2 + e^- \rightarrow {}^{\bullet}O_2^-$). The superoxide molecules are themselves reactive, but can be further converted into other oxidizing agents like hydrogen peroxide ($2\ H^+ + {}^{\bullet}O{-}2 + {}^{\bullet}O{-}2 \rightarrow H_2O_2 + O_2$), and hydroxyl radicals ($H_2O_2 \rightarrow HO^{\bullet} + {}^{\bullet}OH$) [21]. Exogenous oxidizing agents also activate endogenous pathways which augment reactive oxygen species. Diesel exhaust particles, for example, activate mitogen activated protein kinase and nuclear factor kappa-light-chain-enhancer pathway cascades which activate inflammatory cells and rapidly upregulate inflammatory cytokines. Activated neutrophils, eosinophils and macrophages generate reactive oxygen species through one electron transfer to oxygen via membrane-bound nicotinamide adenine dinucleotide phosphate oxidases [18]. In this way, exogenous reactive species can induce activation of endogenous reactive species that contribute a

major source of these harmful compounds. When guanine nucleotides are oxidized at the 8th carbon position, 8-oxoguanine adducts are formed. 8-oxoguanine is a frequently occurring DNA lesion as guanine is the base which is most prone to oxidation [23]. Oxidative stress can be measured using 8-oxoguaning levels as a biomarker [24]. These sites are mended by base excision repair [22]. During base excision repair, 8-oxoguanine DNA glycosylase removes the 8-oxoguanine adduct and also acts as an abasic apurinic/apyrimidinic endonuclease cleaving at the 5' terminal. The gap is repaired with the incorporation of a single nucleotide or in the case of an oxidized 5'-sugar phosphate, long patch repair proceeds with the inclusion of 2-8 nucleotides [25].

DNA is constantly exposed to a barrage of insults which range in type and source. The repair processes initiated by these attacks are not entirely efficient and increased exposure to harmful sources will overload the repair mechanisms and increase baseline DNA damage. Furthermore, inherited mutation of genes involved in DNA response and repair pathways may further exacerbate problems associated with elevated DNA damage due to inadequate repair. Increased replication errors and increased levels of error prone repair eventually bring about oncogenic mutations [26][27]. Mutations activating oncogenes or inactivating tumor suppressor genes, for example, provide a selective advantage for the cell and increase its susceptibility to oncogenic transformation [28]. Mutations in the p53 tumor suppressor gene leading to loss of function of the p53 protein are implicated in most human cancers [29]. P53's protective effect consists of activating DNA repair proteins, arresting the cell cycle at G1/S during DNA damaging events, and activation of apoptosis. Due to its multifunctional role, loss of wild-type function of p53 often leads to oncogenesis [30][31][32]. Chromosomal translocations represent another especially harmful class of mutation. Translocations occur when double strand DNA breaks

rearrange to non-homologous chromosomes through non-homologous recombination [33]. Translocations involving oncogenes are implicated in many cancers such as Burkitt's lymphoma where the c-myc oncogene on chromosome 8 is fused to the immunoglobulin heavy chain locus on chromosome 14 [34].

In the following chapters I have included 4 studies in which we characterize the levels of DNA damage in lymphocyte mediated pathogeneses. In each of these studies, we demonstrate the type and extent of DNA damage or mutagenesis occurring in each experimental condition as well as provide insight into the process by which the damage occurs. With regard to asthma, a multifactorial lymphocytic disease, we have found that IL-13 overexpression in the lungs of CC10-rtTA-IL13 transgenic mice (a well-characterized model of asthma) can initiate systemic genotoxicity. In a genome-wide translocation sequencing study, we have elucidated mechanisms which promote translocations, including AID-dependent translocations, which transpire in stimulated B cells. In another study we've characterized the role of Mef2C, one of the AID-dependent gene translocation hotspots found in the previous study, in the regulation of B cell homeostasis through its involvement with DNA double strand break repair. In the final study, we describe B cell tumors which develop after conditional knockout of the TP53 tumor suppressor gene in mature B cells.

Asthma is a common immune mediated disease initiated by genetic and environmental factors [35]. Preferential differentiation toward type 2 helper T cells over type 1 is a characteristic of the disease [36]. Cytokine IL-13 is a central immune regulator released by type 2 helper T cells. Many studies have shown that overexpression of IL13 in mouse lungs is both necessary and sufficient to induce the airway remodeling indicative of asthma [37][38][39]. Hence, CC10-

rtTA-IL13 transgenic mice which conditionally overexpress IL-13 in the lungs in the presence of doxycycline are a well-characterized model of asthma [40]. The multifaceted influence from both the environment and genetics obscure the discrete role of IL-13 in asthma. In the study included in chapter 1, we used CC10-rtTA-IL13 mice to characterize the systemic and genetic damage initiated by IL-13. We found that in addition to eliciting the hallmark histological features of asthma, IL-13 overexpression in the lungs was sufficient to elicit oxidative DNA damage, single and double strand DNA breaks, and micronucleus formation in the peripheral blood of these transgenic mice. These results have significance regarding the severity of asthma and may indicate an increased risk of other diseases associated with increased and prolonged DNA damage in circulating leukocytes and erythrocytes.

The study included in chapter 2 provides insight into mechanisms which promote the generation of chromosomal translocations. In this study we generated DNA double strand breaks in vivo by infecting with I-SceI expressing retrovirus, isolated B cells of mice containing I-SceI meganuclease recognition sites inserted into the c-myc oncogene or the IgH locus. We then used a high-throughput PCR method to detect and sequence thousands of spontaneously generated translocations entailing these targeted DNA double strand breaks following activation of these isolated B cells. Translocations involving these break sites occurred broadly across all chromosomes with partiality towards proximal and transcribed regions. Comparing results from wildtype versus AID deficient mice under this setup, we also found AID-dependent translocation hotspots. MEF2C was among the genes belonging to these hotspots, and is the focus of chapter 3.

In the third study, we determine the role of MEF2C on DNA repair in B cell progenitors. Using MEF2C deficient adult mouse hematopoietic cells, we found that MEF2C augments expression of DNA repair factors in B cell progenitors. Accordingly MEF2C plays a role in promoting successful V(D)J recombination. MEF2C deficient cells also displayed diminished recuperation after sub-lethal irradiation, further signifying its role in the DNA repair process.

In the final study we determined the effects of inactivation of the p53 tumor suppressor gene in mature B cells of mice using the Cre/Lox method. Mice in this study developed clonal B-cell lymphomas derived from naïve B cells which did not experience class switch recombination. Translocation analysis of these clonal tumors showed that the tumors were not recurrent and did not involve immunoglobulin loci. In this study, we found that p53 deletion was adequate to induce oncogenic transformation of mature B cells.

References

[1] M. Macheret and T. D. Halazonetis, “DNA Replication Stress as a Hallmark of Cancer,” *Annu. Rev. Pathol. Mech. Dis.*, vol. 10, no. 1, pp. 425–448, Jan. 2015.

[2] S. P. Jackson and J. Bartek, “The DNA-damage response in human biology and disease,” *Nature*, vol. 461, no. 7267, pp. 1071–1078, Oct. 2009.

[3] T. A. Kunkel, “DNA Replication Fidelity,” *J. Biol. Chem.*, vol. 279, no. 17, pp. 16895–16898, Apr. 2004.

[4] E. C. Friedberg, L. D. McDaniel, and R. A. Schultz, “The role of endogenous and exogenous DNA damage and mutagenesis,” *Curr. Opin. Genet. Dev.*, vol. 14, no. 1, pp. 5–10, 2004.

[5] A. Sancar, L. A. Lindsey-Boltz, K. Ünsal-Kaçmaz, and S. Linn, “M OLECULAR M ECHANISMS OF M AMMALIAN DNA R EPAIR AND THE DNA D AMAGE C HECKPOINTS,” *Annu. Rev. Biochem.*, vol. 73, no. 1, pp. 39–85, Jun. 2004.

[6] C. Jekimovs, E. Bolderson, A. Suraweera, M. Adams, K. J. O’Byrne, and D. J. Richard, “Chemotherapeutic compounds targeting the DNA double-strand break repair pathways: the good, the bad, and the promising.,” *Front. Oncol.*, vol. 4, p. 86, 2014.

[7] X. Li and W.-D. Heyer, “Homologous recombination in DNA repair and DNA damage tolerance,” *Cell Res.*, vol. 18, no. 1, pp. 99–113, Jan. 2008.

[8] C. H. Bassing, W. Swat, and F. W. Alt, “The Mechanism and Regulation of Chromosomal V(D)J Recombination,” *Cell*, vol. 109, no. 2, pp. S45–S55, 2002.

[9] J. P. Manis, M. Tian, and F. W. Alt, “Mechanism and control of class-switch recombination,” *Trends Immunol.*, vol. 23, no. 1, pp. 31–39, 2002.

[10] A. J. Davis and D. J. Chen, “DNA double strand break repair via non-homologous end-joining.,” *Transl. Cancer Res.*, vol. 2, no. 3, pp. 130–143, Jun. 2013.

[11] H. Wang, M. Wang, H. Wang, W. Böcker, and G. Iliakis, “Complex H2AX phosphorylation patterns by multiple kinases including ATM and DNA-PK in human cells exposed to ionizing radiation and treated with kinase inhibitors.,” *J. Cell. Physiol.*, vol. 202, no. 2, pp. 492–502, Feb. 2005.

[12] B. Jakob, J. Splinter, S. Conrad, K.-O. Voss, D. Zink, M. Durante, M. Löbrich, and G. Taucher-Scholz, “DNA double-strand breaks in heterochromatin elicit fast repair protein recruitment, histone H2AX phosphorylation and relocation to euchromatin.,” *Nucleic Acids Res.*, vol. 39, no. 15, pp. 6489–99, Aug. 2011.

[13] K. L. Cann and G. Dellaire, “Heterochromatin and the DNA damage response: the need to relax.,” *Biochem. Cell Biol.*, vol. 89, no. 1, pp. 45–60, Feb. 2011.

[14] L. J. Kuo and L.-X. Yang, “Gamma-H2AX - a novel biomarker for DNA double-strand

breaks.," *In Vivo*, vol. 22, no. 3, pp. 305–9.

[15] K. Valerie and L. F. Povirk, "Regulation and mechanisms of mammalian double-strand break repair.," *Oncogene*, vol. 22, no. 37, pp. 5792–812, Sep. 2003.

[16] K. Inagaki, C. Ma, T. A. Storm, M. A. Kay, and H. Nakai, "The role of DNA-PKcs and artemis in opening viral DNA hairpin termini in various tissues in mice.," *J. Virol.*, vol. 81, no. 20, pp. 11304–21, Oct. 2007.

[17] J. F. Ruiz, B. Gómez-González, and A. Aguilera, "AID Induces Double-Strand Breaks at Immunoglobulin Switch Regions and c-MYC Causing Chromosomal Translocations in Yeast THO Mutants," *PLoS Genet.*, vol. 7, no. 2, p. e1002009, Feb. 2011.

[18] A. Rahal, A. Kumar, V. Singh, B. Yadav, R. Tiwari, S. Chakraborty, K. Dhama, A. Rahal, A. Kumar, V. Singh, B. Yadav, R. Tiwari, S. Chakraborty, and K. Dhama, "Oxidative Stress, Prooxidants, and Antioxidants: The Interplay," *Biomed Res. Int.*, vol. 2014, pp. 1–19, 2014.

[19] A. Bhattacharyya, R. Chattopadhyay, S. Mitra, and S. E. Crowe, "Oxidative stress: an essential factor in the pathogenesis of gastrointestinal mucosal diseases.," *Physiol. Rev.*, vol. 94, no. 2, pp. 329–54, Apr. 2014.

[20] R. De Bont and N. van Larebeke, "Endogenous DNA damage in humans: a review of quantitative data.," *Mutagenesis*, vol. 19, no. 3, pp. 169–85, May 2004.

[21] J. Lee, N. Koo, and D. B. Min, "Reactive Oxygen Species, Aging, and Antioxidative Nutraceuticals," *Compr. Rev. Food Sci. Food Saf.*, vol. 3, no. 1, pp. 21–33, Jan. 2004.

[22] J. Allgayer, N. Kitsera, C. von der Lippen, B. Epe, and A. Khobta, "Modulation of base excision repair of 8-oxoguanine by the nucleotide sequence.," *Nucleic Acids Res.*, vol. 41, no. 18, pp. 8559–71, Oct. 2013.

[23] S. Kanvah, J. Joseph, G. B. Schuster, R. N. Barnett, C. L. Cleveland, and U. Landman, "Oxidation of DNA: Damage to Nucleobases," *Acc. Chem. Res.*, vol. 43, no. 2, pp. 280–287, Feb. 2010.

[24] A. R. Collins, "Assays for oxidative stress and antioxidant status: applications to research into the biological effectiveness of polyphenols.," *Am. J. Clin. Nutr.*, vol. 81, no. 1 Suppl, p. 261S–267S, Jan. 2005.

[25] F. Coppedè, "An Overview of DNA Repair in Amyotrophic Lateral Sclerosis," *Sci. World J.*, vol. 11, pp. 1679–1691, 2011.

[26] G. Ghosal and J. Chen, "DNA damage tolerance: a double-edged sword guarding the genome," *Transl. Cancer Res.*, vol. 2, no. 3, pp. 107–129, 2013.

[27] C. Bernstein, A. R., V. Nfonsam, and H. Bernstei, "DNA Damage, DNA Repair and Cancer," in *New Research Directions in DNA Repair*, InTech, 2013.

[28] N. Rivlin, R. Brosh, M. Oren, and V. Rotter, “Mutations in the p53 Tumor Suppressor Gene: Important Milestones at the Various Steps of Tumorigenesis.,” *Genes Cancer*, vol. 2, no. 4, pp. 466–74, Apr. 2011.

[29] M. Olivier, M. Hollstein, and P. Hainaut, “TP53 mutations in human cancers: origins, consequences, and clinical use.,” *Cold Spring Harb. Perspect. Biol.*, vol. 2, no. 1, p. a001008, Jan. 2010.

[30] S. Y. Shieh, J. Ahn, K. Tamai, Y. Taya, and C. Prives, “The human homologs of checkpoint kinases Chk1 and Cds1 (Chk2) phosphorylate p53 at multiple DNA damage-inducible sites.,” *Genes Dev.*, vol. 14, no. 3, pp. 289–300, Feb. 2000.

[31] S. Pauklin, A. Kristjuhan, T. Maimets, and V. Jaks, “ARF and ATM/ATR cooperate in p53-mediated apoptosis upon oncogenic stress.,” *Biochem. Biophys. Res. Commun.*, vol. 334, no. 2, pp. 386–94, Aug. 2005.

[32] A. J. Levine, “p53, the cellular gatekeeper for growth and division.,” *Cell*, vol. 88, no. 3, pp. 323–31, Feb. 1997.

[33] M. R. Lieber, J. Gu, H. Lu, N. Shimazaki, and A. G. Tsai, “Nonhomologous DNA end joining (NHEJ) and chromosomal translocations in humans.,” *Subcell. Biochem.*, vol. 50, pp. 279–96, 2010.

[34] D. F. Robbiani and M. C. Nussenzweig, “Chromosome Translocation, B Cell Lymphoma, and Activation-Induced Cytidine Deaminase,” *Annu. Rev. Pathol. Mech. Dis.*, vol. 8, no. 1, pp. 79–103, Jan. 2013.

[35] A. B. Mukherjee and Z. Zhang, “Allergic asthma: influence of genetic and environmental factors.,” *J. Biol. Chem.*, vol. 286, no. 38, pp. 32883–9, Sep. 2011.

[36] N. Zimmermann, N. E. King, J. Laporte, M. Yang, A. Mishra, S. M. Pope, E. E. Muntel, D. P. Witte, A. A. Pegg, P. S. Foster, Q. Hamid, and M. E. Rothenberg, “Dissection of experimental asthma with DNA microarray analysis identifies arginase in asthma pathogenesis,” *J. Clin. Invest.*, vol. 111, no. 12, pp. 1863–1874, 2003.

[37] M. Akdis, S. Burgler, R. Crameri, T. Eiwegger, H. Fujita, E. Gomez, S. Klunker, N. Meyer, L. O’Mahony, O. Palomares, C. Rhyner, N. Ouaked, N. Quaked, A. Schaffartzik, W. Van De Veen, S. Zeller, M. Zimmermann, and C. A. Akdis, “Interleukins, from 1 to 37, and interferon-γ: receptors, functions, and roles in diseases.,” *J. Allergy Clin. Immunol.*, vol. 127, no. 3, pp. 701–21.e1–70, Mar. 2011.

[38] A. Munitz, E. B. Brandt, M. Mingler, F. D. Finkelmant, and M. E. Rothenberg, “Distinct roles for IL-13 and IL-4 via IL-13 receptor alpha 1 and the type II IL-4 receptor in asthma pathogenesis,” *Proc. Natl. Acad. Sci. U. S. A.*, vol. 105, no. 20, pp. 7240–7245, 2008.

[39] M. Wills-Karp, J. Luyimbazi, X. Y. Xu, B. Schofield, T. Y. Neben, C. L. Karp, and D. D. Donaldson, “Interleukin-13: Central mediator of allergic asthma,” *Science (80-.).*, vol. 282, no. 5397, pp. 2258–2261, 1998.

[40] J. A. Elias, T. Zheng, C. G. Lee, R. J. Homer, Q. S. Chen, B. Ma, M. Blackburn, and Z. Zhu, “Transgenic modeling of interleukin-13 in the lung,” *Chest*, vol. 123, no. 3, p. 339S–345S, 2003.

Chapter 2 IL-13 Overexpression in mouse lungs triggers systemic genotoxicity in peripheral blood

Abstract

Asthma is a common heterogeneous disease with both genetic and environmental factors that affects millions of individuals worldwide. Activated type 2 helper T cells secrete a panel of cytokines, including IL-13, a central immune regulator of many of the hallmark type 2 disease characteristics found in asthma. IL-13 has been directly implicated as a potent stimulator of asthma induced airway remodeling. Although IL-13 is known to play a major role in the development and persistence of asthma, the complex combination of environmental and genetic origin of the disease obfuscate the solitary role of IL-13 in the disease. We therefore, used a genetically modified mouse model which conditionally overexpresses IL-13 in the lungs to study the independent role of IL-13 in the progression of asthma. Our results demonstrate IL-13 is associated with a systemic induction of genotoxic parameters such as oxidative DNA damage, single and double DNA strand breaks, micronucleus formation, and protein nitration. Furthermore we show that inflammation induced genotoxicity found in asthma extends beyond the primary site of the lung to circulating leukocytes and erythroblasts in the bone marrow eliciting systemic effects driven by IL-13 over-expression.

Keywords: IL-13, asthma, genotoxicity

Introduction

Asthma affects over 150 million individuals and is clinically diagnosed by a barrage of symptoms which include wheezing, coughing, and shortness of breath [1][2]. Asthma can be subcategorized into two classes: allergic, and non-allergic asthma which constitute roughly 70% and 30% of cases respectively. Although there are almost no observable differences in the types of physiological changes that occur between the two subcategories, non-allergic asthmatics incur

more severe and more frequent symptoms [3]. Airways of asthmatic individuals are distinguished through structural modifications, collectively called airway remodeling that includes bronchiolar inflammation, epithelial sloughing, goblet cell metaplasia, multiplied mucus glands, thickening of the lamina reticularis, increased airway smooth muscle mass, angiogenesis, and alterations in the extracellular matrix components [4][5]. Additionally, B lymphocytes, T lymphocytes, eosinophils, neutrophils, and macrophages also migrate to the airways, triggering the release of immunoglobulin E, leukotrienes, prostaglandins, histamines, and other chemical mediators leading to airway inflammation [6][7].

In asthmatic individuals, T cells differentiate preferentially towards type 2 helper T cells (Th2) [8]. Th2 cells are thought to induce asthma through the secretion of many cytokines that activate inflammatory pathways both directly and indirectly [9]. Notably, Th2 cells secrete IL-13 which triggers STAT6 activation through activation of surface receptors present on eosinophils, mast cells, B lymphocytes, fibroblasts, and airway smooth muscle cells [10][11][12][13][14]. This activation leads to IgE synthesis, mucus hypersecretion, airway hyperreactivity, and tissue fibrosis [15]. Overexpression of IL-13 is necessary and sufficient to induce non-allergic asthma [10][15][16].

Our lab previously published that intestinal mucosal inflammation leads to systemic genotoxicity in mice [17].In this study we sought to determine if IL-13 induced asthma might also lead to systemic genotoxicity in mice. We used a genetically modified mouse model originally developed by the Elias lab [18], which allow for tetracycline activated conditional over-expression of IL-13 in the Clara Cells of the lungs. We then collected peripheral blood from these asthmatic mice and performed genotoxic assays throughout the progression of the disease.

Methods

Transgenic Mice

The CC10-rtTA-IL13 transgenic (TG) mouse is a well-characterized model of asthma [19]. Clara cell 10-kDa (CC10) gene promoter is used for conditionally expression of IL13 in the mouse lung inducible by doxycycline. CC10-rtTA-IL13 transgenic (TG) mice were generated in Dr. Talal Chatila lab David Geffen School of Medicine University of California Los Angeles, USA. Mice were housed and bred in an institutional specific pathogen free animal facility under standard conditions with a 12 hr light/dark cycle and fed a standard diet according to Animal Research Committee regulations at the University of California, Los Angeles.

Doxycycline Treatment

10 TG mice and 9 WT littermate control mice were maintained on normal water until one month of age. After one month of age doxycycline was administered to the drinking water 2 g/L in 4% sucrose and kept in aluminum foil covered bottles to prevent light-induced degradation of doxycycline for a 3 week time period. The IL13 transgene exhibits baseline leakiness in the absence of doxycycline allowing transgenic mice to exhibit minor elevation of IL13 expression and minor allergic airway inflammation [20]. For this reasoning non-treated transgenic mice were not used as controls in our experiments. After the 3 week exposure to doxycycline all mice were euthanized and pathological assessments were conducted on the lungs.

Blood Collection

Peripheral blood was collected by facial vein puncture using 5 mm sterile lancets (Medipoint Inc. Mineola, NY) from experimental mice on specified days throughout the duration of treatment

and on sacrifice day via terminal right ventricle cardiac puncture using a heparin-coated syringe (American Pharmaceutical Partners, Inc. Schaumburg, IL). Blood from each mouse was collected into EDTA-coated tubes (Sarstedt Aktiengesellschaft & Co., Numbrecht.)

Immunofluorescence

50ul of whole peripheral blood was put into erythrocyte lysis buffer, cells were laid over poly - D-lysine-coated coverslips and fixed with 4% paraformaldehyde (Electron Microscopy Sciences) at room temperature as described previously [21]. Subsequently, cells were permeabilized with 0.5% Triton X-100 (Sigma), followed by 5 rinses in PBS. Blocking was done in aluminum-covered plates overnight at 4°C in 10% FBS. Coverslips were then incubated for 1 hour at room temperature with mouse anti-phospho-Histone H2A.X (Upstate, Temecula, CA) at a dilution of 1:400, or Mouse anti-8-oxoguanine clone 483.15 (Upstate, Temecula, CA) at 1:250 respectively. Coverslips were then rinsed with 0.1% Triton X-100. Following a second 10% FBS blocking, cells were stained with FITC-conjugated anti-mouse IgG (Jackson ImmunoResearch, West Grove, PA) at a dilution of 1:150 for samples with γH2AX primary and (1:200) for samples with 8-oxoguanine primary, respectively for 1 hour at room temperature. Coverslips were mounted onto slides using VECTASHIELD with DAPI (Vector Laboratories, Burlingame, CA). For both 8-oxoguanine and γH2AX assay analysis were done on a Zeiss automated microscope. At least 100 cells were counted per sample and cells with more than four distinct foci in the nucleus were considered positive for γH2AX [17] and cells that exhibited elevated fluorescent intensity compared to background were considered positive for 8-oxoguanine respectively. Apoptotic cells, which have an approximate 10-fold increase in nuclear foci in damaged cells, were not included in analyses [17][22]. Statistical analyses were done using Poisson distribution 8-

oxoguanine (STATA statistical analysis software) for γH2AX and using ANOVA and Tukey's post hoc test for 8-oxoguanine analysis (GraphPad Prism).

Micronucleus assay

3µl of whole blood were spread on a microscope slide and stained with Wright-Giemsa solution (Sigma-Aldrich, St. Louis, MO). At least 4000 erythrocytes were counted according to published recommendations [23]. MN were counted and scored with an Olympus Ax70 (Tokyo, Japan) at 100X magnification. Statistical analysis was done using repeated measures ANOVA followed by Tukey's post-tests (GraphPad Prism).

DNA single strand breaks

Oxidative DNA damage and DNA strand breaks were measured in peripheral blood cells using the alkaline comet assay. Peripheral blood was collected before doxycycline administration (day 0), and on days 3, 6, 9, 12, 15, 18 and 21 days of doxycycline treatment. Blood was diluted 1:1 with RPMI + 20% DMSO, slowly frozen and stored at -80°C until the assay was performed. The comet assay was done as described previously [24]. Briefly, cells were mixed with low melting-point agarose, and placed in triplicate onto normal agarose layed over gelbond (Lonza Inc. Rockland, ME). The gel was immersed in lysis buffer (2.5 M NaCl, 0.1 M EDTA, 10 mM Tris, 1% Triton, and 10% DMSO), then alkaline electrophoresis buffer (0.3 M NaOH, 1 mM EDTA). After 20 minutes in the electrophoresis buffer at 4°C, the gel was run for 45 minutes at 300 mA, allowed to dry and then stained with SYBR Gold (Molecular Probes). Comet tail-moments were analyzed using CASP (Comet Assay Software Project,http://casp.sourceforge.net/). To measure oxidative DNA damage, the comet assay was modified to include an incubation step with hOGG1 (New England Biolabs, Ipswich, MA). As described previously, embedded cells were

incubated with hOGG1 (1:300 in NEBuffer1 and BSA) at 37°C for 30 minutes following the lysis step [25]. Tail-moments were normalized to a control to account for inter-experimental variability. Statistical analyses were done using ANOVA (GraphPad Prism).

ELISA analysis

Serum was separated from blood by centrifugation on all mice immediately before doxycycline administration (Day0) and on days 3, 5,7,10,13,16,18, and 21. After collection serum samples were aliquoted into micro-centrifuge tubes and kept at -20°C until analysis. Sandwich ELISAs were conducted on samples that were diluted 1:10. Analysis of total Mouse IgE was done according to manufacturer's instructions (BD biosciences). Each sample was done in triplicate and analyzed using the relative standard curve method optical density vs. concentration. Statistical analysis was done using linear mixed model with repeated measurements nested within each mouse. (STATA statistical analysis software)

Gene expression analysis

Lungs from WT and IL-13 mice at the end of the 3-week doxycycline exposure mice were perfused and lavaged before immersion into RNAlater (Qiagen). Lungs were kept at 4°C for 24 hours then transferred to -80°C until RNA was isolated using the RNeasy Mini kit according to manufacturer's instructions (Qiagen). cDNA was synthesized using SuperscriptIII (Invitrogen) according to manufacturer's recommendations. Quantitative realtime PCR was performed on an ABI Prism 7500 gene expression system (Applied Biosystems) using Taqman gene expression assays for *H2AX, 8-oxoguanine, IL-13, IL-4, IL-5, CCL-11/Eotaxin, TGF-β, Tnfα,* and *Gapdh*was used as an internal control. Each reaction was done in triplicate and analyzed using the relative standard curve method.

Bronchoalveolar lavage

The amount of lung inflammation caused by increased infiltration of immune-circulating cells was assessed by BAL. Briefly, mice were euthanized the trachea was isolated via blunt dissection and small caliber tubing was inserted and secured in the airway. A volume of 1 ml of 1X PBS was flushed and removed 3 times successively from the lungs of WT and IL-13 mice until 3 mL of BAL fluid was collected. BAL fluid was centrifuged at 1600 rpm at 4°C for 10 minutes. After centrifugation cells were re-suspended in 200ul of 1X PBS. A 1:1 ratio of cells to trypan blue was put into a hemocytometer and the number of viable cells was counted. After cell viability was assessed 200 ul of remaining cells were put into cytospin and spun at 400 RPM for 5 minutes. Slides were removed from cytospin and allowed to air dry. After drying the slides were stained using (Thermo Kwik Diff staining kit) using manufactures staining recommendation. Slides were allowed to air dry overnight and were mounted with paramount and a coverslip and allowed to dry. Finally at least 200 cells were differentiated by light microscopy based on conventional morphological criteria for each animal.

Immunohistochemistry

γH2A.X, 8-Hydroxyguanosine, and Nitrotyrosine stains were done on lung tissue of (WT) and IL-13 mice. The slides were placed in xylene to remove paraffin, then a series of ethanol washes. After a wash in tap water, the slides were incubated in 3% Hydrogen peroxide / methanol solution for 10 minutes. The slides were then washed in distilled water, and incubated for 25 minutes in Citrate Buffer pH6 (Invitrogen Corporation) at 95 degrees Celsius using a vegetable steamer. Next, the slides were brought to room temperature, rinsed with PBST (Phosphate Buffered Saline containing 0.05% Tween-20), then incubated at room temperature for 1 hour

with Anti-gamma H2A.X (phosphor S139) antibody (Abcam, ab22551), 2 hours with anti-8-Hydroxyguanosine antibody (Abcam, ab48508), or for 45 minutes with Nitrotyrosine (Millipore, 06-284) at the dilutions of 1: 50 for γH2A.X, and 8-Hydroxyguanosine antibodies and at1:200 for the Nitrotyrosine antibody, respectively. The slides were then rinsed with PBST, and were incubated with Dako EnVision+ System –HRP Labelled Polymer Anti-Mouse (Dako, K4001) at room temperature for 30 minutes. Subsequently after a rinse with PBST, the slides were incubated with DAB (3,3′-Diaminobenzidine) for visualization. Finally, the slides were washed in tap water, counterstained with Harris' Hematoxylin, dehydrated in ethanol, and mounted with media.

Results

Serum IgE levels are induced in IL-13 Mice. Increased level of IgE is a major factor in the etiology of asthma and is found abundantly in the serum of both human and murine models of asthma [26][27][28]. Therefore we assessed the levels of IgE in our transgenic IL-13 over-expression model. We observed that the levels of IgE were higher in the transgenic mice 12 days after IL-13 over-expression and were consistently higher throughout the experiment until terminal day 21 (Figure 1). Although IL-13 mice exhibited higher IgE levels this induction was only significant at day 21 at **,$p<0.007$ IL-13 Mice exhibit increased inflammation of the lung. To understand the role IL-13 induced lung inflammation plays in the genotoxicity and progression of asthma we compared the lungs of WT and IL-13 animals. In (Fig.2A and 2C) WT animals exhibit no increase of inflammation. In contrast IL-13 mice (Fig. 2B and 2D) exhibit significant inflammation of the lung characterized in the airways bronchiolar lumen. IL-13 mice showed increased inflammatory cells migration in the bronchiolar epithelium, marked

hyperplasia, goblet cell metaplasia, and eosinophilic intracytoplasmic inclusion bodies present in clara cells. Thus IL-13 increases inflammation via recruitment of inflammatory cells migrating into airway spaces.

IL-13 mice exhibit increased immune cell infiltration in BAL fluid. To delineate what immune cells may be implicated in the persistent inflammatory and genotoxic response present in the asthma mouse model we determined the cellular composition of the BAL fluid in both the WT and IL-13 mice. IL-13 animals had a near 5-fold increase in eosinophil presence in BAL fluid compared to WT animals at $p<0.04$ (Fig. 3). IL-13 mice also exhibited significantly more circulation of neutrophils in the BAL fluid at ***, $p<0.0004$ compared to WT littermates. IL-13 mice also exhibited an increase induction of lymphocytes although this observation was not significantly different from WT animals.

IL-13 mice exhibit persistent inflammation induced immune response. To elucidate the role IL-13 plays in up-regulation of inflammation in the lung we assessed key mediators of asthma Fig. 4A-4C, inflammatory disease Fig. 4D-F, and genotoxicity Fig. 4G via quantitative real-time PCR. As a measurement of further efficacy of our tissue specific asthma model we measured IL-13 levels in the lungs of both groups of experimental mice. The asthma mouse model exhibited an expected significant increased gene expression of IL-13 at **, $p<0.001$ compared to WT animals. IL-4, TNF-α, IL-5 were significantly up-regulated in IL-13 mice at *,$p<0.01$ compared to WT animals. IL-13 mice also displayed a marked increase of TGF-β at **,$p<0.001$ compared to WT mice. Cc11 transcript levels in IL-13 mice were slightly higher but did not show a

significant increase compared to WT mice. These data are indicative of a chronically activated innate immune response present in IL-13 mice compared to WT mice.

IL-13 Mice have increased staining of markers of genotoxicity in lung tissue. To further assess asthma induced genotoxicity, the lungs of WT and IL-13 mice were stained with γH2AX, anti-8-Hydroxyguanosine, and Nitrotyrosine antibodies. IL-13 mice exhibited increased staining with markers of genotoxicity in the lungs in comparison to WT animals (Fig. 5).

IL-13 Mice show systemically elevated reactive oxygen species induced genotoxicity and double strand breaks in peripheral blood. Because IL-13 is a major mediator of allergic asthma and induces higher levels of inflammation in asthmatic mice [29], we hypothesized that inflammation induced systemic DNA damage would be more prevalent in IL-13 compared to wild type (WT) mice. Increase of asthma induced genotoxicity was assessed in peripheral white blood cells as a systemic measurement of DNA damage. 8-oxoguanine is a mutagenic lesion caused by the interaction of a reactive oxygen species to DNA that causes G:C to T:A transversion mutations during replication [30]. Percent positive 8-oxoguanine staining in peripheral white blood cells was assessed using fluorescent microscopy. Blood was taken on day 0 as an assessment of baseline levels of 8-oxoguanine induction between both WT and IL-13 groups. After 6 days of doxycycline presence in drinking water IL-13 mice exhibited a slight increase of 8-oxoguanine immuno-staining compared to wild type mice this induction persisted and became statistically significant at **,$p<0.001$ at day 15 and remained elevated throughout the 21 day exposure to doxycycline (Fig. 6A). As a measure of the amount of genotoxicity caused by an accumulation of DNA double strand breaks the γH2AX assay was assessed in the WT and IL-13 animals.

H2AX is a member of the histone H2A protein family and becomes rapidly phosphorylated in presence of a DNA damaging event [31]. This rapid phosphorylation causes recruitment of DNA repair proteins to the site of the break and is detectable by specific antibodies to γH2AX. In Fig. 6B we assessed the amount of double strand breaks present in the WT and IL-13 animals. Transgenic animals exhibited an increase in the amount of double strand breaks occurring at every time point after over-expression. This induction of γH2AX was significant on day 9 at **, $p<0.002$, at day 12 at *, $p<0.02$, and at day 18 day at **,$p<0.001$ respectively. A nearly significant induction of γH2AX at $P=0.064$ on day 21 was also observed in the IL-13 mice

I IL-13 mice have systemic single strand breaks and persistent systemic genotoxicity that induces comet and micronucleus formation in peripheral blood leukocytes respectively. The in vivo micronucleus assay was conducted in mature normochromatic erythrocytes circulating in the peripheral blood to determine chromosomal damage. Micronuclei in erythrocytes/erythroblasts from the peripheral blood or bone marrow have been induced in the presence of chromosome breaks, spindle abnormalities, or structurally abnormal chromosomes [23][30]. Mature micronucleated normochromatic erythrocytes represent the final developmental stage of erythroblasts containing micronuclei stemming in the bone marrow, and permit the simultaneous study of the generation and elimination of micronucleated erythrocytes [30][32]. Blood was taken on day 0 as an assessment of baseline levels of 8-oxoguanine induction between both WT and IL-13 groups. After 6 days of doxycycline presence in drinking water IL-13 mice exhibited a significant increase of micronuclei formation in peripheral blood compared to WT animals at *, $p<0.05$. This statistically significant induction at *, $p<0.05$ of micronuclei persisted until terminal date Day 21 (Fig. 7A).

The alkaline comet assay is a gel electrophoresis assay that allows the detection of single and double strand breaks, and alkali labile sites at the single cell level [17]. Asthma is an inflammatory disease that produces large amounts of reactive oxygen species (ROS) [32][33]. Interaction of ROS with DNA may result in mutagenic oxidative base modifications such as 8-hydroxydeoxyguanosine (8-oxo-dGuo) and induce DNA strand breaks [32]. Transgenic animals exhibited an increase in the amount of single strand breaks occurring after 6 days of IL-13 over-expression compared to all other groups where no increase was observed. This induction of strand breaks was significant for indicated groups at *, $p<0.05$. (Fig.7B)

Discussion

Asthma is a chronic obstructive lung disease characterized by chronic inflammation of the airways and recurrent bronchospasms ranging from mild to debilitating [34]. It is well established that Interleukin-13 serves as a major mediator of the asthmatic process [16]. This study is the first to assess IL-13 role in genotoxicity concomitantly with the inflammatory asthmatic process. Our study also demonstrates for the first time that this genotoxicity extends beyond the primary site of the lung to circulating leukocytes and erythroblasts in the bone marrow eliciting systemic effect in peripheral blood driven by IL-13 overexpression.

IL-13 mice exhibited an asthmatic phenotype consistent with previous data. We found a significant increase in IgE. IL-13 mice had sub-epithelial eosinophilic infiltration, peribronchiolar, and perivascular lymphoid infiltration, free floating eosinophilic crystals, many surrounded by aggregates of macrophages, giant cells and neutrophil PMNs [4][16][35]. IL-13 mice showed a significant influx of eosinophils, a cellular hallmark of asthma [36], a significant increase in neutrophils, and non-significant increase of lymphocytes in the bronchoalveolar

lavage fluid. Transgenic mice had increased gene expression of IL-13, IL-4, IL-5,TNFα, Tgfβ, γH2AX, and Ccl11 produced in the lungs [37][29][38][39]. There was a significant increase in γH2AX levels in the lungs of the IL-13 mice and an induced yet non-significant increase in 8-oxoguanine. In IL-13 mice, we detected a significant increase of single and double strand breaks in the peripheral blood and lung, a significant induction of micronucleus formation in the normochromatic erythrocytes present in the peripheral blood leukocytes, as well as increased staining of markers of genotoxicity in the lung [30].

We utilized the well characterized inducible over-expression CC10-rtTA-IL13 transgenic (TG) mouse to elucidate the effect interleukin-13 may have in the genotoxicity of asthma. Recent work has shown that IL-13 signaling is mediated by the type-2 IL-4 receptor, which consists of the IL-4R alpha and IL-13R alpha 1 chains [15][40], yet IL-13 alone is necessary and sufficient to render the major pathophysiological effects of asthma [16]. IL-4 along with IL-13 is a key mediator of inflammation, has an overlapping biological function as IL-13, yet has a distinct role in asthma progression [15]. IL-4 is best known for its role for defining the Th2 phenotype of lymphocytes in asthma, but also exacerbating the asthmatic phenotype by increasing airway hyperresponsiveness, eosinophil recruitment, and mucus over-production [16][35]. We next investigated mRNA levels of CCL-11/eotaxin. There was not a significant increase in CCL-11/eotaxin transcript present in the lung mRNA, however, we did observe a significant increase in IL-5 lung mRNA transcript. A possible explanation to the induced yet nonsignificant increase in CCL11/eotaxin transcript may be found in the work *of Humbles et. al.*[40]. These data suggest, in corroboration with *Conroy, et. al.* [36] that migrating eosinophils in the bronchoalveolar lavage fluid may stimulate release of IL-5, but not CCL11/eotaxin.

With regards to the genotoxicity of IL-13 induced asthma we discovered an increase in the amount of γH2AX and 8-oxoguanine in the blood and lungs of these mice. Phosphorylation of histone H2A to form γH2AX in the presence of a DNA damaging event is used as a biomarker of cellular response to DSBs and has a potential for monitoring DNA damage and repair in human and mice [41][42]. 8-oxo-7,8- dihydroguanine (8oxoG) is an abundant ROS induced lesion that when accumulated has been associated with numerous diseases, including cancer [17][43][44]. We did observe a slight increase of 8oxoG in the WT animals which most likely can be attributed to the repeated blood draws that caused a moderate increase in the production of stress related ROS- induced DNA damage similarly found in *Westbrook, et. al* [45]. As a measure of ongoing DNA damage *Westbrook, et. al* [17] show that an accumulation of double-strand breaks can lead to chromosome breaks and micronucleus formation.

Perturbations to erythroblasts in the bone marrow may be a humoral effect of inflammation-associated DNA damage, as with the peripheral leukocytes. We suggest that increased inflammation in our experimental mice causes a significant induction of migratory cells that preferentially release pro-inflammatory cytokines at sites of inflammation. This re-circulating pool of activated cells may recruit more effector cells, which come into contact with erythroblasts in the bone marrow causing the observed clastogenicity.

To evaluate the inflammatory cell composition we determined the differential cell percentages. The increased prevalence of neutrophils over that of eosinophils in the bronchoalveolar lavage fluid may depict the presence of a more chronic asthmatic phenotype, an idea supported by *Kamath et. al* [46]. Moreover this significant influx of both neutrophils and eosinophils may help generate the enhanced systemic genotoxic response found in the blood. This observation of

an induction of γH2AX mRNA levels further confirms increased genotoxicity in IL-13 mice and correlates with our hypothesis of systemic genotoxicity.

In conclusion, we propose that the key asthmatic mediator interleukin-13, increases important elements of the inflammatory response including ROS derived oxidative stress causing an induction in genotoxicity that has wide reaching systemic genotoxic effects, such as oxidative DNA damage, single and double DNA strand breaks, micronucleus formation, and protein nitration in the peripheral blood. Two potential explanations for the local inflammation and systemic genotoxicity are described by *Westbrook, et. al* [17]. In the first model, innate immune cells activated by inflammation release reactive species that damage circulating leukocytes in the periphery. In the second model, inflammatory cytokines are responsible for systemic genotoxicity through cytokine receptor mediated production of free radicals that damage distant leukocytes. These models are not mutually exclusive, making the second model more likely as it has been shown that injection of cytokines causes systemic genotoxicity in mice [45]. We further suggest increased immune cell infiltration and inflammation byproducts as a possible culprit to this genotoxic induction. The induction of systemic strand breaks which are prevalent in many types of cancer were found to be significantly increased in our IL-13 induced asthma model. Recent studies also point to the fact that asthmatic patients have higher cancer risk [47][48][20]. Previous studies in human asthmatics also identified increased strand breaks produced during the direct interaction of ROS with DNA or during the repair process of damaged DNA [32][49]. In summary, asthma is associated with systemic genotoxicity through single and double DNA strand breaks, oxidative DNA damage, protein nitration, and micronucleus formation. This study further implicates IL-13 as a potential therapeutic target for other pulmonary diseases involving

carcinogenesis. In addition, systemic genotoxicity might be a convenient blood marker for the extent and severity of asthma.

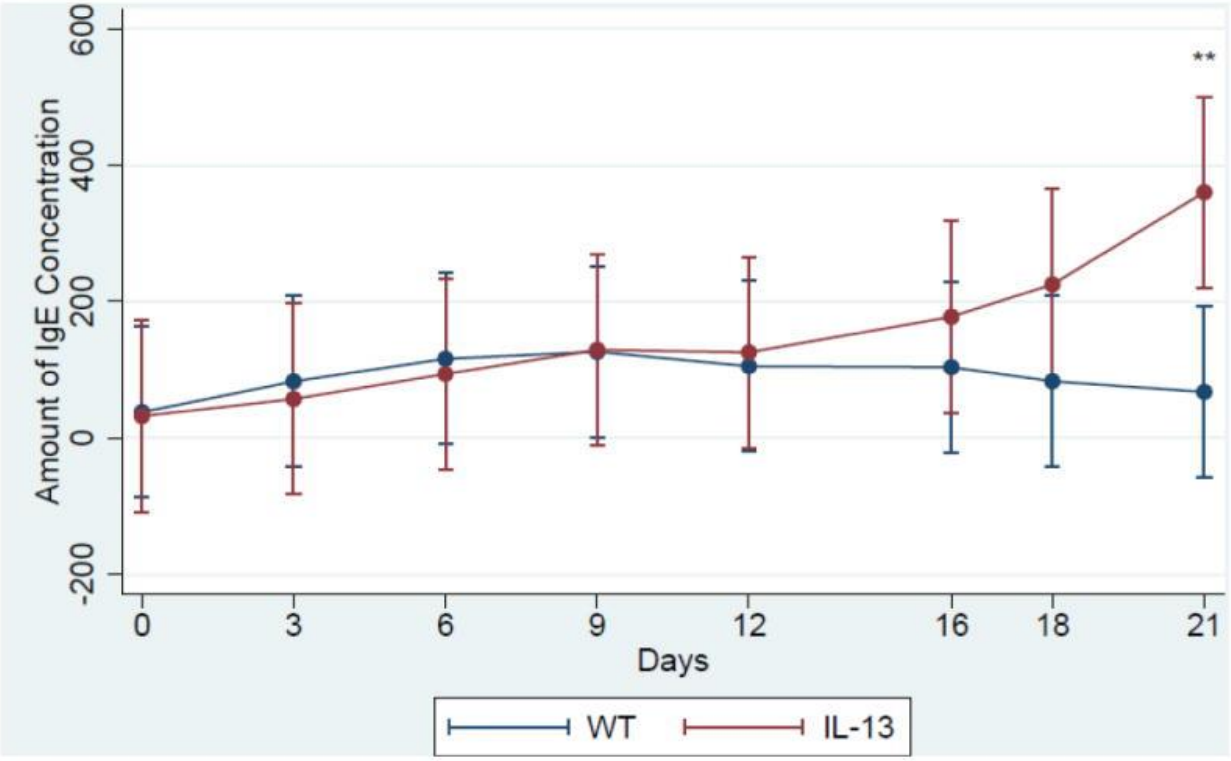

Figure 1

IgE concentration assessed via sandwhich ELISA. **indicates p<, 0.007 n= 5 in both IL-13 and WT animals. Assay was performed with triplicate blood samples from each WT (n=5) and Il-13 (n=5) mouse. (color)

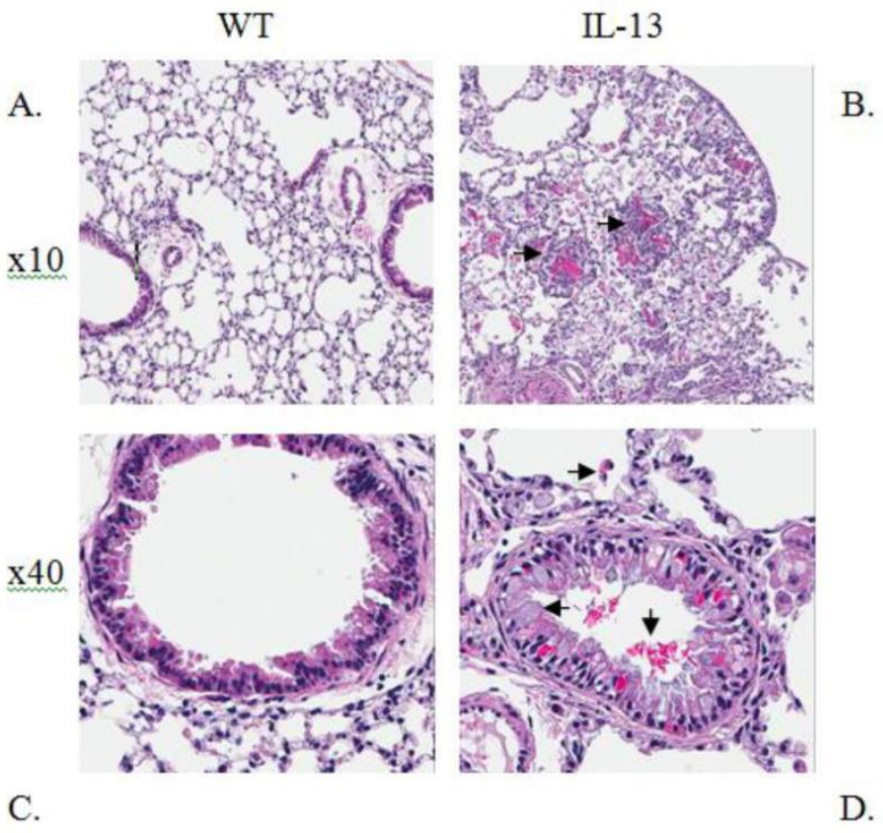

Figure 2

IL-13 over-expression induces lung inflammation in asthmatic mice Representative lung histology Hematoxylin & Eosin (H&E) staining at indicated magnifications. **(A)** 10x image of Wild type (WT) lung and Interleukin 13 over expressed mice **(B)**, both at one month old. Arrows in**(B)** 10x image indicate formation of granuloma metafoci surrounding eosinophilic crystals. 40x image of WT **(C)** and **(D)** 40x image of IL-13 mice. Arrows in **(D)** indicate eosinophil migration, goblet cell metaplasia, and eosinophilic crystal formation in bronchial lumen. n=9 for WT and n=10 for IL-13 mice. (color)

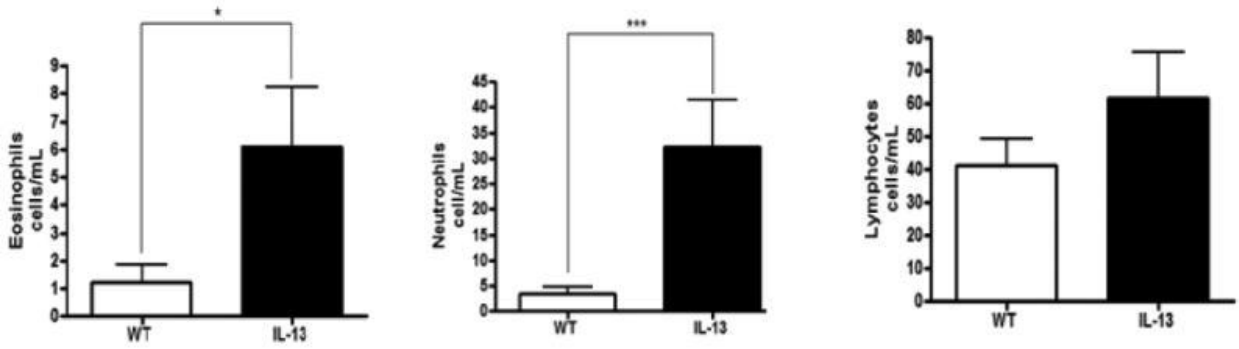

Figure 3

Inflammatory cell composition of bronchial alveolar lavage fluid (BALF)

Differential cell analysis were determined by light microscopic evaluation n=9 for WT, and n=10 for IL-13 animals,* indicates $p<0.05$,*** indicates $p<0.0004$ respectively analysis were conducted using two tailed Student's unpaired T-test with Mann-Whitney determination.

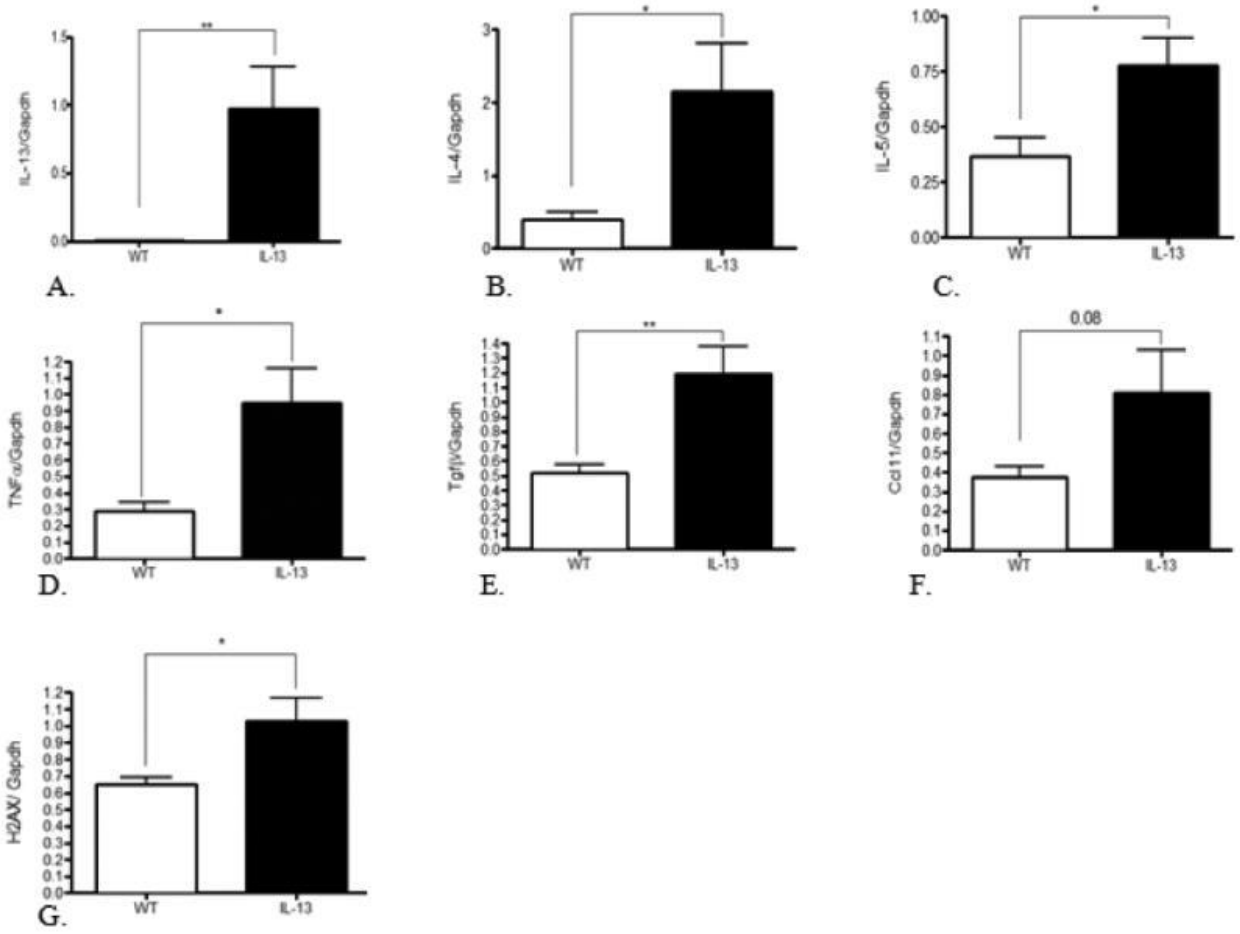

Figure 4

Assessment of cytokine panel in lung mRNA measured by quantitative real-time PCR

Mean expression divided by Gapdh, the internal control gene. * indicates $p<0.01$, ** indicates $p<0.001$, analysis were conducted using two tailed Student's unpaired T-test. n=9 for WT animals and n=10 for IL-13 animals.

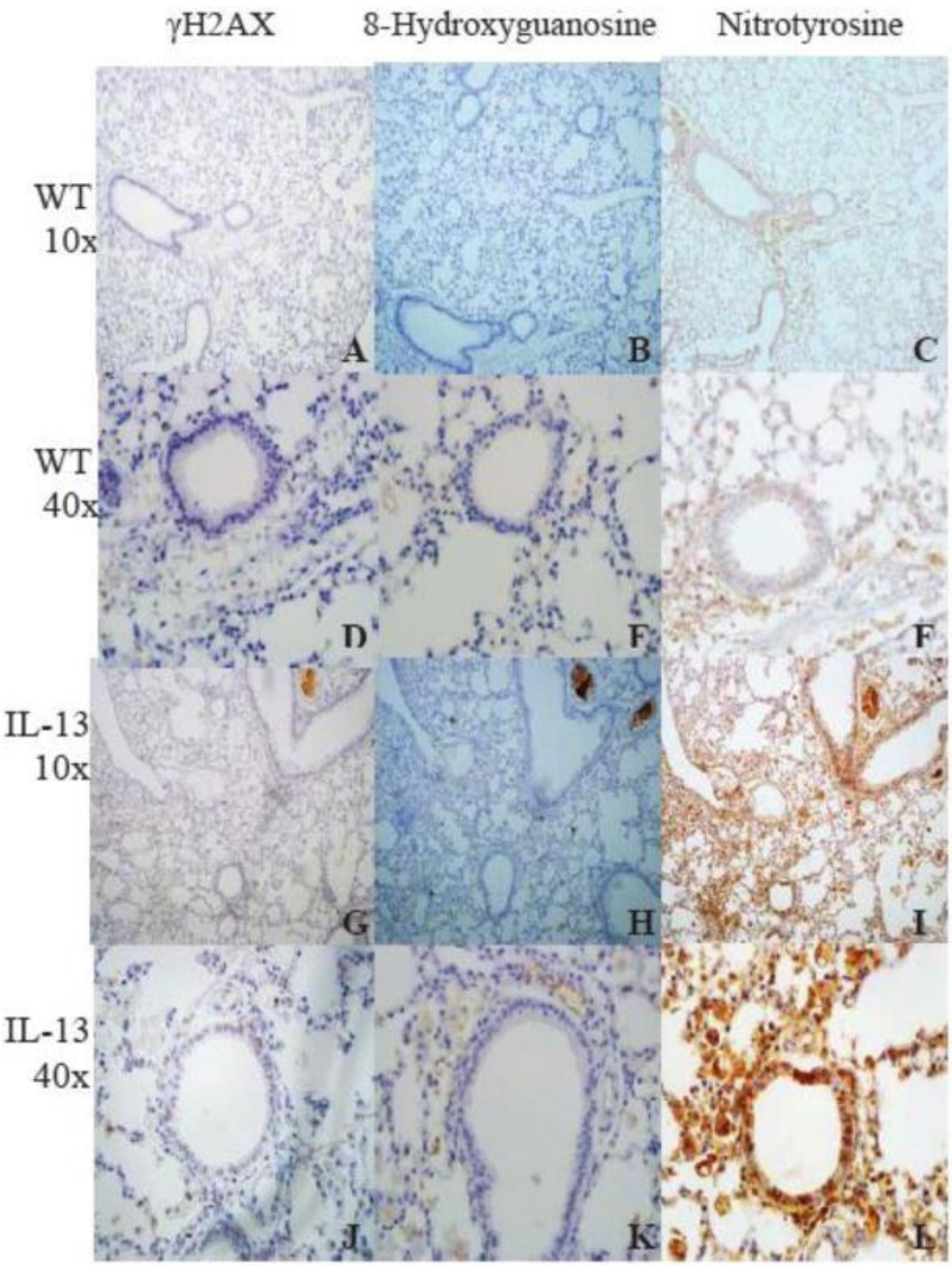

Fig. 5

Staining of markers of genotoxicity and oxidative protein damage in lung tissue as measured by immunohistochemistry

Markers of double strand breaks (A-J), reactive oxygen species (B-K), and inflammation (C-L) induced genotoxicity were stained in WT and IL-13 mice. Lung tissue in IL-13 mice (G-L)

exhibited increased staining in all genotoxic parameters in comparison to WT mice (A-F). n=9 for WT animals and n=10 for IL-13 animals. (color)

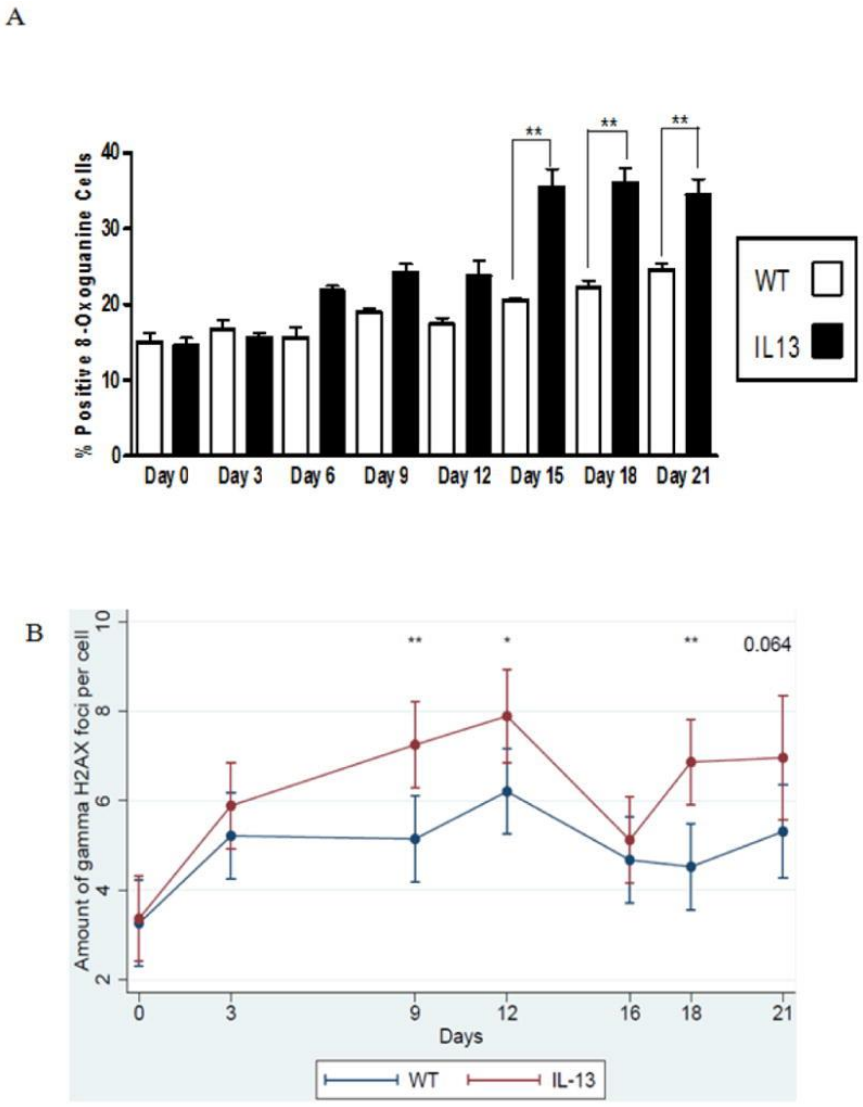

Fig. 6

Persistent genotoxicity measured via inflammation induced 8-oxoguanine and double strand breaks measured via γH2AX in peripheral blood

A.) Percent positive cells for 8-oxoguanine induction in white blood cells. Presence of 8-oxoguanine was confirmed by immunofluorescence. Positive cells stain brightly green compared to no immunofluorescent staining for negative cells. White bars indicate Wild type (WT) animals and black bars indicate IL-13 animals. Data represent mean ± SEM. Statistical analyses were done using ANOVA testing and Tukey's post hoc analysis. n=5 in all groups. ** indicates $p<0.001$.**B** Assessment of double strand breaks measured via γH2AX assay, were counted per

cell using fluorescent microscopy before doxycycline administration at Day 0 and after doxycycline administration at days 3,9,12,16,18 and day 21 using a linear mixed model to determine genotoxic accumulation over time. * indicates p<0.02, ** indicates p<0.002 n=5 for WT and IL-13 animals. (color)

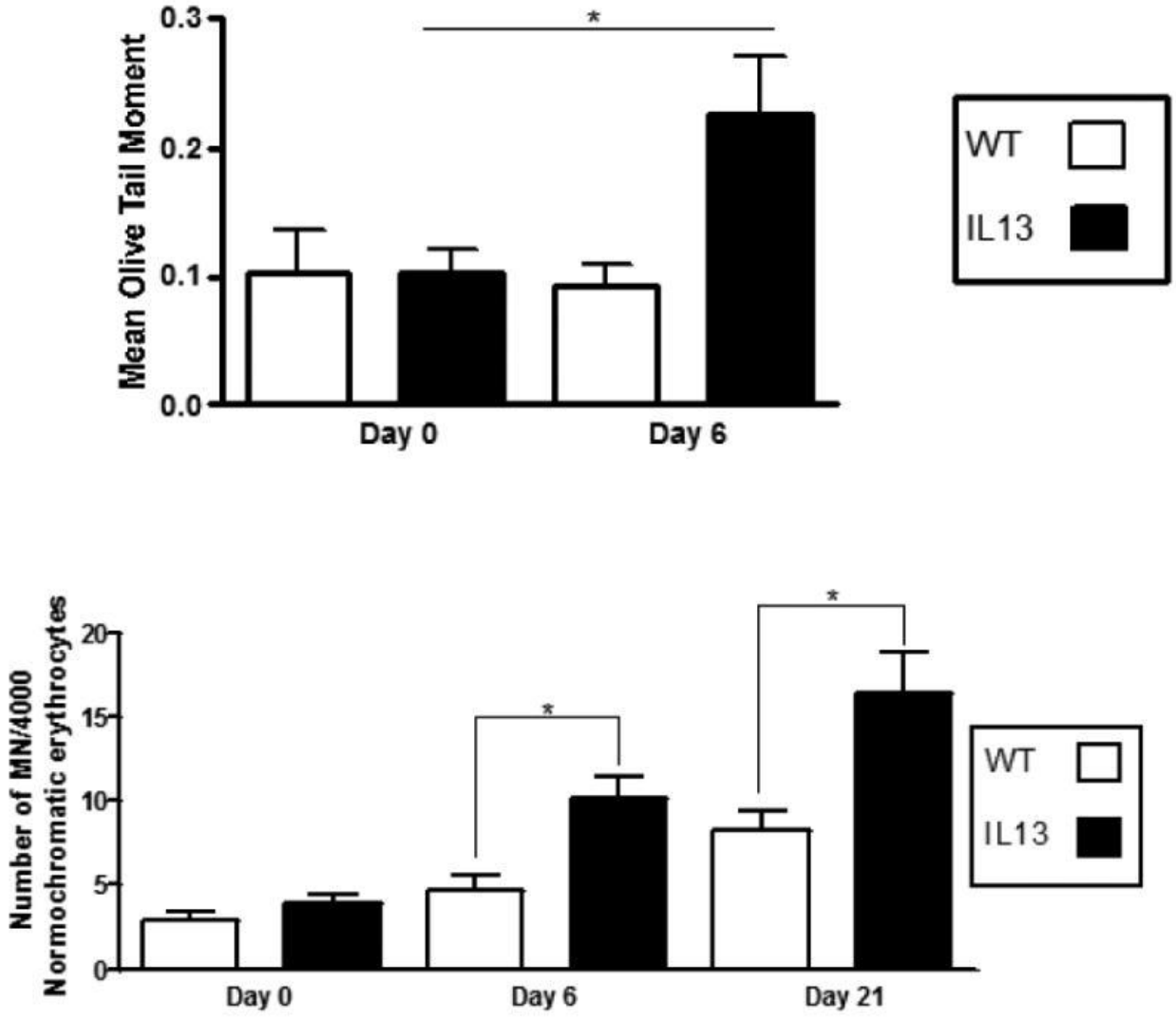

Fig. 7

IL-13 over-expression induced single strand breaks and micronucleated cells in peripheral blood

A.) Assessment of single strand breaks were measured via comet assay before doxycycline administration at Day 0 and after doxycycline administration at days 6. At least 100 olive tail moments were counted via fluorescent microscopy and assessed using CASP software. White bars indicate Wild type (WT) animals and black bars indicate IL-13 animals. Data represent mean ± SEM. Statistical analyses were done using ANOVA testing and Tukey's post hoc analysis. * indicates p<0.05 n=5 for WT and IL-13 animals. **B.)**Number of micronucleated cells

per 4000 normorchromatic erythrocytes. Presence of micronuclei were confirmed by light microscope at 100X. White bars indicate Wild type (WT) animals and black bars indicate IL-13 animals. Data represent mean ± SEM. Statistical analyses were done using ANOVA testing and Tukey's post hoc analysis. n=9 for WT and n=10 for IL-13.* indicates $p<0.05$.

References

[1] L. Akinbami, Moorman JE, and X. Liu, "Asthma prevalence, health care use, and mortality: United States,2005-2009.," 2011.

[2] A. L. Miller, "The etiologies, pathophysiology, and alternative/complementary treatment of asthma," *Altern. Med. Rev.*, vol. 6, no. 1, pp. 20–47, 2001.

[3] S. Romanet-Manent, D. Charpin, A. Magnan, A. Lanteaume, D. Vervloet, and E. C. Grp, "Allergic vs nonallergic asthma: what makes the difference?," *Allergy*, vol. 57, no. 7, pp. 607–613, 2002.

[4] P. Fireman, "Symposium: Understanding asthma pathophysiology," *Allergy Asthma Proc.*, vol. 24, no. 2, pp. 79–83, 2003.

[5] D. M. Hyde, L. A. Miller, E. S. Schelegle, M. V. Fanucchi, L. S. Van Winkle, N. K. Tyler, M. V. Avdalovic, M. J. Evans, R. Kajekar, A. R. Buckpitt, K. E. Pinkerton, J. P. Joad, L. J. Gershwin, R. Wu, and C. G. Plopper, "Asthma: a comparison of animal models using stereological methods," *Eur. Respir. Rev.*, vol. 15, no. 101, 2007.

[6] B. L. Bradley, M. Azzawi, M. Jacobson, B. Assoufi, J. V Collins, A. M. A. Irani, L. B. Schwartz, S. R. Durham, P. K. Jeffery, and A. B. Kay, "EOSINOPHILS, T-LYMPHOCYTES, MAST-CELLS, NEUTROPHILS, AND MACROPHAGES IN BRONCHIAL BIOPSY SPECIMENS FROM ATOPIC SUBJECTS WITH ASTHMA - COMPARISON WITH BIOPSY SPECIMENS FROM ATOPIC SUBJECTS WITHOUT ASTHMA AND NORMAL CONTROL SUBJECTS AND RELATIONSHIP TO BRON," *J. Allergy Clin. Immunol.*, vol. 88, no. 4, pp. 661–674, 1991.

[7] W. R. Henderson, D. B. Lewis, R. K. Albert, Y. Zhang, W. J. E. Lamm, G. K. S. Chiang, F. Jones, P. Eriksen, Y. T. Tien, M. Jonas, and E. Y. Chi, "The importance of leukotrienes in airway inflammation in a mouse model of asthma," *J. Exp. Med.*, vol. 184, no. 4, pp. 1483–1494, 1996.

[8] N. Zimmermann, N. E. King, J. Laporte, M. Yang, A. Mishra, S. M. Pope, E. E. Muntel, D. P. Witte, A. A. Pegg, P. S. Foster, Q. Hamid, and M. E. Rothenberg, "Dissection of experimental asthma with DNA microarray analysis identifies arginase in asthma pathogenesis," *J. Clin. Invest.*, vol. 111, no. 12, pp. 1863–1874, 2003.

[9] L. E. Harrington, R. D. Hatton, P. R. Mangan, H. Turner, T. L. Murphy, K. M. Murphy,

and C. T. Weaver, “Interleukin 17-producing CD4(+) effector T cells develop via a lineage distinct from the T helper type 1 and 2 lineages,” *Nat. Immunol.*, vol. 6, no. 11, pp. 1123–1132, 2005.

[10] M. Akdis, S. Burgler, R. Crameri, T. Eiwegger, H. Fujita, E. Gomez, S. Klunker, N. Meyer, L. O’Mahony, O. Palomares, C. Rhyner, N. Ouaked, N. Quaked, A. Schaffartzik, W. Van De Veen, S. Zeller, M. Zimmermann, and C. A. Akdis, “Interleukins, from 1 to 37, and interferon-γ: receptors, functions, and roles in diseases.,” *J. Allergy Clin. Immunol.*, vol. 127, no. 3, pp. 701–21.e1–70, Mar. 2011.

[11] T. A. Chatila, “Interleukin-4 receptor signaling pathways in asthma pathogenesis,” *Trends Mol. Med.*, vol. 10, no. 10, pp. 493–499, 2004.

[12] H. Jiang, M. B. Harris, and P. Rothman, “IL-4/IL-13 signaling beyond JAK/STAT,” *J. Allergy Clin. Immunol.*, vol. 105, no. 6, pp. 1063–1070, 2000.

[13] L. Cohn, J. A. Elias, and G. L. Chupp, “ASTHMA: Mechanisms of disease persistence and progression,” *Annu. Rev. Immunol.*, vol. 22, pp. 789–815, 2004.

[14] B. D. Medoff, S. Y. Thomas, and A. D. Luster, “T cell trafficking in allergic asthma: The ins and outs,” in *Annual Review of Immunology*, vol. 26, 2008, pp. 205–232.

[15] A. Munitz, E. B. Brandt, M. Mingler, F. D. Finkelmant, and M. E. Rothenberg, “Distinct roles for IL-13 and IL-4 via IL-13 receptor alpha 1 and the type II IL-4 receptor in asthma pathogenesis,” *Proc. Natl. Acad. Sci. U. S. A.*, vol. 105, no. 20, pp. 7240–7245, 2008.

[16] M. Wills-Karp, J. Luyimbazi, X. Y. Xu, B. Schofield, T. Y. Neben, C. L. Karp, and D. D. Donaldson, “Interleukin-13: Central mediator of allergic asthma,” *Science (80-.).*, vol. 282, no. 5397, pp. 2258–2261, 1998.

[17] A. M. Westbrook, B. Wei, J. Braun, and R. H. Schiestl, “Intestinal Mucosal Inflammation Leads to Systemic Genotoxicity in Mice,” *Cancer Res.*, vol. 69, no. 11, pp. 4827–4834, 2009.

[18] Z. Zhu, B. Ma, R. J. Homer, T. Zheng, and J. A. Elias, “Use of the tetracycline-controlled transcriptional silencer (tTS) to eliminate transgene leak in inducible overexpression transgenic mice,” *J. Biol. Chem.*, vol. 276, no. 27, pp. 25222–25229, 2001.

[19] T. Zheng, Z. Zhu, Z. D. Wang, R. J. Homer, B. Ma, R. J. Riese, H. A. Chapman, S. D. Shapiro, and J. A. Elias, “Inducible targeting of IL-13 to the adult lung causes matrix metalloproteinase-and cathepsin-dependent emphysema,” *J. Clin. Invest.*, vol. 106, no. 9, pp. 1081–1093, 2000.

[20] M. T. Garcia Sanz, F. J. Gonzalez Barcala, J. M. Alvarez Dobano, and L. Valdes Cuadrado, “Asthma and risk of lung cancer,” *Clin. Transl. Oncol.*, vol. 13, no. 10, pp. 728–730, 2011.

[21] J. V Goldstine, S. Nahas, K. Gamo, S. M. Gartler, R. S. Hansen, J. H. Roelfsema, R. A. Gatti, and Y. Marahrens, “Constitutive phosphorylation of ATM in lymphoblastoid cell

lines from patients with ICF syndrome without downstream kinase activity," *DNA Repair (Amst).*, vol. 5, no. 4, pp. 432–443, 2006.

[22] A. Muslimovic, I. H. Ismail, Y. Gao, and O. Hammarsten, "An optimized method for measurement of gamma-H2AX in blood mononuclear and cultured cells," *Nat. Protoc.*, vol. 3, no. 7, pp. 1187–1193, 2008.

[23] M. Hayashi, R. R. Tice, J. T. Macgregor, D. Anderson, D. H. Blakey, M. Kirshvolders, F. B. Oleson, F. Pacchierotti, F. Romagna, H. Shimada, S. Sutou, and B. Vannier, "IN-VIVO RODENT ERYTHROCYTE MICRONUCLEUS ASSAY," *Mutat. Res.*, vol. 312, no. 3, pp. 293–304, 1994.

[24] N. P. Singh, M. T. McCoy, R. R. Tice, and E. L. Schneider, "A SIMPLE TECHNIQUE FOR QUANTITATION OF LOW-LEVELS OF DNA DAMAGE IN INDIVIDUAL CELLS," *Exp. Cell Res.*, vol. 175, no. 1, pp. 184–191, 1988.

[25] C. A. Smith, "Untitled," *Cogn. Emot.*, vol. 20, no. 1, pp. 1–2, 2006.

[26] E. Hamelmann, K. Tadeda, A. Oshiba, and E. W. Gelfand, "Role of IgE in the development of allergic airway inflammation and airway hyperresponsiveness - a murine model," *Allergy*, vol. 54, no. 4, pp. 297–305, 1999.

[27] J. Mora, E. K. Riggs, J. Fu, D. W. MacGlashan Jr., S. A. Fox, B. Yu, M. C. Tobin, and L. L. Thomas, "Expression of the high affinity IgE receptor by neutrophils of individuals with allergic asthma is both minimal and insensitive to regulation by serum IgE," *Clin. Immunol.*, vol. 132, no. 1, pp. 132–140, 2009.

[28] X. Wang, W. Zhao, S. Liu, and X. Feng, "Correlation of IL-4 and IL-13 gene polymorphisms with asthma and total serum IgE levels," *Zhonghua Jiehe He Huxi Zazhi*, vol. 32, no. 3, pp. 161–164, 2009.

[29] J. A. Elias, T. Zheng, C. G. Lee, R. J. Homer, Q. S. Chen, B. Ma, M. Blackburn, and Z. Zhu, "Transgenic modeling of interleukin-13 in the lung," *Chest*, vol. 123, no. 3, p. 339S–345S, 2003.

[30] A. M. Westbrook and R. H. Schiestl, "Atm-Deficient Mice Exhibit Increased Sensitivity to Dextran Sulfate Sodium-Induced Colitis Characterized by Elevated DNA Damage and Persistent Immune Activation," *Cancer Res.*, vol. 70, no. 5, pp. 1875–1884, 2010.

[31] W. M. Bonner, C. E. Redon, J. S. Dickey, A. J. Nakamura, O. A. Sedelnikova, S. Solier, and Y. Pommier, "OPINION gamma H2AX and cancer," *Nat. Rev. Cancer*, vol. 8, no. 12, pp. 957–967, 2008.

[32] C. Hasbal, B. Y. Aksu, S. Himmetoglu, Y. Dincer, E. E. Koc, S. Hatipoglu, and T. Akcay, "DNA damage and glutathione level in children with asthma bronchiale: Effect of antiasthmatic therapy," *Pediatr. Allergy Immunol.*, vol. 21, no. 4, pp. E674–E678, 2010.

[33] I. G. Luzina, A. D. Keegan, N. M. Heller, G. A. W. Rook, T. Shea-Donohue, and S. P. Atamas, "Regulation of inflammation by interleukin-4: a review of 'alternatives,'" *J.*

Leukoc. Biol., vol. 92, no. 4, pp. 753–764, 2012.

[34] Y. Bosse, M. Lemire, A. H. Poon, D. Daley, J.-Q. He, A. Sandford, J. H. White, A. L. James, A. W. Musk, L. J. Palmer, B. A. Raby, S. T. Weiss, A. L. Kozyrskyj, A. Becker, T. J. Hudson, and C. Laprise, "Asthma and genes encoding components of the vitamin D pathway," *Respir. Res.*, vol. 10, 2009.

[35] G. Grunig, M. Warnock, A. E. Wakil, R. Venkayya, F. Brombacher, D. M. Rennick, D. Sheppard, M. Mohrs, D. D. Donaldson, R. M. Locksley, and D. B. Corry, "Requirement for IL-13 independently of IL-4 in experimental asthma," *Science (80-.).*, vol. 282, no. 5397, pp. 2261–2263, 1998.

[36] D. M. Conroy, A. A. Humbles, S. M. Rankin, R. T. Palframan, P. D. Collins, D. A. Griffiths-Johnson, P. J. Jose, and T. J. Williams, "The role of the eosinophil-selective chemokine, eotaxin, in allergic and non-allergic airways inflammation," *Mem. Inst. Oswaldo Cruz*, vol. 92, pp. 183–191, 1997.

[37] B. Ma, W. Liu, R. J. Homer, P. J. Lee, A. J. Coyle, J. M. Lora, C. G. Lee, and J. A. Elias, "Role of CCR5 in the pathogenesis of IL-13-induced inflammation and remodeling," *J. Immunol.*, vol. 176, no. 8, pp. 4968–4978, 2006.

[38] T. A. Wynn, "IL-13 effector functions," *Annu. Rev. Immunol.*, vol. 21, pp. 425–456, 2003.

[39] J. A. J. Vanoirbeek, M. Tarkowski, V. De Vooght, B. Nemery, and P. H. M. Hoet, "Immunological Determinants in a Mouse Model of Chemical-Induced Asthma After Multiple Exposures," *Scand. J. Immunol.*, vol. 70, no. 1, pp. 25–33, 2009.

[40] A. A. Humbles, D. M. Conroy, S. Marleau, S. M. Rankin, R. T. Palframan, A. E. I. Proudfoot, T. N. C. Wells, D. C. Li, P. K. Jeffery, D. A. GriffithsJohnson, T. J. Williams, and P. J. Jose, "Kinetics of eotaxin generation and its relationship to eosinophil accumulation in allergic airways disease: Analysis in a guinea pig model in vivo," *J. Exp. Med.*, vol. 186, no. 4, pp. 601–612, 1997.

[41] V. Valdiglesias, S. Giunta, M. Fenech, M. Neri, and S. Bonassi, "gamma H2AX as a marker of DNA double strand breaks and genomic instability in human population studies," *Mutat. Res. Mutat. Res.*, vol. 753, no. 1, pp. 24–40, 2013.

[42] M. L. Yamamoto, R. Reliene, J. Oshima, and R. H. Schiestl, "Effects of human Werner helicase on intrachromosomal homologous recombination mediated DNA deletions in mice," *Mutat. Res. Mol. Mech. Mutagen.*, vol. 644, no. 1–2, pp. 11–16, 2008.

[43] M. D. Evans, M. Dizdaroglu, and M. S. Cooke, "Oxidative DNA damage and disease: induction, repair and significance," *Mutat. Res. Mutat. Res.*, vol. 567, no. 1, pp. 1–61, 2004.

[44] P. Fortini, B. Pascucci, E. Parlanti, M. D'Errico, V. Simonelli, and E. Dogliotti, "8-Oxoguanine DNA damage: at the crossroad of alternative repair pathways," *Mutat. Res. Mol. Mech. Mutagen.*, vol. 531, no. 1–2, pp. 127–139, 2003.

[45] A. M. Westbrook, B. Wei, J. Braun, and R. H. Schiestl, “Intestinal inflammation induces genotoxicity to extraintestinal tissues and cell types in mice,” *Int. J. Cancer*, vol. 129, no. 8, pp. 1815–1825, 2011.

[46] A. V Kamath, I. D. Pavord, P. R. Ruparelia, and E. R. Chilvers, “Is the neutrophil the key effector cell in severe asthma?,” *Thorax*, vol. 60, no. 7, pp. 529–530, 2005.

[47] P. Boffetta, W. Ye, G. Boman, and O. Nyren, “Lung cancer risk in a population-based cohort of patients hospitalized for asthma in Sweden,” *Eur. Respir. J.*, vol. 19, no. 1, pp. 127–133, 2002.

[48] D. W. Brown, K. E. Young, R. F. Anda, V. J. Felitti, and W. H. Giles, “Re: Asthma and the risk of lung cancer. Findings from the adverse childhood experiences (ACE),” *Cancer Causes Control*, vol. 17, no. 3, pp. 349–350, 2006.

[49] D. Zeyrek, A. Cakmak, A. Atas, A. Kocyigit, and O. Erel, “DNA damage in children with asthma bronchiale and its association with oxidative and antioxidative measurements,” *Pediatr. Allergy Immunol.*, vol. 20, no. 4, pp. 370–376, 2009.

Chapter 3 Genome-Wide Translocation Sequencing Reveals Mechanisms of Chromosome Breaks and Rearrangements in B cells

Summary

Whereas chromosomal translocations are common pathogenetic events in cancer, mechanisms that promote them are poorly understood. To elucidate translocation mechanisms in mammalian cells, we developed high-throughput, genome-wide translocation sequencing (HTGTS). We employed HTGTS to identify tens of thousands of independent translocation junctions involving fixed I-SceI meganuclease-generated DNA double-strand breaks (DSBs) within the *c-myc* oncogene or *IgH* locus of B lymphocytes induced for activation-induced cytidine deaminase (AID)-dependent *IgH*class switching. DSBs translocated widely across the genome but were preferentially targeted to transcribed chromosomal regions. Additionally, numerous AID-dependent and AID-independent hot spots were targeted, with the latter comprising mainly cryptic I-SceI targets. Comparison of translocation junctions with genome-wide nuclear run-ons revealed a marked association between transcription start sites and translocation targeting. The majority of translocation junctions were formed via end-joining with short microhomologies. Our findings have implications for diverse fields, including gene therapy and cancer genomics.

Introduction

Recurrent oncogenic translocations are common in hematopoietic malignancies including lymphomas [1] also occur frequently in solid tumors such as prostate and lung cancers [2]. DNA double-strand breaks (DSBs) are common intermediates of these genomic aberrations [3]. DSBs are generated by normal metabolic processes, by genotoxic agents including some cancer therapeutics, and by V(D)J and immunoglobulin (Ig) heavy (H) chain (IgH) class switch recombination (CSR) in lymphocytes [4]. Highly conserved pathways repair DSBs to preserve

genome integrity [5]. Nevertheless, repair can fail, resulting in unresolved DSBs and translocations. Recurrent translocations in tumors usually arise as low-frequency events that are selected during oncogenesis. However, other factors influence the appearance of recurrent translocations including chromosomal location of oncogenes [6]. Chromosomal environment likely affects translocation frequency by influencing mechanistic factors, including DSB frequency at translocation targets, factors that contribute to juxtaposition of broken loci for joining, and mechanisms that circumvent repair functions that promote intrachromosomal DSB joining [4].

IgH CSR is initiated by DSBs that result from transcription-targeted AID-cytidine deamination activity within *IgH* switch (S) regions that lie just 5′ of various sets of $C_H$exons. DSBs within the donor Sμ region and a downstream acceptor S region are fused via end-joining to complete CSR and allow expression of a different antibody class [7]. Clonal translocations in human and mouse B cell lymphomas often involve *IgH* S regions and an oncogene, such as *c-myc* [1][8]. In this regard, AID-generated *IgH* S region DSBs directly participate in translocations to *c-myc* and other genes [9][10][11]. Through its role in somatic hypermutation (SHM) of *IgH* and Ig light (*IgL*) variable region exons, AID theoretically might generate lower frequency DSBs in Ig loci that serve as translocation intermediates [12]. In addition, AID mutates many non-Ig genes in activated B cells at far lower levels than Ig genes [13]; such off-target AID activity also may contribute to translocations of non-Ig genes [14]. Indeed, AID even has been suggested to initiate lesions leading to translocations in nonlymphoid cancers, including prostate cancer [15]. However, potential roles of AID in generating DSBs genome-wide have not been addressed. In this regard, other sources of translocation-initiating DSBs could include intrinsic factors, such as

oxidative metabolism, replication stress, and chromosome fragile sites, or extrinsic factors such as ionizing radiation or chemotherapeutics [4].

DSBs lead to damage response foci formation over 100 kb or larger flanking regions, promoting DSB joining and suppressing translocations [4][16]. *IgH* class switching in activated B cells can be mediated by yeast I-SceI endonuclease-generated DSBs without AID or S regions, suggesting general mechanisms promote efficient intrachromosomal DSB joining over at least 100 kb [17]. In somatic cells, classical nonhomologous end-joining (C-NHEJ) repairs many DSBs [4]. C-NHEJ suppresses translocations by preferentially joining DSBs intrachromosomally [18]. Deficiency for C-NHEJ leads to frequent translocations, demonstrating that other pathways fuse DSBs into translocations [4]. Correspondingly, an alternative end-joining pathway (A-EJ), that prefers ends with short microhomologies (MHs), supports CSR in the absence of C-NHEJ [19] and joins CSR DSBs to other DSBs to generate translocations [4]. Indeed, C-NHEJ suppresses p53-deficient lymphomas with recurrent *IgH/c-myc* translocations catalyzed by A-EJ [20]. Various evidence suggests that A-EJ may be translocation prone (e.g., [21]).

The mammalian nucleus is occupied by nonrandomly positioned genes and chromosomes [22]. Fusion of DSBs to generate translocations requires physical proximity; thus, spatial disposition of chromosomes might impact translocation patterns [4]. Cytogenetic studies revealed that certain loci involved in oncogenic translocations are spatially proximal [22]. Studies of recurrent translocations in mouse B cell lymphomas suggested that aspects of particular chromosomal regions, as opposed to broader territories, might promote proximity and influence translocation frequency [11]. Nonrandom position of genes and chromosomes in the nucleus led to two general models for translocation initiation. “Contact-first” poses translocations to be restricted to proximally positioned chromosomal regions, whereas “breakage-first” poses that distant DSBs

can be juxtaposed [22]. In-depth evaluation of how chromosomal organization influences translocations requires a genome-wide approach.

To elucidate translocation mechanisms, we developed approaches that identify genome-wide translocations arising from a specific DSB in vivo. Our studies isolate large numbers of translocations from primary B cells, which were activated for CSR, and provide a comprehensive analysis of the relationships among particular classes of DSBs, transcription, chromosome domains, and translocation events.

Results

Development of High-Throughput Genomic Translocation Sequencing

We developed high-throughput genomic translocation (HTGTS) to isolate junctions between a chromosomal DSB introduced at a fixed site and other sequences genome-wide. Such junctions, other than those involving breaksite resection, mostly should result from end-joining of introduced DSBs to other genomic DSBs. Thus, HTGTS will identify other genomic DSBs capable of joining to the test DSBs. With HTGTS, we isolated from primary mouse B cells junctions that fused *IgH* or *c-myc* DSBs to sequences distributed widely across the genome (Figures 1A and 1B). We chose *c-myc* and *IgH* as targets because they participate in recurrent oncogenic translocations in B cell lymphomas. To generate *c-myc*- or *IgH*-specific DSBs, we employed an 18 bp canonical I-SceI meganuclease target sequence, which is absent in mouse genomes [23]. One*c-myc* target was a cassette with 25 tandem I-SceI sites, to increase cutting efficiency, within *c-myc* intron 1 on chromosome (chr)15 (termed c-*myc*$^{25xI\text{-}SceI}$; Figure 1C; [11]). For comparison, we employed an allele with a single I-SceI site in the same position (termed c-*myc*$^{1xI\text{-}SceI}$) (Figure 1C; see Figures S1A–S1C available online). For*IgH*, we employed an allele

with two I-SceI sites in place of endogenous Sγ1 (termed $\Delta S\gamma1^{2xI\text{-}SceI}$) on chr12 [17]. As a cellular model, we used primary splenic B cells activated in culture with αCD40 plus IL4 to induce AID, transcription, DSBs and CSR at Sγ1 (IgG1) and Sε (IgE), during days 2–4 of activation. At 24 hr, we infected B cells with I-SceI-expressing retrovirus to induce DSBs at I-SceI targets [17]. Cells were processed at day 4 to minimize doublings and potential cellular selection. As high-titer retroviral infection can impair C-NHEJ [11], we also assayed B cells that express from their *Rosa26* locus an I-SceI-glucocorticoid receptor fusion protein (I-SceI-GR) that can be activated via triamcinolone acetonide (TA) (Figure 1D; Figures S1D–S1F). The c-$myc^{25xI\text{-}SceI}$ cassette was frequently cut in TA-treated c-$myc^{25xI\text{-}SceI}$/$ROSA^{I\text{-}SceI\text{-}GR}$ B cells (Figure S1G).

We employed two HTGTS methods. For the adaptor-PCR approach (Figure 1) [24], genomic DNA was fragmented with a frequently cutting restriction enzyme, ligated to an asymmetric adaptor, and further digested to block amplification of germline or unrearranged target alleles. We then performed nested PCR with adaptor- and locus-specific primers. Depending on the locus-specific PCR primers, one or the other side of the I-SceI DSB provides the "bait" translocation partner (Figure 1C), with the "prey" provided by DSBs at other genomic sites. As a second approach, we employed circularization PCR (Figure 1E) [25], in which enzymatically fragmented DNA was intramolecularly ligated and digested with blocking enzymes and nested PCR was performed with locus-specific primers. Following sequencing of PCR products, we aligned HTGTS junctions to reference genomes and scripted filters to remove artifacts from aligned databases. We experimentally controlled for potential background by generating HTGTS libraries from mixtures of human DNA and mouse DNA from activated I-SceI-infected c-$myc^{25xI\text{-}SceI}$ or $\Delta S\gamma1^{2xI\text{-}SceI}$ B cells; junctions fusing mouse and human sequences were less than

1% of the total (Figure 1F). We identified nearly 150,000 independent junctions from numerous libraries from different mice (Table S1). Resulting genome-wide junction maps are shown either as colored dot plots of overall distribution of translocation numbers in selected size bins (useful for visualizing hot spots) or bar plots that compress hot spots and illustrate translocation site density. HTGTS yields an average of 1 unique junction/5 ng of DNA, corresponding to about one junction/1000 genomes. Major findings were reproduced with both HTGTS methods (e.g., Figure S2A). Moreover, while the largest portion of data was obtained with c-*myc*$^{25xI\text{-}SceI}$ alleles cut via retroviral I-SceI, major findings were reproduced via HTGTS from the c-*myc*$^{25xI\text{-}SceI}$ allele cleaved by I-SceI-GR and the c-*myc*$^{1xI\text{-}SceI}$ allele cleaved by retroviral I-SceI

Analysis of Genome-wide Translocations from *c-myc* DSBs

For HTGTS of c-*myc*$^{25xI\text{-}SceI}$ or c-*myc*$^{1xI\text{-}SceI}$ alleles, we used primers about 200 bp centromeric to the cassette (Figure 1C) to detect junctions involving broken ends (BEs) on the 5′ side of *c-myc* I-SceI DSBs ("5′ *c-myc*-I-SceI BEs"). Based on convention, prey sequences joined to 5′ c-*myc*-I-SceI BEs are in (+) orientation if read from the junction in centromere to telomere direction and in (−) orientation if read in the opposite direction (Figures S3A–S3D). Joins in which 5′ c-*myc*-I-SceI BEs are fused to resected 3′ c-*myc*-I-SceI BEs would be (+) (Figure S3A). Intrachromosomal joins to DSBs centromeric or telomeric to 5′ c-*myc*-I-SceI BEs would be (+) or (−) depending on the side of the second DSB to which they were joined, with potential outcomes including deletions, inversions, and extrachromosomal circles (Figures S3B and S3C). Junctions to DSBs on different chromosomes could be (+) or (−) and derivative chromosomes centric or dicentric (Figure S3D). Analyses of over 100,000 independent junctions from 5′ c-*myc*-I-SceI BEs from WT and *AID*$^{-/-}$ backgrounds revealed prey to be distributed widely

throughout the genome with similar general distribution patterns (Figure 2; Figures S2B, S2E, and S2F). Other than 200 kb downstream of the bait DSB, intrachromosomal and interchromosomal junctions were evenly distributed into (+) and (−) orientation (Figure 2;Figure S3I). This finding implies that extrachromosomal circles and acentric fragments are represented similarly to other translocation classes, suggesting little impact of cellular selection on junction distribution. The junctions of 5′ c-*myc*-I-SceI BE from c-*myc*$^{25xI\text{-}SceI}$, c-*myc*$^{1xI\text{-}SceI}$, and c-*myc*$^{25xI\text{-}SceI}$/ROSA$^{I\text{-}SceI\text{-}GR}$ models were all consistent with end-joining, and most (75%–90%) had short junctional MHs (Table S1).

WT and *AID*$^{-/-}$ HTGTS maps for 5′ c-*myc*-I-SceI BEs had other common features. First, the majority of junctions (75%) arose from joining 5′ c-*myc*-I-SceI BEs to sequences within 10 kb, with most lying 3′ of the breaksite (Figure 3A; Figure S4A). The density of joins remained relatively high within a region 200 kb telomeric to the breaksite (Figure 3A;Figure S4A). Notably, most junctions within this 200 kb region, but not beyond, were in the (+) orientation, consistent with joining to resected 3′ *c-myc*-I-SceI BEs (Figure 3A;Figure S4A). About 15% of junctions occurred within the region 100 kb centromeric to the breaksite. As these could not have resulted from resection (due to primer removal), they may reflect the known propensity for joining intrachromosomal DSBs separated at such distances [17]. Compared with other chromosomes, chr15 had a markedly high density of translocations along its 50 Mb telomeric portion and also a high density along its centromeric portion (Figure 2). Many chromosomes had smaller regions of relatively high or low translocation density, with such overall patterns conserved between WT and *AID*$^{-/-}$ backgrounds (Figure 2; Figures S2A–S2F). Finally, although the majority of hot spots were WT specific, a number were shared between WT and *AID*$^{-/-}$backgrounds (see below).

Analysis of HTGTS Libraries from *IgH* DSBs

For HTGTS of the $\Delta S\gamma 1^{2xI\text{-}SceI}$ alleles, we used primers about 200 bp telomeric to the I-SceI cassette (Figure 1C), allowing detection of junctions involving BEs on the 5′ side of Sγ1 I-SceI DSBs ("5′ Sγ1-I-SceI BEs"). Intra- and interchromosomal joins involving 5′ Sγ1-I-SceI BEs result in (+) or (−) junctions with the range of potential chromosomal outcomes including deletions, inversions, extrachromosomal circles, and acentrics (Figures S3E–S3H). We isolated and analyzed approximately 9000 and 8000 5′ Sγ1-I-SceI BE junctions from WT and $AID^{-/-}$ libraries, respectively (Figures S2G and S2H). Reminiscent of the 5′ c-*myc*-I-SceI junctions, about 75% of these junctions were within 10 kb of the breaksite, with a larger proportion on the 3′ side and predominantly in the (−) orientation, consistent with joining to resected 3′ Sγ1-I-SceI BEs (Figures S4B–S4D). Outside the breaksite region, the general 5′ Sγ1-I-SceI BE translocation patterns resembled those observed for 5′ c-*myc*-I-SceI BEs, with both (+) and (−) translocations occurring on all chromosomes (Figures S3J and S2G). Though we analyzed more limited numbers of 5′ Sγ1-I-SceI BE junctions (Table S2 and Figures S2G and S2H), the broader telomeric region of chr12 had a notably large number of hits, and within this region, there were *IgH* hot spots in WT, but not $AID^{-/-}$, libraries (Figure 3B).

Sμ and Sε are major targets of AID-initiated DSBs in B cells activated with αCD40/IL4. Correspondingly, substantial numbers of 5′ Sγ1-SceI BE junctions from WT, but not $AID^{-/-}$, B cells joined to either Sμ or to Sε, which, respectively, lie approximately 100 kb upstream and downstream of the $\Delta S\gamma 1^{2xI\text{-}SceI}$ cassette (Figure 3B; Figures S4B–S4D). These findings support the notion that DSBs separated by 100–200 kb can be joined at high frequency by general repair mechanisms [17]. We also observed frequent junctions from WT libraries specifically within

Sγ3, which lies about 20 kb upstream of the breaksite, a finding of interest as joining Sγ3 to donor Sμ DSBs during CSR in αCD40/IL4-activated B cells occurs at low levels (see below). Notably, in WT, but not in *AID*$^{-/-}$ libraries, we found numerous junctions within Sγ1 (Figure S4D), which is also targeted by AID in αCD40/IL4-activated B cells. As Sγ1 is present only on the non-targeted chr12 homolog due to the ΔSγ1$^{2xI\text{-}SceI}$ replacement, these findings demonstrate robust translocation of 5′ Sγ1-I-SceI BEs to AID-dependent Sγ1 DSBs on the homologous chromosome, consistent with trans-CSR [26]. Finally, while AID deficiency greatly reduced junctions into S regions, we observed a focal cluster of five 5′ Sγ1-I-SceI BE junctions in or near Sμ in *AID*$^{-/-}$ ΔSγ1$^{2xI\text{-}SceI}$ libraries (Figure 3B;Figure S4C).

Most *c-myc* Translocation Hot Spots Are Targeted by AID

To identify 5′ c-*myc*-I-SceI BE translocation hot spots in an unbiased manner, we separated the genome into 250 kb bins and identified bins containing a statistically significant enrichment of translocations (Extended Experimental Procedures). This approach identified 55 hot spots in WT libraries and 15 in *AID*$^{-/-}$ libraries (Table S3;Figure 4A). Among the 43 most significant hot spots, 39 were in genes and 4 were in intergenic regions. Of these 43 hot spots, 21 were present at significantly greater levels in WT versus *AID*$^{-/-}$ backgrounds, and, therefore, classified as AID dependent; while 9 more were enriched (from 3- to 6-fold) in the WT background and were potentially AID dependent (Table S3; Figure 4A). The other 13 were equally represented between WT and *AID*$^{-/-}$ backgrounds (Table S3; Figure 4A). Of these 13, two exist in multiple copies (*Sfi1 and miR-715*), which may have contributed to their classification as hot spots [27]); five reached hot spot significance in only one of the two backgrounds (Table S3; Figure 4A).

The Sμ, Sγ1, and Sε regions, which are targeted for CSR DSBs by αCD40/IL4 treatment, were by far the strongest AID hot spots for 5′ c-*myc*-I-SceI BEs, with other non-*IgH* AID-dependent hot spots ranging from 1% to 10% of Sμ levels (Figure 4A). Translocation specificity to these three S regions, which together comprise less than 20 kb, was striking; there were only a few junctions in the remainder of the C_H locus, which includes 4 other S regions not substantially activated by αCD40/IL4 (Figure 3C). Notably, there was only one 5′ c-*myc*-I-SceI BE junction with Sγ3, even though Sγ3 was a marked hot spot for 5′ Sγ1-I-SceI BEs. In this regard, while AID-dependent DSBs in Sγ3 likely are much less frequent than in Sμ, Sγ1, and Sε under αCD40/IL4 stimulation conditions, Sγ3 DSBs may be favored targets of 5′ Sγ1-I-SceI BEs because of linear proximity. Finally, translocations occurred in Sμ and Sγ1 in *AID*$^{-/-}$ B cells at much lower levels than in WT, but frequently enough to qualify them as AID-independent hot spots (Figure 4A).

Several top AID SHM or binding targets in activated B cells [13][28] were translocation hot spots for 5′ c-*myc*-I-SceI BEs, including our top 3 non-*IgH* hot spots (*Il4ra*, *CD83*, and *Pim1*) and probable AID-dependent translocation targets (e.g., *Pax5* and *Rapgef1*) (Figure 4A; Table S3). We also identified other AID-dependent translocation hot spots including the *Aff3*, *Il21r*, and *Socs2* genes, and a nonannotated intergenic transcript on chr4 (Gm12493, Figure 4A; Table S3). We confirmed the ability of such hot spots to translocate to the c-*myc*$^{25xI\text{-}SceI}$ cassette by direct PCR (Table S4). We conclude that AID not only binds and mutates numerous non-Ig target genes but also acts on them to cause DSBs and translocations.

Translocations Genome-wide Frequently Occur Near Active Transcription Start Sites

To quantify transcription genome-wide, we applied unbiased global run-on sequencing (GRO-seq; [29]) to αCD40/IL4-activated, I-SceI-infected B cells. GRO-seq measures elongating Pol II activity and distinguishes transcription on both strands. For all analyses, we excluded junctions within 1 Mb of the *c-myc* breaksite to avoid biases from this dominant class of junctions. To analyze remaining junctions from WT and *AID*$^{-/-}$backgrounds, we determined nearest transcription start sites (TSSs) and divided translocations based on whether or not the TSS had promoter proximal activity based on GRO-seq (Extended Experimental Procedures). Strikingly, both WT and *AID*$^{-/-}$junctions, when dominant *IgH* translocations were excluded, showed a distinct peak that reached a maximum about 300–600 bp on the sense side of the active TSSs and spanned from about 600 bp on the antisense side to about 1 kb on the sense side (Figures 4B and 4C). Translocation hot spot genes, including *Il4ra*, *CD83*, *Gm12493*,*Pim1*, as well as potential hot spots including *Pax5* and *Bcl11a*, had a substantial proportion of their translocations within 1–2 kb regions starting 200–400 bp in the sense direction from their bidirectional TSSs (Figures 5A and 5B). In one striking example of TSS-proximal translocation targeting, there were distinct translocation peaks downstream of the TSSs of *Il4ra* and *Il21r*, which lies just 20 kb downstream; yet, there were no detected translocations into the 3′ portion of *Il4ra* even though it was highly transcribed (Figure 5A). While lower level translocations into some AID hot spot genes in*AID*$^{-/-}$ mice had less correlation with TSS proximity (Figures 5A and 5B), the overall correlation of translocations and active TSS appeared similar in WT and *AID*$^{-/-}$mice (Figures 4B and 4C; Figures S5A and S5B). Together, our findings indicate a relationship between active TSSs and AID-dependent and independent translocations genome-wide. In this context, we did not find a marked TSS correlation for translocations into nontranscribed genes (Figures 4B and 4C).

When the dominant *IgH* hot spots were included in the translocation/transcription analyses, the translocation peak shifted from about 300–600 bp to about 1.5 kb downstream of the TSS in the sense direction (compare Figures 4B and 4C to Figures S5C and S5D). In B cells, transcription through Sμ initiates from the V(D)J exon and Iμ exon promoters upstream of Sμ. B cell activation with αCD40/IL4 stimulates CSR between Sμ and Sγ1 or Sε by inducing AID and by activating Iγ1 and Iε promoters upstream of Sγ1 and Sε. Indeed, most translocations into germline C_H genes in WT αCD40/IL4-activated B cell were tightly clustered 1-2 kb downstream in the 5′ portion of Sμ, Sγ1, and Sε, consistent with transcription robustly targeting AID to S regions (Figure 5C). Finally, AID-independent *IgH* translocations were scattered more broadly through S and C regions, suggesting that DSBs that initiate them arise by a different, AID-independent mechanism of S region instability (Figure 5C).

For 5′ c-*myc*-I-SceI BEs (outside the breaksite region), 55% of translocations were within genes, whereas genes account for only 36% of the genome (Table S5). Therefore, we asked whether translocations from 5′ c-*myc*-I-SceI BEs varied with gene density. For this purpose, we compared translocation densities to available gene density maps and to our GRO-seq transcription maps of all genes (Figure 6; Figure S6 and Figure S7). Strikingly, translocation distribution was highly correlated with gene density and transcription level. In general, chromosomal regions with highest transcriptional activity had highest translocation density. In contrast, regions with very low or undetectable transcription generally were very low in translocations
(Figure 6; Figure S6 and Figure S7). Notably, we found no obvious regions with high overall transcription and low translocation levels, supporting a direct relationship between active transcription and translocation targeting genome-wide. In this context, we observed several robust AID-independent hot spot peaks that were relatively distant to the TSS and/or occurred in

nonactive genes (Figures 4B and 4C, asterisks); these hot spots were generated by I-SceI activity at cryptic endogenous I-SceI sites as discussed next.

HTGTS Libraries Reveal Numerous Cryptic Genomic I-SceI Target Sites

Eleven AID-independent translocation targets for 5′ c-*myc*-I-SceI BEs were in genes and two were in intergenic regions (Table S3). Eight of these hot spot regions, in which junctions were tightly clustered, contained potential I-SceI-related sites, many of which were very near (within 50 bp) or actually contributed to translocation junctions. These putative cryptic I-SceI sites had from 1 to 5 divergent nucleotides with respect to the canonical 18 bp target site (Figure 7A). We scanned the mouse genome for potential cryptic I-SceI sites that diverged up to three positions and identified ten additional sites that map within 400 bp of one or more 5′ c-*myc*-I-SceI BE translocation junctions (Figure 7A). In vitro I-SceI digestion of PCR-amplified genomic fragments demonstrated that all eight putative I-SceI targets at hot spots, and six of seven tested additional putative I-SceI targets, were bona fide I-SceI substrates (Figures 7A and 7B). We performed direct translocation PCRs with three selected cryptic I-SceI sites and confirmed I-SceI-dependent translocation to the c-*myc*$^{25\text{xI-SceI}}$ cassette (Figure 7C). Finally, GRO-seq analyses showed that five of eight cryptic I-SceI translocation hot spots were in transcriptionally silent areas and that two I-SceI-generated hot spots in transcribed genes were distant from the TSS (Figures 4B and 4C, asterisks; Figures 7D and 7E), highlighting the distinction between the I-SceI-generated hot spots and most other genomic translocation hot spots.

Discussion

With HTGTS, we have identified the genome-wide translocations that emanate from DSBs introduced into c-*myc* or *IgH* in activated B cells. A substantial percentage of these

translocations (80%–90%) join introduced DSBs to sequences on the same chromosome proximal to the breaksite, likely reflecting the strong preference for C-NHEJ to join DSBs intrachromosomally [18][17][25]. The remaining 10%–20% translocate broadly across all chromosomes, with translocation density correlating with transcribed gene density. Translocations are most often near TSSs within individual genes. Despite *c-myc* and *IgH*DSBs translocating broadly, there are translocation hot spots, with the majority being generated by cellular AID activity and most of the rest by ectopically expressed I-SceI activity at cryptic genomic I-SceI target sequences. Notably, targeted DSBs join at similar levels to both (+) and (−) orientations of hot spot sequences, arguing against a role for cellular selection in their appearance. This finding also suggests that both sides of hot spot DSBs have similar opportunity to translocate to a DSB on another chromosome.

The majority of HTGTS junctions from the *c-myc* I-SceI DSBs are mediated by end-joining and contain short MHs, reminiscent of joins in cancer genomes [3] and consistent with roles for either (or both) C-NHEJ or A-EJ [4]. Recurrence of translocations in cancer genomes is a characteristic used to consider them as potential oncogenic "drivers." Our HTGTS studies establish that many recurrent translocations form in the absence of selection and, thus, are caused by factors intrinsic to the translocation mechanism [11][15]. HTGTS also provides a method to discover recurrent genomic DSBs, as evidenced by ability of HTGTS to find known DSBs, such as AID-initiated DSBs in S regions, and previously unrecognized genomic I-SceI targets. HTGTS should be readily applicable for genome-wide screens for translocations and recurrent DSBs in a wide range of cell types.

AID Has a Dominant Role in Targeting Recurrent Translocations Genome-wide

Prior studies demonstrated that AID binds to and mutates non-Ig genes [30][13][28]. We find that AID also induces DSBs and translocations in non-Ig genes with the peak of translocation junctions spanning the region of the TSS. Thus, processes closely associated with transcription and, potentially, transcriptional initiation may attract AID activity to these non-Ig gene targets, consistent with ectopically expressed AID mutating yeast promoter regions [31]. *IgH* translocation junctions mostly fall 1.5–2 kb downstream of the activated I region TSSs within S regions, which are known to be specialized AID targets. Thus, transcription through S regions attracts and focuses AID activity, at least in part via pausing mechanisms and by generating appropriate DNA substrates, such as R-loops, for this single-strand DNA-specific cytidine deaminase [32][33][7]. Notably, S regions still qualified as translocation hot spots for 5′ c-*myc*-I-SceI BEs in $AID^{-/-}$ B cells, supporting suggestions that these regions, perhaps via transcription, may be intrinsically prone to DSBs [34][35]. Given the differential targeting of CSR and SHM [12], application of HTGTS to germinal center (GC) B cells, in which AID initiates SHM within variable region exons, may reveal novel AID genomic targets not observed in B cells activated for *IgH* CSR in culture, potentially including genes that could contribute to GC B cell lymphoma [1].

A General Role for Transcription and Transcription Initiation in Targeting Translocations

We find a remarkable genome-wide correlation between transcription and translocations even in $AID^{-/-}$ cells, with a peak of translocation junctions lying near active TSSs. In this context, while the majority of junctions were located in the sense transcriptional direction, junctions also occurred at increased levels close to the TSS on the antisense side (e.g.,Figures 4B and 4C; Figure 5), correlating with focal antisense transcription in the immediate vicinity of active

promoters [29] (Figure 5). Notably, we observed a number of regions genome-wide that were quite low in or devoid of translocations and transcription, but few, if any, that were low in translocations but high in transcription (Figure 6). On the other hand, we found that transcription is not required for high-frequency translocations, since many I-SceI-dependent hot spots are in nontranscribed regions. Together, our observations are consistent with transcription mechanistically promoting translocations by promoting DSBs. Thus, our findings strongly support the long-standing notion of a mechanistic link between transcription, DSBs, and genomic instability [36][37][38].

Potential Influences of Genome Organization on Translocations

The high level of translocations of 5′ c-*myc*-I-SceI BEs to other sequences along much the length of chr15, while generally correlated with transcription, likely may be further promoted by high relative proximity of many intrachromosomal regions [39]. Proximity might also contribute to the apparently increased frequency of 5′ c-*myc*-I-SceI BEs to certain regions of various chromosomes (e.g., Figure 2). In this regard, the relative frequency of chr15 5′ c-*myc*-I-SceI BE translocations to the Sμ and Sε regions on chr12 were only 5 and 7 fold less, respectively, than levels of intra-*IgH* 5′ Sγ1-I-SceI BE joins to Sμ and Sε (Figure 3C). Thus, even though DSBs are rare in *c-myc*, their translocation to *IgH* when they do occur is driven at a high rate by other mechanistic aspects, most likely proximal position [11]. However, we also note that sequences lying in regions across all chromosomes translocate to DSBs in *c-myc* on chr15 and *IgH* in chr12, suggesting the possibility that, in some cases, DSBs might move into proximity before joining, perhaps during the cell cycle or via other mechanisms (e.g. [40]).

HTGTS Reveals an Unexpectedly Large Number of Genomic I-SceI Targets

Our HTGTS studies revealed 18 cryptic genomic I-SceI sites as translocation targets. There could potentially be more cryptic I-SceI sites; to find the full spectrum, bait sequences may need to be introduced into a variety of chromosomal locations to neutralize position effects. Beyond I-SceI, the HTGTS approach could readily be extended through the use Zinc finger nucleases [41], meganucleases [42], or TALENs [43] designed to cleave specific endogenous sites, thereby obviating the need to introduce a cutting site and greatly facilitating the process. The above three classes of endonucleases are being developed for targeted gene correction of human mutations in stem cells for gene therapy. One major concern with such nucleases is relative activity on the specific target versus off-target activity, with the latter being difficult to assess. HTGTS provides a means for identifying off-target DSBs generated by such enzymes, for assessing ability of such off-target DSBs to translocate, and for identifying the sequences to which they translocate.

Experimental Procedures

Mouse Strains Utilized

$\Delta S\gamma 1^{2xI\text{-}SceI}$, c-*myc*$^{25xI\text{-}SceI}$ and *AID*$^{-/-}$ mice were described [17][11][44]. c-*myc*$^{1xI\text{-}SceI}$ mice were generated similarly to c-*myc*$^{25xI\text{-}SceI}$ mice (see Extended Experimental Procedures). ROSA$^{I\text{-}SceI\text{-}GR}$ mice were generated by targeting an I-SceI-GR/IRES-tdTomato expression cassette into *Rosa26* (Extended Experimental Procedures). All mice used were heterozygous for modified alleles containing I-SceI cassettes. The Institutional Animal Care and Use Committee of Children's Hospital, Boston approved all animal work.

Splenic B Cell Purification, Activation in Culture, and Retroviral Infection

All procedures were performed as previously described [11]. c-*myc*$^{25xI\text{-}SceI}$/ROSA$^{I\text{-}SceI\text{-}GR}$ B cells were cultured in medium containing charcoal-stripped serum and I-SceI-GR was activated with 10 μM triamcinolone acetate (TA, Sigma).

Generation of HTGTS Libraries

Genomic DNA was digested with HaeIII for c-*myc*$^{25xI\text{-}SceI}$ samples or MspI for ΔSγ1$^{2xI\text{-}SceI}$ samples. For adaptor-PCR libraries, an asymmetric adaptor was ligated to cleaved genomic DNA. Ligation products were incubated with restriction enzymes chosen to reduce background from germline and unrearranged targeted alleles. Three rounds of nested PCR were performed with adaptor- and locus-specific primers. For circularization-PCR libraries, HaeIII- or MspI-digested genomic DNA was incubated at 1.6 ng/μl to favor intramolecular ligation and samples treated with blocking enzymes as above. Two rounds of nested PCR were performed with primers specific for sequences upstream of the I-SceI cassette. Libraries were sequenced by Roche-454. See Extended Experimental Procedures for details.

Data Analysis

Alignment and Filtering

Sequences were aligned to the mouse reference genome (NCBI37/mm9) with the BLAT program. Custom filters were used to purge PCR repeats and multiple types of artifacts including those caused by in vitro ligation and PCR mispriming.

Hot Spot Identification

Translocations from WT or *AID*$^{-/-}$ libraries minus those on chr15 or the *IgH* locus were pooled. The adjusted genome was then divided into 250 kb bins and bins containing five or more hits constituted a hot spot (details in Extended Experimental Procedures).

In Vitro Testing of Putative Cryptic I-SceI Sites

A genomic region encompassing each candidate I-SceI site was PCR-amplified and 500 ng of purified products were incubated with 5 units of I-SceI for 3 hr. Reactions were separated on agarose gel and relative intensity of uncut and I-SceI-digested bands calculated with the FluorchemSP program (Alpha Innotech) (see Extended Experimental Procedures).

PCR Detection of Translocations between c-*myc* and Cryptic I-SceI Sites

Translocation junctions between *c-myc* and cryptic I-SceI targets were PCR-amplified according to the standard protocol [11]. Primers and PCR conditions are detailed in Extended Experimental Procedures.

PCR Detection of Translocations between c-*myc* and Cryptic I-SceI Sites

Translocation junctions between *c-myc* and cryptic I-SceI targets were PCR-amplified according to the standard protocol [11]. Primers and PCR conditions are detailed in Extended Experimental Procedures.

GRO-Seq

Nuclei were isolated from day 4 αCD40/IL4-stimulated and I-SceI-infected c-*myc*$^{25xI\text{-}SceI}$B cells as described [45]. GRO-seq libraries were prepared from 5×10^6 cells from two independent

mice using a described protocol [29]. Both libraries were sequenced on the Hi-Seq 2000 platform with single-end reads and analyzed as described (see Extended Experimental Procedures). After filtering and alignment, we obtained 34,212,717 reads for library 1 and 15,913,244 reads for library 2. As results between libraries were highly correlated, we show results only from replicate 1.

Accession Numbers

The Gro-Seq data sets are deposited in SRA (http://www.ncbi.nlm.nih.gov/sra) under accession number SRA049000.

SUPPLEMENTAL INFORMATION Supplemental Information includes Extended Experimental Procedures, seven figures, and seven tables and can be found with this article online at doi:10.1016/j.cell.2011.07.049.

Acknowledgments

We thank Barry Sleckman for providing unpublished information about circular PCR translocation cloning of RAG-generated DSBs. This work was supported by NIH grant 5P01CA92625 and a Leukemia and Lymphoma Society of America (LLS) SCOR grant to F.W.A., grants from AIRC and grant FP7 ERC-2009-StG (Proposal No. 242965—"Lunely") to R.C., an NIH KO8 grant AI070837 to C.C.G., and a V Foundation Scholar award to M.G. Y.Z. was supported by CRI postdoctoral fellowship and R.L.F. by NIH training grant 5T32CA070083-13. F.W.A. is an Investigator of the Howard Hughes Medical Institute. F.W.A. is a member of the scientific advisory board of Cellectis Pharmaceuticals.

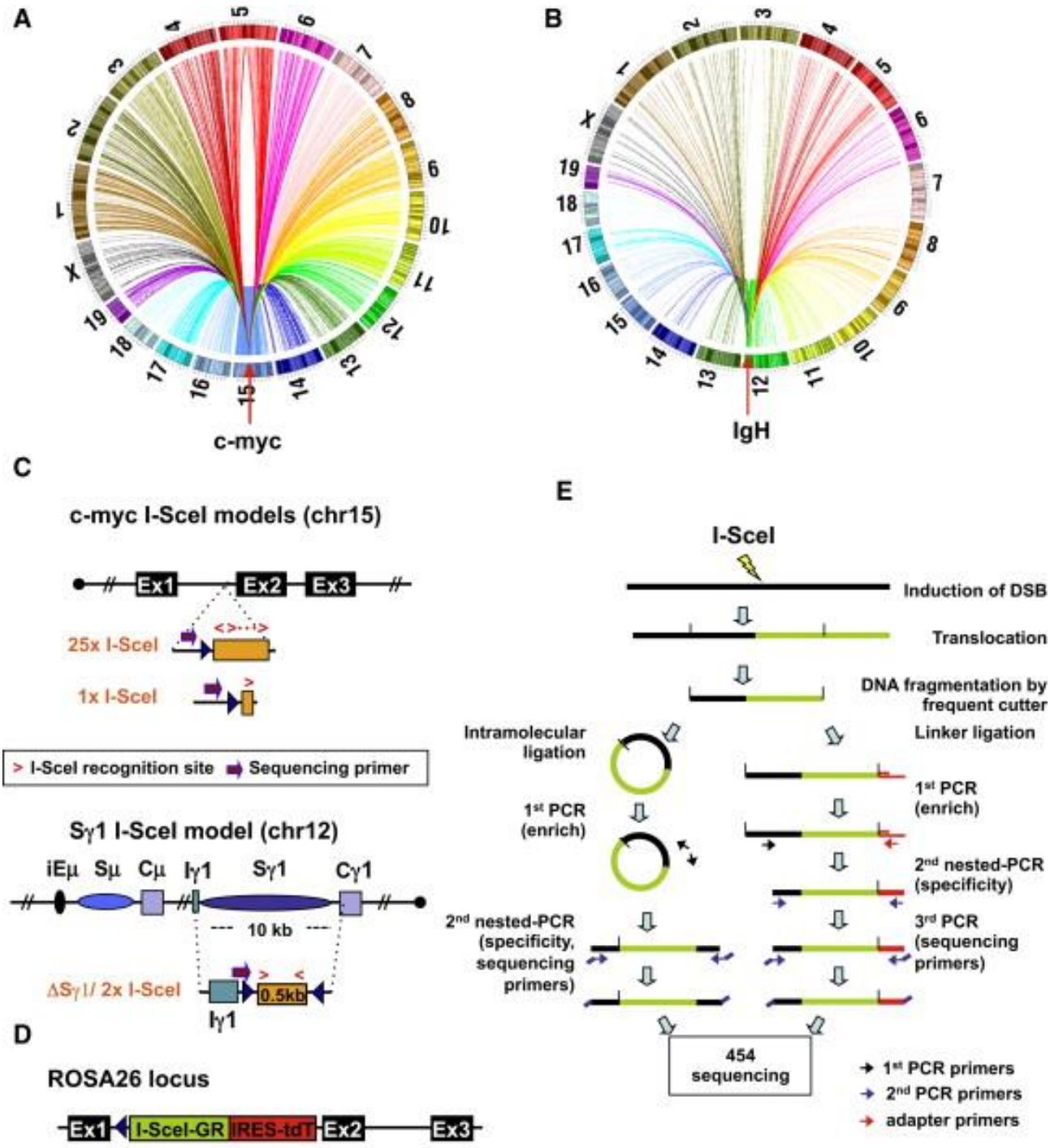

F

method	ad-PCR	ad-PCR	ad-PCR	circ-PCR
mouse DNA	c-myc$^{25x\ I\text{-}SceI}$ WT	c-myc$^{25x\ I\text{-}SceI}$ AID-/-	ΔSγ1$^{2x\ I\text{-}SceI}$ WT	c-myc$^{25x\ I\text{-}SceI}$ WT
human DNA	K562	K562	K562	K562
mouse junc.	2257	1957	1837	316
human junc.	12	11	6	2
background	**0.53%**	**0.56%**	**0.33%**	**0.63%**

Figure 1.
High-Throughput Genomic Translocation Sequencing
(A and B) Circos plots of genome-wide translocation landscape of representative *c-myc* (A) or *IgH* (B) HTGTS libraries. Chromosome ideograms comprise the circumference. Individual translocations are represented as arcs originating from specific I-SceI breaks and terminating at partner site.
(C) Top: a cassette containing either 25 or one I-SceI target(s) was inserted into intron 1 of *c-myc* (seeFigures S1A–S1C). Bottom: a cassette composed of a 0.5 kb spacer flanked by I-SceI target replaced the*IgH* Sγ1 region. Relative orientation of I-SceI sites is indicated by red arrows. Position of primers for generation and sequencing HTGTS libraries is shown.
(D) An expression cassette for I-SceI fused to a glucocorticoid receptor (I-SceI-GR) was targeted into*Rosa26* (see Figures S1D–S1G). The red fluorescent protein Tomato (tdT) is coexpressed via an IRES.
(E) Schematic representation of HTGTS methods; left: circularization-PCR, right: adaptor-PCR. See text for details.
(F) Background for HTGTS approaches, calculated as percent of artifactual human:mouse hybrid junctions when human DNA was mixed 1:1 with mouse DNA from indicated samples.

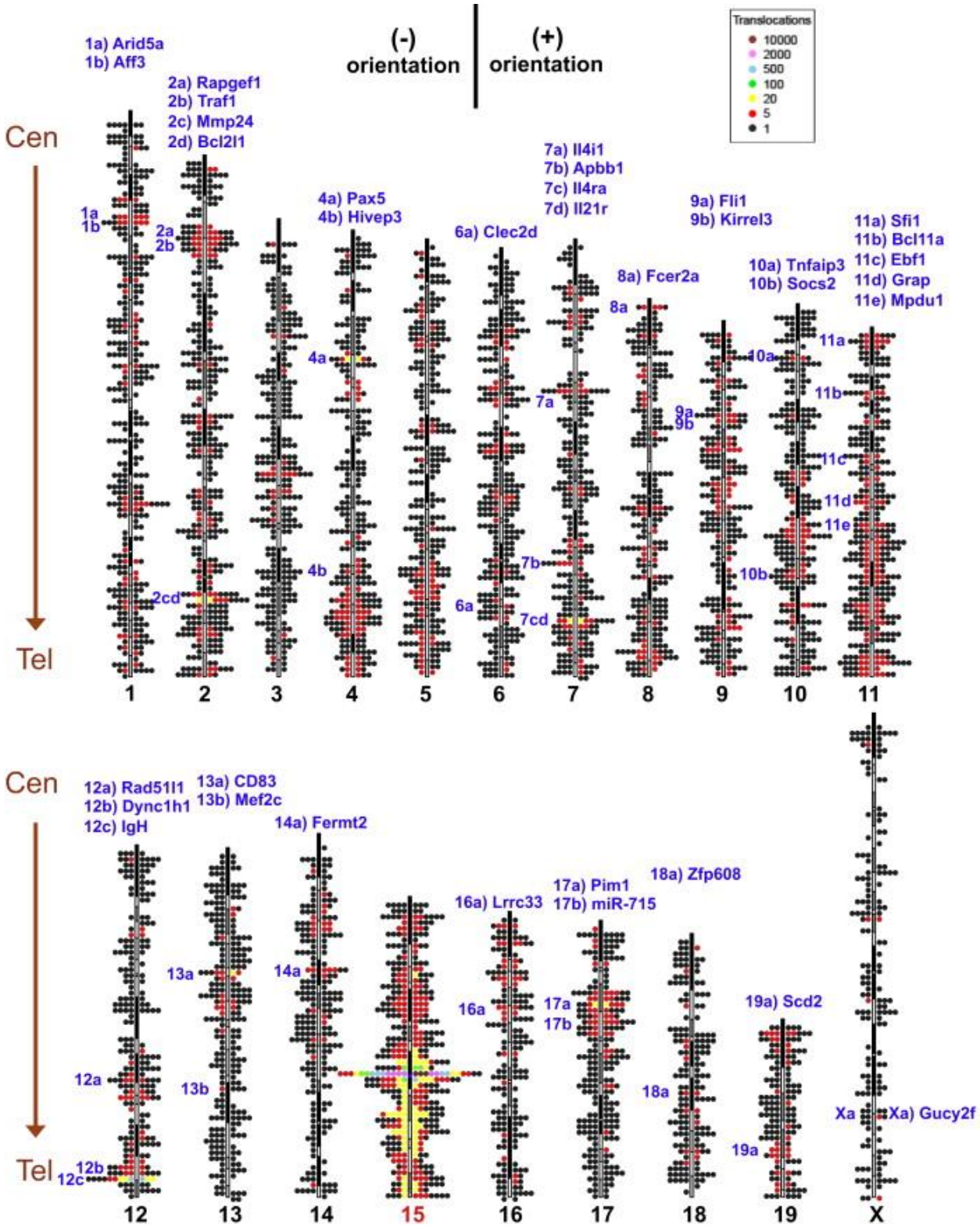

Figure 2.
Genome-wide Distribution and Orientation of Translocations from *c-myc* DSBs

Genome-wide map of translocations originating from the c-*myc*$^{25xI\text{-}SceI}$ cassette (chr15) in αCD40/IL4-activated and I-SceI-infected B cells. Single junctions are represented by dots located at corresponding chromosomal position. The dot scale is 2 Mb. Clusters of translocations are indicated with color codes, as shown in legend. (+) and (−) orientation junctions (see Figure S3) are plotted on right and left side of each ideogram, respectively. Hot spots (see Figure 4A) are listed in blue on top, with notation on the left side of chromosomes to indicate position. Data are from HTGTS libraries from seven different mice. Centromere (Cen) and telomere (Tel) positions are indicated. See also Figure S2.

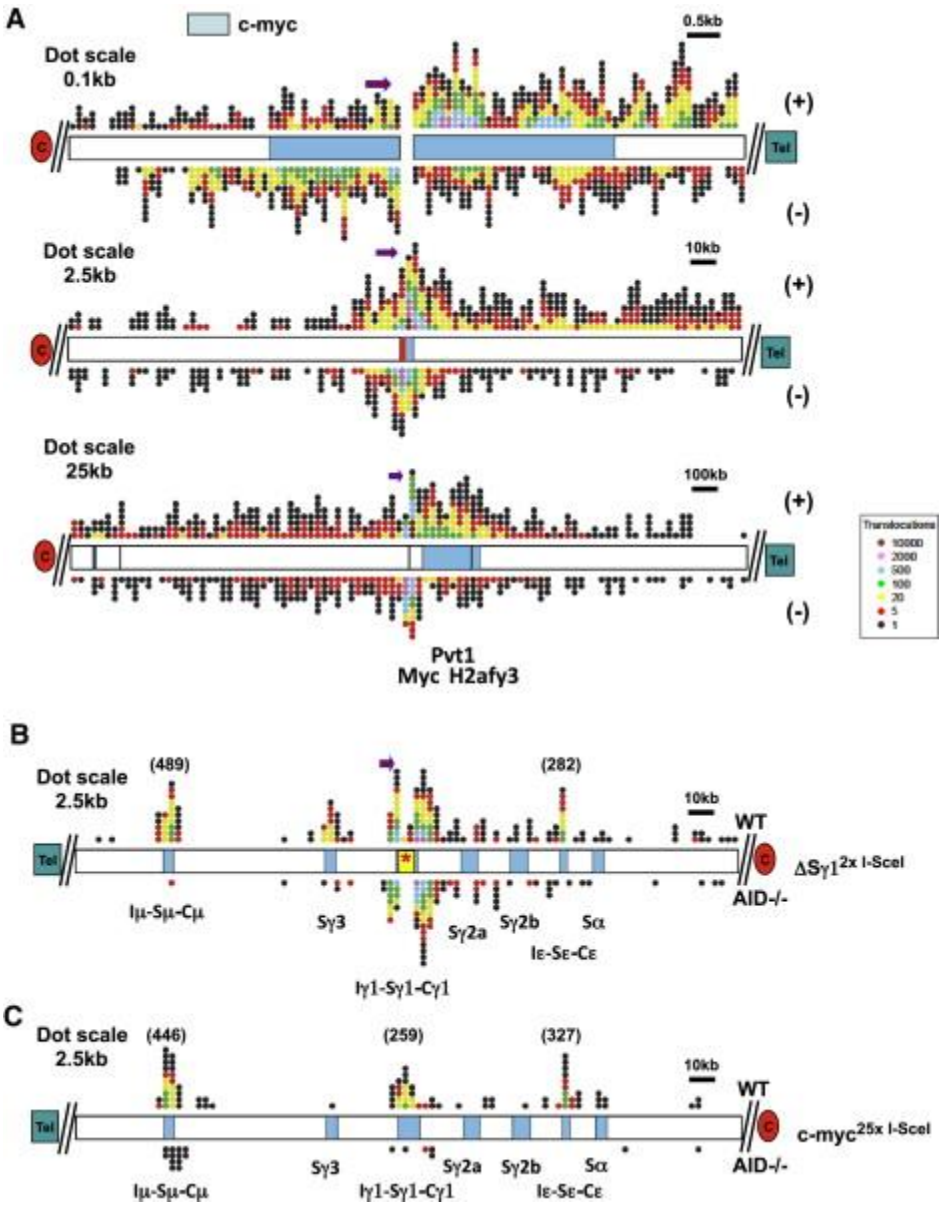

Figure 3.
Distribution of *IgH*- and *c-myc*-Proximal Junctions
(A) Distribution of junctions around chr15 breaksite in the pooled c-*myc*$^{25xI\text{-}SceI}$ HTGTS library. Top: 10 kb around breaksite (represented as a split). Middle: 250 kb around breaksite (represented by red bar); Bottom: 2.5 Mb around breaksite. (+) and (−)-oriented junctions are plotted on top and bottom of chromosome diagrams, respectively.
(B and C) Distribution of translocation junctions at *IgH* in the pooled ΔSγ1$^{2xI\text{-}SceI}$ (B) or c-*myc*$^{25xI\text{-}SceI}$ (C) HTGTS libraries. Translocations in WT (top) and *AID*$^{-/-}$ (bottom) B cells are shown. Positions of S regions within the 250 kb *IgH* C_H region are indicated. Color codes are as in Figure 2. Dot size, position of centromere (red oval) and telomere (green rectangle), and orientation of the sequencing primer are indicated. See also Figure S4.

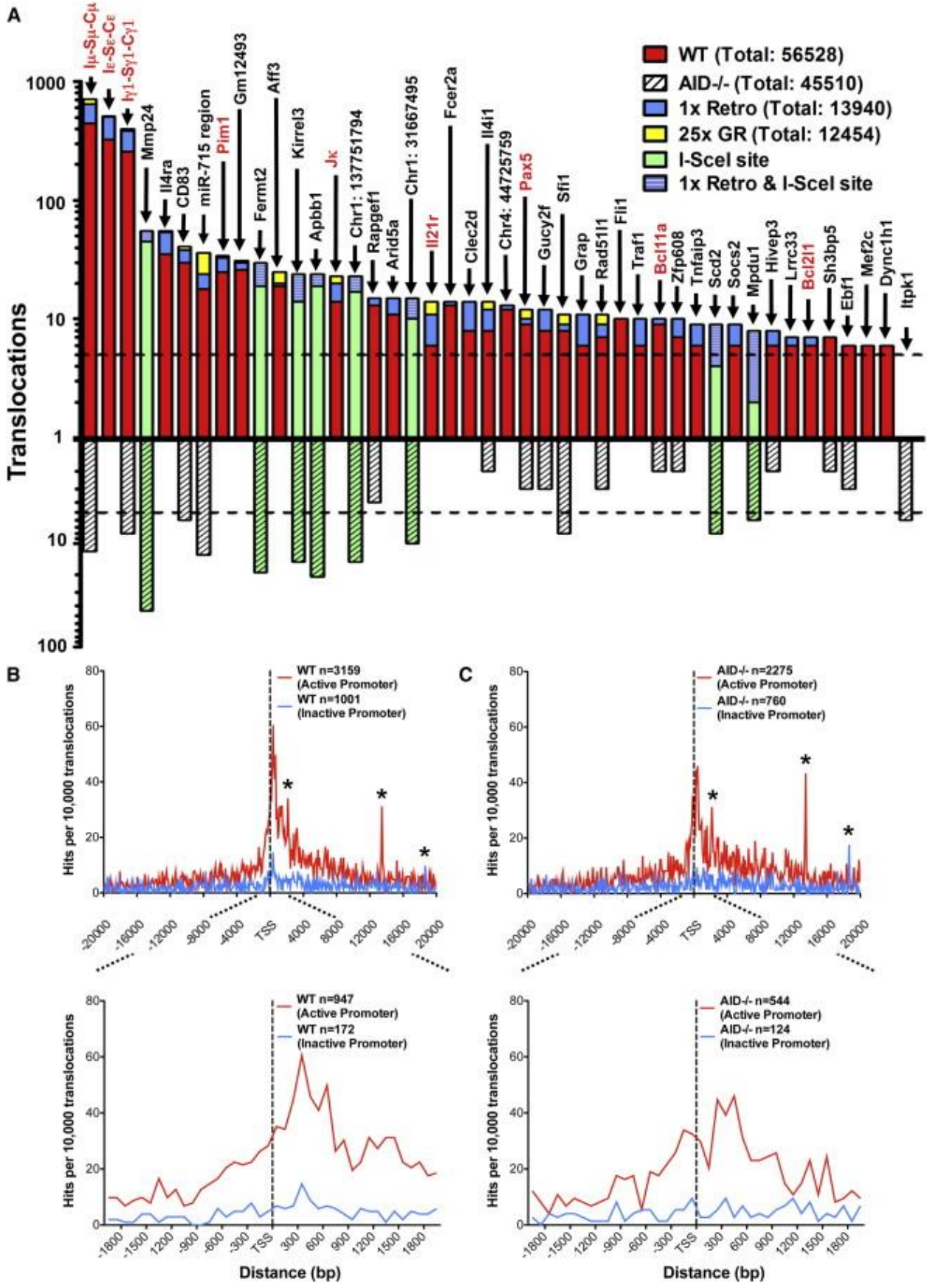
A
WT (Total: 56528)
AID-/- (Total: 45510)
1x Retro (Total: 13940)
25x GR (Total: 12454)
I-SceI site
1x Retro & I-SceI site
Translocations
1000
100
10
1
10
100
Iμ-Sμ-Cμ
Iε-Sε-Cε
Iγ1-Sγ1-Cγ1
Mmp24
Il4ra
CD83
miR-715 region
Pim1
Gm12493
Fermt2
Aff3
Kirrel3
Apbb1
Jκ
Chr1: 137751794
Rapgef1
Arid5a
Chr1: 31667495
Il21r
Fcer2a
Clec2d
Il4i1
Chr4: 44725759
Pax5
Gucy2f
Sfi1
Grap
Rad51l1
Fli1
Traf1
Bcl11a
Zfp608
Tnfaip3
Scd2
Socs2
Mpdu1
Hivep3
Lrrc33
Bcl2l1
Sh3bp5
Ebf1
Mef2c
Dync1h1
Itpk1
B
WT n=3159
(Active Promoter)
WT n=1001
(Inactive Promoter)
Hits per 10,000 translocations
WT n=947
(Active Promoter)
WT n=172
(Inactive Promoter)
Distance (bp)
C
AID-/- n=2275
(Active Promoter)
AID-/- n=760
(Inactive Promoter)
AID-/- n=544
(Active Promoter)
AID-/- n=124
(Inactive Promoter)

Figure 4.
Identification of Specific and General Translocation Hot Spots
(A) Graph representing translocation numbers in frequently hit genes and non-annotated chromosomal regions. Only hot spots with more than five hits are shown and are ordered based on frequency of translocations in the pooled c-*myc*$^{25xI\text{-}SceI}$/WT HTGTS library (top bars). Respective frequencies of translocations in the pooled c-*myc*$^{25xI\text{-}SceI}$/*AID*$^{-/-}$ HTGTS library are displayed underneath (bottom bars). Green bars represent frequent hits involving cryptic I-SceI sites. Blue and yellow portions of top bars represent translocations found in c-*myc*$^{1xI\text{-}SceI}$ and c-*myc*$^{25xI\text{-}SceI}$/ROSA$^{I\text{-}SceI\text{-}GR}$ libraries, respectively. Genes translocated in human and mouse lymphoma or leukemia are in red. The dashed line represents the cutoff for significance over random occurrence for each of the two groups (see Table S3).
(B and C) Genome-wide distribution of translocations relative to TSSs. Junctions from c-*myc*$^{25xI\text{-}SceI}$/WT (B) or c-*myc*$^{25xI\text{-}SceI}$/*AID*$^{-/-}$ (C) libraries (excluding 2 Mb around chr15 breaksite and *IgH* S regions) are assigned a distance to the nearest TSS and separated into "active" and "inactive" promoters as determined by GRO-seq. Translocation junctions are binned at 100 bp intervals. n represents the number of junctions within 20 kb (upper panels) or 2 kb (lower panels) of TSS. Asterisks indicate cryptic genomic I-SceI sites. See also Figure S5.

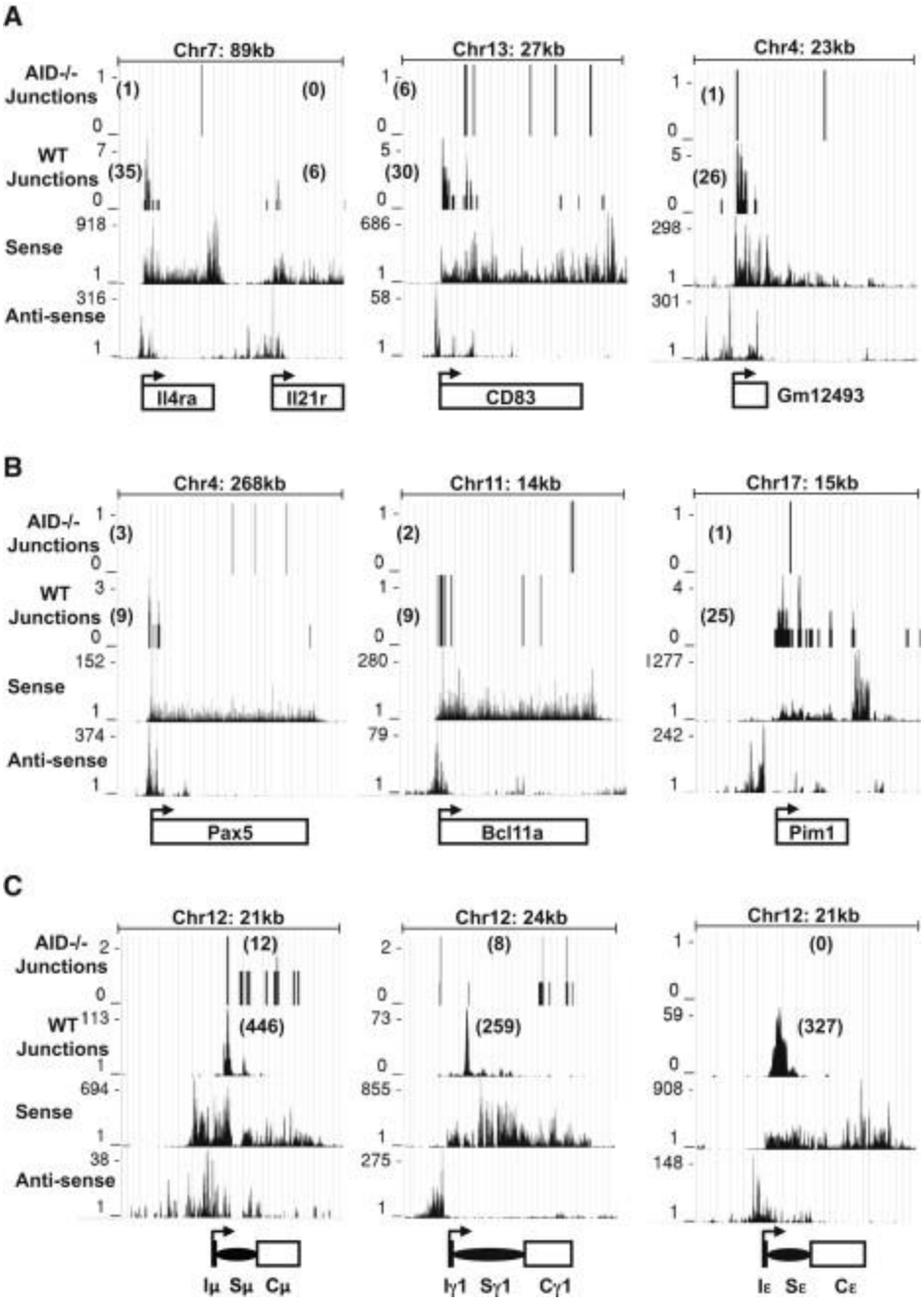

Figure 5.
Translocations Preferentially Occur Near TSSs
WT and *AID*$^{-/-}$ c-*myc*$^{25xI\text{-}SceI}$ HTGTS libraries were analyzed. In each panel, translocation junctions are in the first and second rows (WT and *AID*$^{-/-}$ as indicated). The third and fourth rows represent sense and antisense nascent RNA signals from GRO-seq. The *IgH* μ, γ1, ε genes are shown in (C), the next most frequently hit hot spots in (A) and three selected oncogene hot spots in (B). The transcriptional start site (arrow) is at the bottom of each panel. The size of each genomic region and number of junctions in each are shown.

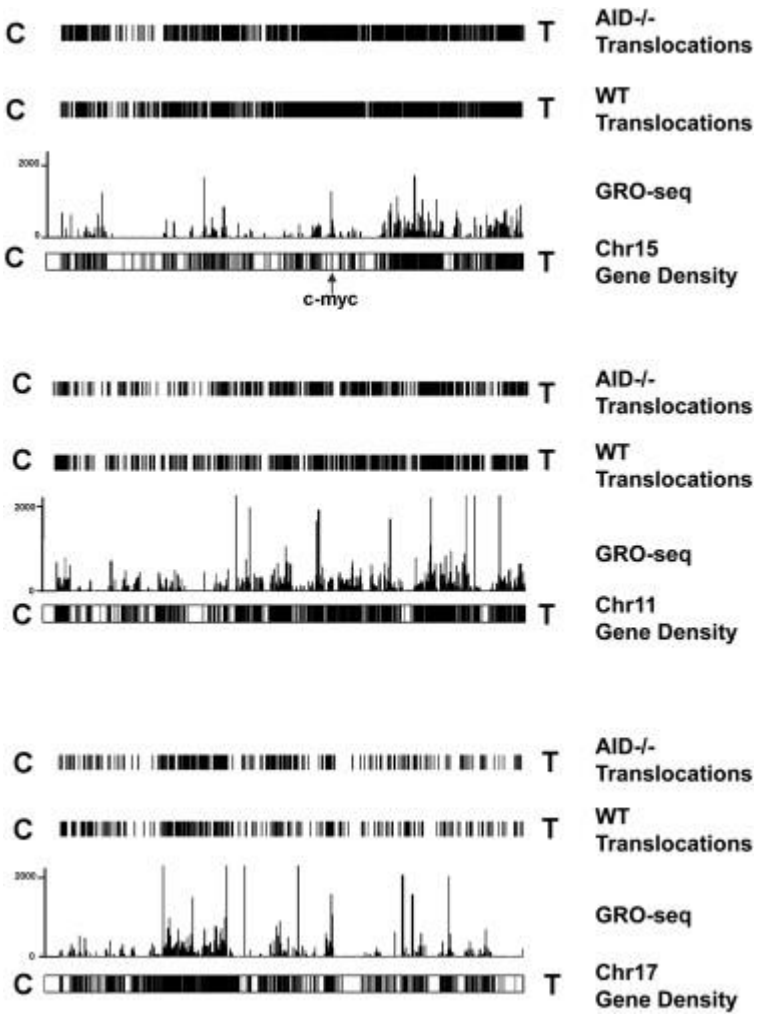

Figure 6.
Translocations Cluster to Transcribed Regions
Translocation density maps from pooled c-*myc*$^{25xI\text{-}SceI}$/WT and c-*myc*$^{25xI\text{-}SceI}$/*AID*$^{-/-}$ HTGTS libraries are aligned with combined sense and antisense nascent RNA signals for chr 15, 11, and 17 using the UCSC genome browser. Chromosome gene densities are displayed below GRO-seq traces. Chromosomal orientation from left to right is centromere (C) to telomere (T). See also Figure S6 and Figure S7.

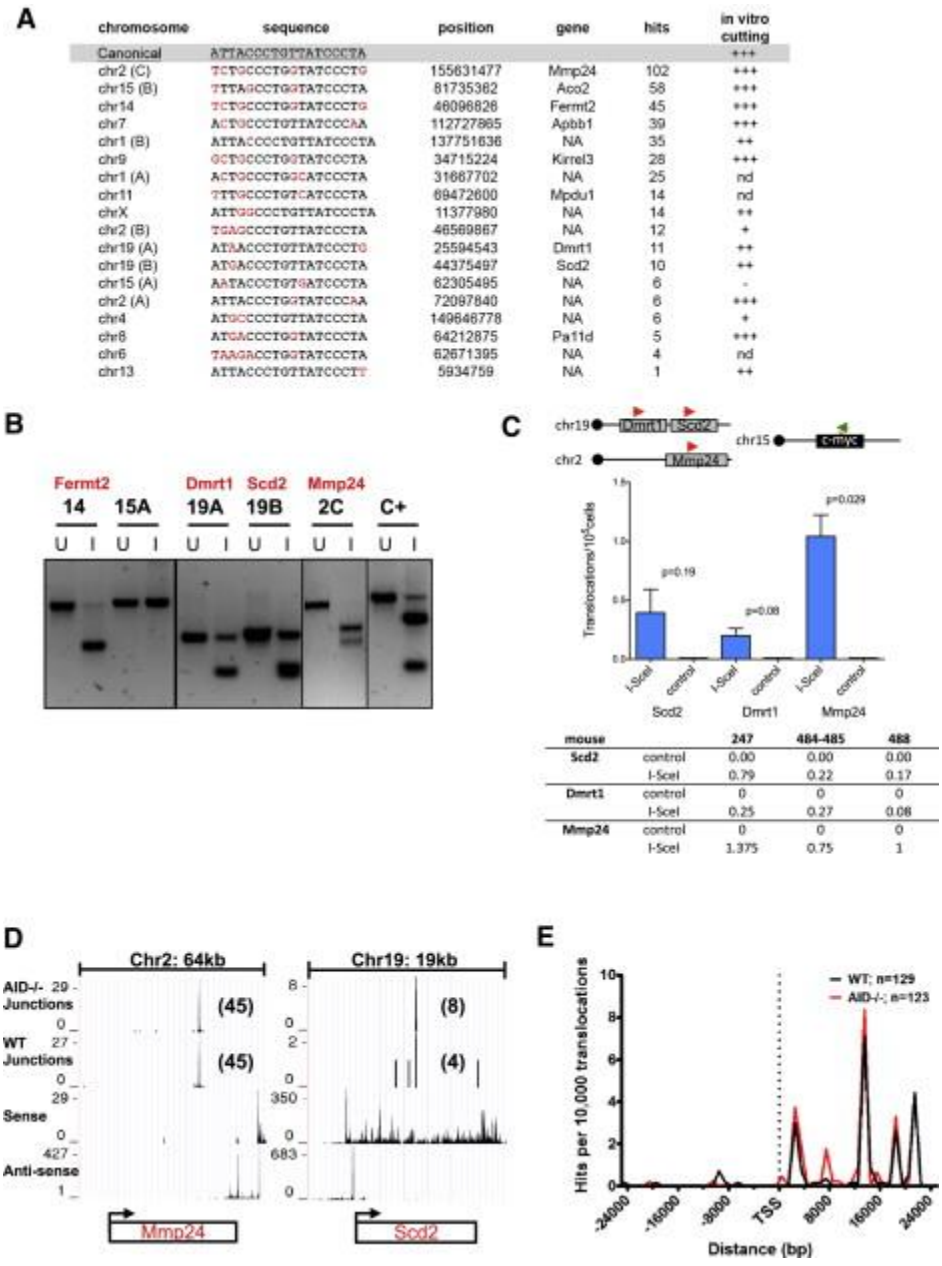

Figure 7.

Identification of Cryptic I-SceI Sites in the Mouse Genome by HTGTS

(A) Cryptic I-SceI site translocation targets. The canonical I-SceI recognition sequence is on top; nucleotides divergent from the consensus are in red. Chromosomal position and gene location of each cryptic site are indicated. “Hits” represent total number of unique junctions in a 4 kb region centered around each site in the pool of all HTGTS libraries (see also Table S6). In vitro cutting efficiency, evaluated as in Extended Experimental Procedures, is indicated. NA, intergenic or not annotated; and, not determined.

(B) In vitro cutting of PCR products encompassing indicated cryptic I-SceI sites. C+, positive control: PCR fragment containing a canonical I-SceI site. U, uncut; I, I-SceI-digested.

(C) PCR to detect translocations between c-*myc*$^{25xI\text{-}SceI}$ and cryptic I-SceI sites in *Scd2*, *Dmrt1*, and*Mmp24* genes. (Top) Position of primers used for PCR amplification. (Middle) Average frequency of translocations ± SEM (Bottom) Number of translocations/10^5 cells from three independent c-*myc*$^{25xI\text{-}SceI}$WT mice.
(D) Transcription in genes containing I-SceI sites determined by GRO-seq. Translocation junctions are in the first (*AID*$^{-/-}$) and second (WT) rows; sense and antisense nascent RNA signals are in the third and fourth rows.
(E) Distance of cryptic I-SceI hot spots from the nearest TSS in pooled HTGTS libraries from WT and *AID*$^{-/-}$ c-*myc*$^{25xI\text{-}SceI}$ B cells.

References

[1] R. Kuppers and R. Dalla-Favera, “Mechanisms of chromosomal translocations in B cell lymphomas,” *Oncogene*, vol. 20, no. 40, pp. 5580–5594, 2001.

[2] D. R. Shaffer and P. P. Pandolfi, “Breaking the rules of cancer,” *Nat. Med.*, vol. 12, no. 1, pp. 14–15, 2006.

[3] M. R. Stratton, P. J. Campbell, and P. A. Futreal, “The cancer genome,” *Nature*, vol. 458, no. 7239, pp. 719–724, 2009.

[4] Y. Zhang, M. Gostissa, D. G. Hildebrand, M. S. Becker, C. Boboila, R. Chiarle, S. Lewis, and F. W. Alt, “The Role of Mechanistic Factors in Promoting Chromosomal Translocations Found in Lymphoid and Other Cancers,” in *Advances in Immunology, Vol 106*, vol. 106, F. W. Alt, Ed. 2010, pp. 93–133.

[5] M. R. Lieber, “The Mechanism of Double-Strand DNA Break Repair by the Nonhomologous DNA End-Joining Pathway,” in *Annual Review of Biochemistry, Vol 79*, vol. 79, R. D. Kornberg, C. R. H. Raetz, J. E. Rothman, and J. W. Thorner, Eds. 2010, pp. 181–211.

[6] M. Gostissa, S. Ranganath, J. M. Bianco, and F. W. Alt, “Chromosomal location targets different MYC family gene members for oncogenic translocations,” *Proc. Natl. Acad. Sci. U. S. A.*, vol. 106, no. 7, pp. 2265–2270, 2009.

[7] J. Chaudhuri, U. Basu, A. Zarrin, C. Yan, S. Franco, T. Perlot, B. Vuong, J. Wang, R. T. Phan, A. Datta, J. Manis, and F. W. Alt, “Evolution of the immunoglobulin heavy chain class switch recombination mechanism,” *Adv. Immunol.*, vol. 94, pp. 157–214, 2007.

[8] M. Gostissa, F. W. Alt, and R. Chiarle, “Mechanisms that Promote and Suppress Chromosomal Translocations in Lymphocytes,” in *Annual Review of Immunology, Vol 29*, vol. 29, W. E. Paul, D. R. Littman, and W. M. Yokoyama, Eds. 2011, pp. 319–350.

[9] S. Franco, M. Gostissa, S. Zha, D. B. Lombard, M. M. Murphy, A. A. Zarrin, C. Yan, S. Tepsuporn, J. C. Morales, M. M. Adams, Z. K. Lou, C. H. Bassing, J. P. Manis, J. J. Chen, P. B. Carpenter, and F. W. Alt, “H2AX prevents DNA breaks from progressing to chromosome breaks and translocations,” *Mol. Cell*, vol. 21, no. 2, pp. 201–214, 2006.

[10] A. R. Ramiro, M. Jankovic, E. Callen, S. Difilippantonio, H. T. Chen, K. M. McBride, T. R. Eisenreich, J. J. Chen, R. A. Dickins, S. W. Lowe, A. Nussenzweig, and M. C. Nussenzweig, “Role of genomic instability and p53 in AID-induced c-myc-Igh translocations,” *Nature*, vol. 440, no. 7080, pp. 105–109, 2006.

[11] J. H. Wang, M. Gostissa, C. T. Yan, P. Goff, T. Hickernell, E. Hansen, S. Difilippantonio, D. R. Wesemann, A. A. Zarrin, K. Rajewsky, A. Nussenzweig, and F. W. Alt, “Mechanisms promoting translocations in editing and switching peripheral B cells,” *Nature*, vol. 460, no. 7252, pp. 231–U94, 2009.

[12] M. Liu and D. G. Schatz, “Balancing AID and DNA repair during somatic hypermutation,” *Trends Immunol.*, vol. 30, no. 4, pp. 173–181, 2009.

[13] M. Liu, J. L. Duke, D. J. Richter, C. G. Vinuesa, C. C. Goodnow, S. H. Kleinstein, and D. G. Schatz, “Two levels of protection for the B cell genome during somatic hypermutation,” *Nature*, vol. 451, no. 7180, pp. 841–U11, 2008.

[14] D. F. Robbiani, A. Bothmer, E. Callen, B. Reina-San-Martin, Y. Dorsett, S. Difilippantonio, D. J. Bolland, H. T. Chen, A. E. Corcoran, A. Nussenzweig, and M. C. Nussenzweig, “AID Is Required for the Chromosomal Breaks in c-myc that Lead to c-myc/IgH Translocations,” *Cell*, vol. 135, no. 6, pp. 1028–1038, 2008.

[15] C. Lin, L. Yang, B. Tanasa, K. Hutt, B. Ju, K. Ohgi, J. Zhang, D. W. Rose, X.-D. Fu, C. K. Glass, and M. G. Rosenfeld, “Nuclear Receptor-Induced Chromosomal Proximity and DNA Breaks Underlie Specific Translocations in Cancer,” *Cell*, vol. 139, no. 6, pp. 1069–1083, 2009.

[16] A. Nussenzweig and M. C. Nussenzweig, “Origin of Chromosomal Translocations in Lymphoid Cancer,” *Cell*, vol. 141, no. 1, pp. 27–38, 2010.

[17] A. A. Zarrin, C. Del Vecchio, E. Tseng, M. Gleason, P. Zarin, M. Tian, and F. W. Alt, “Antibody class switching mediated by yeast endonuclease-generated DNA breaks,” *Science (80-.).*, vol. 315, no. 5810, pp. 377–381, 2007.

[18] D. O. Ferguson, J. M. Sekiguchi, S. Chang, K. M. Frank, Y. J. Gao, R. A. DePinho, and F. W. Alt, “The nonhomologous end-joining pathway of DNA repair is required for genomic stability and the suppression of translocations,” *Proc. Natl. Acad. Sci. U. S. A.*, vol. 97, no. 12, pp. 6630–6633, 2000.

[19] C. T. Yan, C. Boboila, E. K. Souza, S. Franco, T. R. Hickernell, M. Murphy, S. Gumaste, M. Geyer, A. A. Zarrin, J. P. Manis, K. Rajewsky, and F. W. Alt, “IgH class switching and translocations use a robust non-classical end-joining pathway,” *Nature*, vol. 449, no. 7161, pp. 478–U9, 2007.

[20] C. M. Zhu, K. D. Mills, D. O. Ferguson, C. Lee, J. Manins, J. Fleming, Y. J. Gao, C. C. Morton, and F. W. Alt, “Unrepaired DNA breaks in p53-deficient cells lead to oncogenic gene amplification subsequent to translocations,” *Cell*, vol. 109, no. 7, pp. 811–821, 2002.

[21] D. Simsek and M. Jasin, “Alternative end-joining is suppressed by the canonical NHEJ component Xrcc4-ligase IV during chromosomal translocation formation,” *Nat. Struct. Mol. Biol.*, vol. 17, no. 4, pp. 410–U43, 2010.

[22] K. J. Meaburn, T. Misteli, and E. Soutoglou, “Spatial genome organization in the formation of chromosomal translocations,” *Semin. Cancer Biol.*, vol. 17, no. 1, pp. 80–90, 2007.

[23] M. Jasin, “Genetic manipulation of genomes with rare-cutting endonucleases,” *Trends Genet.*, vol. 12, no. 6, pp. 224–228, 1996.

[24] P. D. Siebert, A. Chenchik, D. E. Kellogg, K. A. Lukyanov, and S. A. Lukyanov, "AN IMPROVED PCR METHOD FOR WALKING IN UNCLONED GENOMIC DNA," *Nucleic Acids Res.*, vol. 23, no. 6, pp. 1087–1088, 1995.

[25] G. K. Mahowald, J. M. Baron, M. A. Mahowald, S. Kulkarni, A. L. Bredemeyer, C. H. Bassing, and B. P. Sleckman, "Aberrantly resolved RAG-mediated DNA breaks in Atm-deficient lymphocytes target chromosomal breakpoints in cis," *Proc. Natl. Acad. Sci. U. S. A.*, vol. 106, no. 43, pp. 18339–18344, 2009.

[26] S. Reynaud, L. Delpy, L. Fleury, H. L. Dougier, C. Sirac, and M. Cogne, "Interallelic class switch recombination contributes significantly to class switching in mouse B cells," *J. Immunol.*, vol. 174, no. 10, pp. 6176–6183, 2005.

[27] A. R. Quinlan, R. A. Clark, S. Sokolova, M. L. Leibowitz, Y. Zhang, M. E. Hurles, J. C. Mell, and I. M. Hall, "Genome-wide mapping and assembly of structural variant breakpoints in the mouse genome," *Genome Res.*, vol. 20, no. 5, pp. 623–635, 2010.

[28] A. Yamane, W. Resch, N. Kuo, S. Kuchen, Z. Li, H. Sun, D. F. Robbiani, K. McBride, M. C. Nussenzweig, and R. Casellas, "Deep-sequencing identification of the genomic targets of the cytidine deaminase AID and its cofactor RPA in B lymphocytes," *Nat. Immunol.*, vol. 12, no. 1, pp. 62–U85, 2011.

[29] L. J. Core, J. J. Waterfall, and J. T. Lis, "Nascent RNA Sequencing Reveals Widespread Pausing and Divergent Initiation at Human Promoters," *Science (80-.).*, vol. 322, no. 5909, pp. 1845–1848, 2008.

[30] L. Pasqualucci, P. Neumeister, T. Goossens, G. Nanjangud, R. S. K. Chaganti, R. Kuppers, and R. Dalla-Favera, "Hypermutation of multiple proto-oncogenes in B-cell diffuse large-cell lymphomas," *Nature*, vol. 412, no. 6844, pp. 341–346, 2001.

[31] B. Gomez-Gonzalez and A. Aguilera, "Activation-induced cytidine deaminase action is strongly stimulated by mutations of the THO complex," *Proc. Natl. Acad. Sci. U. S. A.*, vol. 104, no. 20, pp. 8409–8414, 2007.

[32] K. F. Yu, F. Chedin, C. L. Hsieh, T. E. Wilson, and M. R. Lieber, "R-loops at immunoglobulin class switch regions in the chromosomes of stimulated B cells," *Nat. Immunol.*, vol. 4, no. 5, pp. 442–451, 2003.

[33] R. Pavri and M. C. Nussenzweig, "AID Targeting in Antibody Diversity," in *Advances in Immunology, Vol 110*, vol. 110, F. W. Alt, K. F. Austen, T. Honjo, F. Melchers, J. W. Uhr, and E. R. Unanue, Eds. 2011, pp. 1–26.

[34] D. D. Dudley, J. P. Manis, A. A. Zarrin, L. Kaylor, M. Tian, and F. W. Alt, "Internal IgH class switch region deletions are position-independent and enhanced by AID expression," *Proc. Natl. Acad. Sci. U. S. A.*, vol. 99, no. 15, pp. 9984–9989, 2002.

[35] S. Unniraman, S. M. Zhou, and D. G. Schatz, "Identification of an AID-independent pathway for chromosomal translocations between the Igh switch region and Myc," *Nat. Immunol.*, vol. 5, no. 11, pp. 1117–1123, 2004.

[36] A. Aguilera, “The connection between transcription and genomic instability,” *Embo J.*, vol. 21, no. 3, pp. 195–201, 2002.

[37] M. C. Haffner, A. M. De Marzo, A. K. Meeker, W. G. Nelson, and S. Yegnasubramanian, “Transcription-Induced DNA Double Strand Breaks: Both Oncogenic Force and Potential Therapeutic Target?,” *Clin. Cancer Res.*, vol. 17, no. 12, pp. 3858–3864, 2011.

[38] X. Li and J. L. Manley, “Cotranscriptional processes and their influence on genome stability,” *Genes Dev.*, vol. 20, no. 14, pp. 1838–1847, 2006.

[39] E. Lieberman-Aiden, N. L. van Berkum, L. Williams, M. Imakaev, T. Ragoczy, A. Telling, I. Amit, B. R. Lajoie, P. J. Sabo, M. O. Dorschner, R. Sandstrom, B. Bernstein, M. A. Bender, M. Groudine, A. Gnirke, J. Stamatoyannopoulos, L. A. Mirny, E. S. Lander, and J. Dekker, “Comprehensive Mapping of Long-Range Interactions Reveals Folding Principles of the Human Genome,” *Science (80-.).*, vol. 326, no. 5950, pp. 289–293, 2009.

[40] N. Dimitrova, Y.-C. M. Chen, D. L. Spector, and T. de Lange, “53BP1 promotes non-homologous end joining of telomeres by increasing chromatin mobility,” *Nature*, vol. 456, no. 7221, pp. 524–U51, 2008.

[41] E.-M. Haendel and T. Cathomen, “Zinc-Finger Nuclease Based Genome Surgery: It’s All About Specificity,” *Curr. Gene Ther.*, vol. 11, no. 1, pp. 28–37, 2011.

[42] S. Arnould, C. Delenda, S. Grizot, C. Desseaux, F. Paques, G. H. Silva, and J. Smith, “The I-CreI meganuclease and its engineered derivatives: applications from cell modification to gene therapy,” *Protein Eng. Des. Sel.*, vol. 24, no. 1–2, pp. 27–31, 2011.

[43] M. Christian, T. Cermak, E. L. Doyle, C. Schmidt, F. Zhang, A. Hummel, A. J. Bogdanove, and D. F. Voytas, “Targeting DNA Double-Strand Breaks with TAL Effector Nucleases,” *Genetics*, vol. 186, no. 2, pp. 757–U476, 2010.

[44] M. Muramatsu, K. Kinoshita, S. Fagarasan, S. Yamada, Y. Shinkai, and T. Honjo, “Class switch recombination and hypermutation require activation-induced cytidine deaminase (AID), a potential RNA editing enzyme,” *Cell*, vol. 102, no. 5, pp. 553–563, 2000.

[45] C. C. Giallourakis, A. Franklin, C. Guo, H.-L. Cheng, H. S. Yoon, M. Gallagher, T. Perlot, M. Andzelm, A. J. Murphy, L. E. Macdonald, G. D. Yancopoulos, and F. W. Alt, “Elements between the IgH variable (V) and diversity (D) clusters influence antisense transcription and lineage-specific V(D)J recombination,” *Proc. Natl. Acad. Sci. U. S. A.*, vol. 107, no. 51, pp. 22207–22212, 2010.

Chapter 4 Mef2C Protects Bone Marrow B Lymphopoiesis by Enhancing DNA Repair and V(D)J Recombination

Abstract

Efficient DNA double strand break (DSB) repair is critical for bone marrow (BM) B lymphopoiesis. We found that Mef2C promotes BM B cell progenitor survival by enhancing the transcription of DNA repair factors and Rag recombinases. Mef2C ablation by Vav-Cre resulted in increased DSBs, inefficient V(D)J recombination and reduced survival of BM B cell progenitors, a phenotype resembling B lymphoid aging. Mef2C became essential for B lymphoid recovery after irradiation, with pre-B cells being the bottleneck in recovery. ChIP-sequencing analysis documented Mef2C binding at promoters and enhancers of DNA repair factors and V(D)J initiators in human B lymphoblasts. These data identify Mef2C as a B lineage specific enhancer of DNA repair machinery with a critical function during regenerative stress.

Introduction

The ability to sustain efficient bone marrow (BM) B lymphopoiesis is critical for proper immune function. B lymphoid progenitors in the BM go through a series of V(D)J recombination steps to generate diverse B cell receptors (BCRs). The success of V(D)J recombination is critical for humoral immunity as diverse BCRs are required to recognize foreign antigens and generate antibodies against them. V(D)J rearrangement is initiated by the generation of DNA double strand breaks (DSBs) by Rag recombinases at the border of two recombining immunoglobulin (Ig) gene segments, which are repaired by non-homologous end joining (NHEJ) DSB repair machinery. Defective DNA DSB repair during this process results in cell death or creates mutations or abnormal chromosome rearrangements, making BM B lymphopoiesis an inherently vulnerable process. To ensure genomic integrity, B lymphoid progenitors have adopted a tight regulation of cell survival and induce apoptosis in cells that undergo abnormal rearrangement [1]. However, during physiological aging, this homeostatic balance is altered due to reduced V(D)J rearrangement efficiency and increased B lymphoid progenitor death [2]. These defects contribute to the lymphoid/myeloid lineage skewing and impaired immune function in the aged. It is unknown, however, if B lymphoid progenitors possess cell type specific regulatory mechanisms to ensure efficient DNA repair and V(D)J recombination during homeostasis and stress.

Recent studies have identified Myocyte enhancer factor 2C (Mef2C) as a novel regulator of B lymphoid homeostasis. Mef2C is a MADS box transcription factor that was originally discovered as a regulator of cardiogenesis and myogenesis [3]. Depletion of Mef2C by B-cell

specific CD19-Cre revealed a critical requirement for Mef2C in the B lymphoid system, and showed that Mef2C regulates BCR-induced proliferation of mature B cells in the spleen [4][5][6]. In the BM, Mef2C is highly expressed in common lymphoid progenitors (CLPs) and B cell progenitors while its expression is barely detectable in T cells, granulocytes or erythrocytes [7]. Inducible deletion of Mef2C using the Mx1-Cre proposed a role for Mef2C in myeloid vs. lymphoid fate choice [7]. We uncovered a function for Mef2C within the B lymphoid cells in the bone marrow; hematopoietic specific loss of Mef2C by Vav-Cre resulted in the reduction of BM prepro-B & pre-B cells without affecting the peripheral B cells, a phenotype reminiscent of B lymphoid aging [8]. Others also showed a requirement for Mef2C in BM B lymphoid compartment by documenting that B-cell specific Mef2C deficiency, induced by the Mb-1-Cre transgene, leads to reduced B lymphoid subsets in both BM and spleen, although the defect in peripheral B cells was overcome as the mice matured [9]. Although these studies proposed an intrinsic requirement for Mef2C within BM B-lymphoid progenitor cells, the mechanism underlying the inefficient BM B lymphopoiesis in the absence of Mef2C is unknown.

Here, we report that Mef2C protects the survival of all stages of BM B lymphoid progenitors and thereby maintains efficient BM B lymphopoiesis. The requirement for Mef2C to protect B cell progenitors was greatly increased during the recovery from sub-lethal total body irradiation, with pre-B cells being the most notable bottleneck in B lymphoid recovery. Our data suggests that Mef2C sustains B lymphopoiesis by enhancing the transcription of crucial factors involved in DNA repair and recombination, which function together to ensure the fidelity of V(D)J rearrangement. Mef2C binds to genes encoding key DNA repair and V(D)J factors in human B lymphoid cells, co-localizing with epigenetic marks of active enhancers and promoters. These findings uncover a central role for Mef2C as a lineage specific enhancer of DNA repair

machinery in B cell progenitors, and provide new insights to mechanisms that may be affected during B lymphoid aging.

Results

Mef2C promotes BM B lymphoid progenitor survival to maintain the integrity of the B lymphoid compartment

To define the cellular and molecular processes that Mef2C regulates in B lymphoid system, VavCre Mef2C$^{fl/fl}$ mice were used to induce Mef2C depletion in the hematopoietic compartment, VavCre^{+} Mef2C$^{fl/+}$ or VavCre^{-} Mef2C$^{fl/fl}$ mice of same age were used as controls. We focused our study in mid-aged adult mice (7-10 month) when the B lymphoid defect associated with Mef2C deficiency is consistently observed [8]. Loss of Mef2C in hematopoietic cells resulted in a specific reduction of BM B cells, while B lymphocytes in peripheral blood and spleen were not significantly affected (Fig. 1a). To define the specific stages that Mef2C regulates during BM B lymphopoiesis, FACS analysis of CLPs and B lymphoid progenitors was performed in mid-aged VavCre Mef2C$^{fl/fl}$ mice. In contrast to previous studies with MxCre Mef2C$^{fl/fl}$ mice where a reduction of CLPs (defined as Lin^{-}AA4.1^{+}IL-7Rα^{+} or Lin^{-}IL-7R^{+}Sca1^{lo}cKit^{lo}) was reported [7], we observed no significant difference in the percentage of phenotypic CLPs, defined as Lin^{-} cKit^{lo}AA4.1^{+}IL-7Rα^{+} Flt3^{+} (Fig. 1b,c) or Lin^{-}IL-7R^{+}Sca1^{lo}cKit^{lo} (Supplementary Fig. 1), in VavCre Mef2C$^{fl/fl}$ mice. While our previous study revealed a reduction of prepro-B and pre-B cells in Mef2C deficient mice[8], further analysis of a larger cohort using Hardy fractions by

FACS suggested that all compartments of BM B lymphoid progenitors (Fr. A to E) were significantly reduced in Mef2C deficient mid-aged adults. In contrast, the mature B cells (Fr.F) that circulate through the BM were not affected (Fig. 1d,e). These data together suggested that Mef2C has a specific function within BM B lymphoid progenitor compartment to protect B lymphopoiesis.

As physiological aging significantly impairs BM B lymphopoiesis, we assessed the impact of Mef2C loss on BM B lymphopoiesis compared to control mice at different stages of post-natal life. FACS analysis of BM B lymphoid progenitors in Mef2C deficient mice at 2, 9 and 20 month of age documented that loss of Mef2C results in profound decline of BM B lymphoid progenitors already in young and mid-aged adults, whereas control mice exhibited similar phenotype only later in life (Supplementary Fig. 2). This suggests that Mef2C protects BM B cell progenitors from a defect that resembles premature B lymphoid aging.

Regulation of cell viability is a critical mechanism by which B lymphoid progenitors maintain homeostasis and exclude cells with errors in BCR rearrangement [1]. FACS analysis of Annexin V expression revealed increased cell death of B lymphoid progenitors in Mef2C deficient mice, while the sIgM+ mature B lymphocytes in BM and total BM cell viability were unaffected (Fig. 1f,g). These data suggest that Mef2C has a distinct function in ensuring the survival of BM B lymphoid progenitors.

Mef2C promotes B lymphoid recovery upon sub-lethal irradiation

Sub-lethal irradiation results in profound depletion of BM hematopoietic cells, including B lymphoid cells [10]. The recovery of B lymphoid compartment requires rapid proliferation and differentiation of BM B cell progenitors. To investigate the function of Mef2C during the recovery from irradiation induced BM ablation, 6Gy sub-lethal total body irradiation (TBI) was performed on mid-aged VavCre Mef2C$^{fl/fl}$ and control mice, and the recovery of the hematopoietic lineages was monitored at various time points post irradiation (Fig. 2a). Peripheral blood cell counts were determined by complete blood count (CBC) analysis, and the differentiation into B, T and myeloid lineages was assessed by FACS analysis. Loss of Mef2C did not affect the kinetics of red blood cell (RBC) or white blood cell (WBC) counts before or after sub-lethal irradiation, while the previously identified defect in platelets [8] was retained during the recovery from irradiation (Supplementary Fig. 3a). 2 days post irradiation, peripheral blood B, T and myeloid cells in both Mef2C deficient and control mice were significantly reduced, B cells being affected the most (Fig. 2b,c). While peripheral blood B cell counts in control mice returned to steady state levels by 6 weeks after irradiation, Mef2C deficient mice failed to recover the ablated B cell compartment (Fig. 2b,c). In contrast, the recovery of T lymphoid and myeloid lineages in Mef2C deficient mice was comparable to controls (Fig. 2c, Supplementary Fig. 3b,c). FACS analysis of B cell markers in the spleen also showed impaired B lymphoid recovery in Mef2C deficient mice, excluding possible sequestration of B lymphocytes into peripheral lymphoid organs as an underlying cause for the impaired recovery of blood B cells (Fig. 2d,e). Nevertheless, both blood and spleen B cells in irradiated Mef2C deficient mice recovered to levels comparable to un-irradiated Mef2C deficient littermates by week 16 (data not shown), implying that loss of Mef2C severely delayed rather than completely blocked the recovery of peripheral B lymphoid compartment.

To understand why peripheral B lymphoid recovery is delayed in VavCre Mef2C$^{fl/fl}$ mice post irradiation, we investigated the kinetics of recovery of BM B lymphoid progenitor subsets (Fig. 2a). Cellularity of all B lymphoid progenitors was greatly reduced in both mutant and control mice at 2 days after irradiation (Fig. 3a). Consistent with the recovery of peripheral B lymphocytes being completed at week 6 in control mice, the cellularity of BM B lymphoid progenitors in control mice also reached to level comparable to un-irradiated mice by 6 weeks post irradiation (Fig. 3a). While the loss of Mef2C significantly affected the early recovery of all B cell progenitors at week 2 (Fig. 3a,b), the recovery of prepro-B and pro-B cells in VavCre Mef2C$^{fl/fl}$ mice eventually caught up with the controls by week 6 (Fig. 3a,c). In contrast, the recovery of pre-B cells and downstream sIgM+ mature B cells in Mef2C deficient BM was severely compromised even at 6 weeks (Fig. 3a,b). These data suggested that the impaired recovery of peripheral B lymphocytes in Mef2C deficient mice results from the requirement for Mef2C to promote BM B lymphoid regeneration, and identified pre-B cell stage as a major bottleneck in B lymphoid recovery in Mef2C deficient mice.

To investigate whether the increased requirement for Mef2C upon irradiation induced stress is due a critical function in promoting B lymphoid progenitor survival, we assessed the viability of BM B progenitor subsets at week 2 post irradiation. At this stage, the recovery pre-B cells in control mice had reached to a level similar to un-irradiated mice, but the recovery of Mef2C deficient pre-B cells was lagging behind (Fig. 3a). Annexin V expression analysis showed that the increase of cell death in Mef2C deficient B lymphoid progenitors observed at steady state was further exaggerated 2 weeks post irradiation (Fig. 3d). These data documented a heightened requirement for Mef2C to protect BM B lymphopoiesis, especially at pre-B cell stage, upon increased regenerative stress during the recovery from irradiation.

Mef2C regulates DNA double strand break repair in pre-B cells to protect the B lymphoid compartment

To determine the mechanism by which Mef2C protects BM lymphopoiesis, we proceeded to identify the molecular pathways regulated by Mef2C in B lymphoid progenitors. As the requirement for Mef2C during the recovery from irradiation was most notable at pre-B cell stage, we performed Affymetrix microarray analysis of Mef2C deficient pre-B cells from mid-aged (9 mo) adults. Loss of Mef2C significantly ($|FC| \geq 2.0$ & p-value≤ 0.05) reduced the expression of 1,941 genes and significantly increased the expression of 824 genes in pre-B cells (Fig. 4a). Gene Ontology (GO) analysis of differentially expressed genes identified regulation of transcription, cell cycle and DNA repair processes among the top categories down-regulated in Mef2C deficient pre-B cells (Fig. 4b), while there were few significantly enriched GO categories among the up-regulated genes (data not shown). These data raised the hypothesis that Mef2C functions as an activator that ensures proper transcriptional control of a critical cellular process, DNA repair, in pre-B cells.

To assess the functional requirement for Mef2C in promoting DNA repair, we performed alkaline comet assay, which detects both single and double strand DNA breaks. Mef2C deficient pre-B cells harbored longer comet tails than controls (Fig. 4c), and quantitative analysis of comet tail moments confirmed significantly higher level of DNA damage in Mef2C deficient pre-B cells (Fig. 4d).

As DNA DSB repair is critical for normal lymphoid development, we examined the accumulation of DSBs in Mef2C deficient pre-B cells by immunostaining for γH2AX.

Quantification of γH2AX foci revealed that loss of Mef2C in pre-B cells results in increased DNA DSBs (Fig. 4f,g), confirming the functional requirement for Mef2C in promoting DSB repair in B lymphoid progenitors. In response to DNA DSBs, homologous recombination (HR) pathway is activated in cycling cells while non-homologous end joining (NHEJ) pathway is activated in quiescent cells. Analysis of microarray data suggested that loss of Mef2C affects both HR & NHEJ repair pathways as DSB sensor (Mre11a & Rad50) and critical effectors in both pathways (Chek1&2, Rad51 & Rad54l for HR; Xrcc4, Xrcc6 & Lig4 for NHEJ) were significantly down-regulated in Mef2C deficient pre-B cells (Fig. 4g). While pre-B cells are mostly quiescent, a significant fraction of pro-B cells are proliferating. Affymetrix microarray analysis of Mef2C deficient pro-B cells revealed that similar processes are regulated by Mef2C in both pro-B cells and pre-B cells (Supplementary Fig. 4). These data suggested that Mef2C governs both HR & NHEJ DSB repair pathways at different stages of BM B lymphopoiesis.

In summary, both gene expression and DNA repair analysis revealed a critical function for Mef2C in promoting the DNA repair machinery, specifically DSB repair, in BM B lymphoid progenitors

Mef2C regulates DNA repair and V(D)J rearrangement machinery to promote BCR rearrangement during B lymphoid development

In addition to maintaining genomic integrity, DNA repair, and specifically NHEJ DSB repair pathway, is also required for normal B lymphoid differentiation. During V(D)J rearrangement, DSBs are induced by Rag recombinases at the border of Ig segments and repaired by NHEJ machinery. Successful BCR rearrangement is critical for B cell survival, and requires that the

expression of key rearrangement factors such as Rag recombinases are precisely regulated at distinct B cell progenitor stages [11][12]. Analysis of microarray data showed up-regulation of transcription of Rag1 and 2 during pro-B to pre-B transition. This was also the case for key factors in NHEJ machinery (Xrcc4 &6 and Lig4), but not for the HR factor Rad51 (Fig. 5a), implying a stage specific regulation for NHEJ DNA repair factors during B lymphoid development. The up-regulation of NHEJ machinery during pro-B to pre-B transition was also confirmed by analysis of published gene expression studies (The Immunological Genome Project [13] and GEO data base Series GSE39554) (data not shown). Analysis of Mef2C deficient BM pro-B and pre-B cells showed that loss of Mef2C impaired the induction of all these critical factors in pre-B cells (Fig. 5a), indicating a role for Mef2C in promoting V(D)J rearrangement through transcriptional enhancement of key effectors.

To investigate functional consequences of the compromised DNA repair and V(D)J rearrangement machinery, we isolated Mef2C deficient BM sIgM+ B cells and performed quantitative PCR analysis of IgL rearrangement. Loss of Mef2C significantly reduced the rearrangement efficiency of both κ and λ (λ1-3) light chains (Fig. 5b). Since loss of Mef2C resulted in the reduction of all BM B lymphoid progenitors, and similar biological processes were identified to be down-regulated in both Mef2C deficient pro-B and pre-B cells, we sought to define if Mef2C also promotes IgH rearrangement. Quantitative PCR analysis in Mef2C deficient pro-B cells revealed a significant reduction in rearrangement frequency of J558 family, the IgH family, which represents 62.5% [14] of B cells in adult mice, while no difference was noted in the fetal dominating 7183 IgH family [15], which only represents 7% [14] of adult B cells (Fig. 5c). These data together suggest that Mef2C is required for proper heavy and light chain V(D)J rearrangement in BM B lymphoid progenitors.

The ability to successfully execute V(D)J rearrangement is also a requirement for the rapid regeneration of B lymphoid progenitors during the recovery from BM ablation. To quantify the rearranged IgH & IgL chains at protein level, we performed intracellular FACS of IgM in pro-B cells and Igκ in BM pre-B B cells from Mef2C deficient mice both before and 2 weeks after sub-lethal irradiation. At steady state, the protein level of both IgM / Igκ in Mef2C deficient pro-B and pre-B cells were slightly reduced compared to controls, whereas at week 2 post irradiation, the reduction in IgM and Igκ protein expression in Mef2C deficient pro-B and pre-B cells was greatly exaggerated (Fig. 5d,e). These data showed a heightened requirement for Mef2C in promoting V(D)J recombination upon regenerative stress.

MEF2C binds to the enhancers and promoters of genes encoding critical DNA repair and V(D)J factors

We next sought to identify candidate direct target genes that MEF2C binds to in B lymphoid cells by analyzing the ChIP-seq data for MEF2C in human B lymphoblast cells (available via Encode project [16]). GO analysis of MEF2C bound genes in human B lymphoblast cells revealed significant enrichment of transcription regulation, cell cycle regulation and B cell differentiation categories (Fig. 6a). Intersection of the human ChIP-seq data with the mouse microarray data revealed that a considerable fraction of genes down-regulated in Mef2C deficient pre-B cells are associated with MEF2C peaks, and that they are enriched in genes that function in transcription regulation and DNA repair (Fig. 6a).

Majority of MEF2C binding sites localized at 5kb to 500kb away from transcription start site (TSS) while 8% of Mef2C binding sites localized within 5kb from TSS (Fig. 6b), suggesting that MEF2C functions at both promoters and enhancers. Analysis of active and repressive histone marks and co-factors around MEF2C binding sites in human B lymphoblasts showed that MEF2C binding is strongly correlated with co-activator p300 binding and active histone marks, including H3K4Me1 (enhancers), H3K4Me3 (promoters), H3K27Ac (active enhancers and promoters), while no enrichment of repressive histone marks H3K9Me3 or H3K27Me3 was observed around MEF2C binding sites (Fig. 6c). These data supported the notion that Mef2C primarily acts as an activator in B lymphoid cells.

Analysis of MEF2C ChIP-seq data at individual Mef2C candidate target genes revealed that MEF2C directly binds to genes encoding Rag recombinases, DSB sensor components (Mre11a & Rad50) and key NHEJ effectors (Xrcc4 & Lig4) (Fig. 6d), suggesting that Mef2C may directly regulate their expression. MEF2C peaks were also identified at genes encoding master B lymphoid transcription regulators (E2a & EBF1) (Fig. 6d), raising the questions whether MEF2C could also regulate V(D)J effectors indirectly through E2a and/or EBF1, or in co-operation with these B-cell factors. Indeed, intersection of MEF2C, E2a and EBF1 binding sites in human B lymphoblasts revealed significant co-localization in genes enriched for functions in transcription, cell survival, immune response and cell cycle regulation (Supplementary Fig. 5a). Furthermore, co-localization of MEF2C binding with EBF1 and/or E2a binding was identified at key MEF2C candidate targets (B cell factors: E2a, EBF1 & RAG1; DSB repair factors: RAD50, LIG4 & XRCC4) (Supplementary Fig. 5b). Together, these data propose that MEF2C may assist E2a and EBF1 in regulating the transcription of critical V(D)J and DNA repair factors. Moreover, MEF2C binding in all key candidate target genes was associated with co-factor p300 binding and

active histone marks (H3K27Ac, H3K4Me1 & H3K4Me3) (Fig. 6d), indicating that MEF2C binds to active regulatory regions of target genes to enhance their transcription.

Discussion

The ability of a stem or progenitor cell to repair DNA damage is vital to the integrity of its genome and thus the normal function of the tissue/organism. In addition to serving fundamental housekeeping functions in all cell types, efficient DNA repair, and DSB repair specifically, is critical for normal lymphoid development due to its necessity in V(D)J recombination. However, it is unknown if B lymphoid cells possess lineage specific regulatory mechanisms that connect the general DNA repair machinery with B cell specific functions. Our study identified for the first time the existence of a B cell specific transcriptional regulator of DNA repair machinery, Mef2C.

We discovered that Mef2C enhances the expression of essential components of DSB repair machinery as well as lymphoid specific Rag recombinases in BM B cell progenitors, thereby enabling efficient V(D)J recombination and protecting the survival of BM B lymphoid progenitors. Analysis of V(D)J rearrangement in BM B cell progenitors revealed that loss of Mef2C reduces the efficiency of both heavy and light chain rearrangement, thus compromising

BM B lymphopoiesis at multiple stages downstream of the CLP. Future studies will be required to assess if the BCR repertoire of peripheral B compartment is compromised as a result of the reduced V(D)J rearrangement efficiency in Mef2C deficient BM, and whether such defect compromises B cell mediated immune response upon exposure to foreign antigens.

Due to the similarity in the developmental processes of B and T lymphoid cells, our data prompts the question whether T cell progenitors also possess lineage specific regulators that enhance DNA repair machinery and V(D)J recombination. Mef2C itself is not robustly expressed in the T cell lineage [7][17], and loss of Mef2C did not affect T lymphopoiesis during steady state or even during the recovery from irradiation. However, as previous studies suggested that primary T lymphocytes express Mef2D [17], it will be important to address if Mef2D or other broadly expressed MEF2 family members function in T lineage to regulate DNA repair machinery and V(D)J recombination.

Analysis of B cell progenitors upon hematopoietic deletion of Mef2C revealed a phenotype that was highly reminiscent of B cell aging, but occurred already in young/mid-aged adults. These included a profound loss of BM pre-B cells without immediate effects on peripheral (blood and spleen) B cell compartment. Mef2C deficiency resembled B lymphoid aging at multiple cellular and molecular processes, as aging of B lymphoid compartment is also associated with increased apoptosis of B cell progenitors [2] and defective BCR rearrangement. Such defects have been linked to reduced E2a & Rag expression and defective DNA repair in the elderly [18][19]. It is therefore intriguing to propose that Mef2C protects BM B progenitors from

premature aging. Future studies will be needed to determine at molecular and cellular level the degree to which Mef2C deficiency models physiological B lymphoid aging, and to define if a failure to respond to Mef2C or its downstream effectors underlies B lymphoid aging.

Analysis of Mef2C ChIP-sequencing data in human B lymphoblasts identified Mef2C binding at enhancers and/or promoters of critical B cell transcription factors as well as V(D)J initiator and DNA repair effectors. These data suggested two possible mechanisms of how Mef2C regulates V(D)J recombination and DNA repair in B lymphoid progenitors: (1) Mef2C may directly enhance the transcription of genes encoding Rag proteins and DNA repair machinery, and/or (2) Mef2C may regulate these factors indirectly by, or in co-operation with, intermediate transcription factors such as E2a and Ebf1. Analysis of the shared binding sites for these factors in human lymphoblasts suggest that both models may be true. As the MADS box of Mef2C is able to bind and recruit p300 directly to enhance transcription [20][21], one possible mechanism is that Mef2C recruits p300 to key target genes, which then establishes H3K27Ac and enhances gene transcription.

In addition to emerging as a key regulator of normal immune cell development, Mef2C is also known as a co-operating oncogene in multiple types of leukemia [21]. Mef2C became abnormally expressed in leukemic GMPs in MLL-AF9 driven leukemias and knockdown of Mef2C attenuated the proliferative potential of these cells [22], while loss of Mef2C in MLL-ENL driven leukemias reduced the homing and invasiveness of leukemia cells [23]. It is still unclear how ectopic activation of Mef2C expression promotes leukemia progression. Although

defective DNA repair is a common cause for tumorigenesis, in established tumor cells, DNA repair pathways can enable tumor cell to survive DNA damage that is associated with high proliferation rate or induced by chemotherapeutic treatments [24]. Future studies will be required to test the hypothesis that Mef2C may protect leukemic cells from DNA damage by enhancing DNA repair machinery. Moreover, it will be important to define whether the ability of Mef2C to enhance DNA repair is restricted to the hemato-lymphoid system, or is also utilized during the development of other tissues, such as muscle, heart and vasculature. Identification of Mef2C as a unique lineage specific co-ordinator of DNA repair provides a new model how this critical cellular process is efficiently integrated to bone marrow B lymphopoiesis to ensure proper development and maintenance of the immune system.

Methods

Mice: VavCre mice were bred with $Mef2C^{fl/fl}$ mice to generate $VavCre^{+}$ $Mef2C^{fl/fl}$ mice. $VavCre^{+}$ $Mef2C^{fl/+}$ or $VavCre^{-}$ $Mef2C^{fl/fl}$ mice of same age were used as controls. Genotyping analysis was done as previously described [8]. All mice were maintained according to the guidelines of the University of California Los Angeles Animal Research Committee.

Analysis of Peripheral Blood Counts: Peripheral blood was harvested from the retro-orbital sinus into Vacutainer tubes (BD Biosciences) and sent to the University of California Los Angeles Division of Laboratory Animal Medicine laboratory for complete blood cytometry (CBC) analysis.

FACS Analysis and Isolation of B Lymphoid Progenitors: Hematopoietic cells were analyzed using antibodies listed. Dead cells were excluded with 7-amino-actinomycin D and cell populations were analyzed using an LSR II or Fortessa flow cytometer or sorted using a FACS Aria & Aria-H cell sorter. Data were analyzed with FlowJo software version 9.2.

RNA Purification: Total RNA was isolated from sorted cells using QIAshredder and RNEasy Micro & Mini Kit (QIAGEN). cDNAs were prepared by the Quantitect reverse transcription kit (QIAGEN), and qPCR was performed with LightCycler 480 SYBR Green I Master (Roche) using LightCycler 480 real-time PCR system (Roche). Samples were normalized to βActin. All primer sequences are available upon request.

Gene Expression Profiling: Affymetrix microarray analysis was performed on three independent control and three independent Mef2C deficient sorted pro-B & pre-B cells. The R package Limma provided through the open source project Bioconductor was used for assessing differential expression. To calculate absolute mRNA expression levels, the RMA (Robust Multiarray Averaging) method was used to obtain background adjusted, quantile normalized and

probe level data summarized values for all probe sets. The Affymetrix Mouse Genome 430 2.0 Array GeneChip platform was used for the analysis. Official gene symbols for probe sets were obtained using the Bioconductor annotation database mouse4302.db. The mas5calls algorithm through the R package of affy was used for calculating PMA detection calls for each array sample. Differentially expressed genes were uploaded into the DAVID interface to identify significantly over-represented functional GO biological process categories.

Quantitative Analysis of Ig Gene Rearrangements: cDNA were generated from sorted B cell populations as described above. Quantitative analysis of 7183 & J558 heavy chain as well as κ, λ1, λ2, and λ3 light chain rearrangements were performed by qPCR using published primer (light chain primers [25] and heavy chain primers [26]). Rearrangement frequencies were calculated as $2^{\Delta Ct}$ with $\Delta Ct = Ct_{\text{Actin}} - Ct_{\text{Ig}}$.

Statistical analysis: Student's unpaired two-tailed t-test was used for statistical analysis and differences with P values of 0.05 or less were considered significant.

Irradiation: Sub-lethal (6Gy) total body irradiation was performed with Co-60 pool irradiator.

Immunofluorescence microscopy (γH2AX): IF microscopy of γH2AX was performed as described [27]. In brief, FACS purified cells were pipetted onto poly-lysine coated slides, fixed

with 4% PFA for 10 min at room temperature, permeabilized in 0.15% Triton X-100 for 2 min at room temperature and blocked in 10% donkey serum / PBS overnight at 4°C. Slides were then incubated for 1-2 hr at room temperature with anti-phospho-H2AX (Ser 139) (Millipore, 05-636). Slides were washed three times in PBS and incubated for 1 hr at room temperature with A488-conjugated goat anti-mouse (Life Technologies, A11029) antibody. Slides were then washed three times in PBS and mounted using ProLong® Gold Antifade Reagent with DAPI (Life Technologies, P36935). Microscopy imaging was performed using Zeiss LSM 700 confocal microscope (100x objective) and Nikon ECLIPSE E600 microscope (100x objective). Cells were scored as positive (≥4 foci) or negative (0-3 foci) based on the number of foci observed by eye. All scoring was done blind and more than 50 cells were counted per sample.

Alkaline Comet assay: Alkaline comet assay was performed with Enzo comet SCGE assay kits according to the manufacturer's protocols. In brief, FACS purified cells were embedded in low melting point agarose and transferred onto comet slides. Cells were then lysed and treated with freshly made alkaline solution followed by electrophoresis in alkaline electrophoresis solution. Slides were dried for at least 2 days before imaging. Nuclei were stained with Sybr Green for 20 min. Pictures of individual cells were taken with microscope (×40 objective) and analyzed using the CASP software (http://casplab.com/). The tail moment of all comets analyzed was used to define outliers and non-outliers based on calculated absolute deviation. Cells were defined as outliers when their tail moment absolute deviation was ≥3 median absolute deviation (MAD). Statistical significance was calculated in Prism (GraphPad) utilizing the Mann-Whitney test.

ChIP-sequencing analysis: ChIP-sequencing data from ENCODE project [28] were used for analysis. Alignment images were generated with the UCSC Genome Browser [29] and peaks identification was based on the peak calling process of ENCODE project. Peak intersection was done with Galaxy [30] and peaks were mapped to nearby genes within 200kb range from TSS using Genomic Regions Enrichment of Annotations Tool (Great) [31]. The following publically available ChIP-seq datasets in GM12878 cells from ENCODE projects were used for analysis: MEF2C GSM803420, p300 GSM935562, H3K4Me1 GSM733772, H3K4Me3 GSM733708, H3K27Ac GSM733771, H3K9Me3 GSM733664, H3K27Me3 GSE50893, E2A GSM1010745, EBF1 GSM803386.

Acknowledgements

We thank E. Passegué and J. Flach (UCSF) for discussions and immunofluorescence microscopy protocol; E. Montecino-Rodriguez, K. Dorshkind and S. Smale (UCLA) for critical discussions of the data; UCLA BSCRC Flow Cytometry Core for help with FACS; UCLA Clinical Microarray Core for performing the microarrays. This work was funded by the Leukemia & Lymphoma Society Scholar Award for HKAM and The Jonsson Cancer Center Fund at UCLA. W.W received fellowship from the Whitcome Foundation and the California Institute for Regenerative Medicine Pre-doctoral Training Grant. A.M-H was funded by the Human Frontiers Science Program. TO was supported by the Leukemia & Lymphoma Society postdoctoral fellowship (57537-13) and by the European Union through the European Social Fund (Mobilitas Grant No. MJD284).

Antibody	Flour	Clone	Company
B220	APC	RA3-6B2	BD Bioscience
B220	APC Cy7	RA3-6B2	BD Bioscience
B220	PerCP Cy5.5	RA3-6B2	eBioscience
B220	PE	RA3-6B2	BD Bioscience
CD19	PE	1D3	BD Bioscience
CD127 (Il7rα)	PECy7	A7R34	eBioscience
cKit	APC	2B8	eBioscience
Sca1	PECy7	D7	eBioscience
AA4.1	PE	AA4.1	BD Bioscience
CD135 (Flt3)	Biotin	A2F10	eBioscience
Gr1	APC	RB6-8C5	BD Bioscience
Mac1	PE	M1/70	BD Bioscience
CD4	APC	RM4-5	BD

			Bioscience
CD8a	PE	53-6.7	BD Bioscience
IgD	FITC	11-26C.2A	BD Bioscience
IgM	PE	R6-60.2	BD Bioscience
IgM	FITC	II/41	BD Bioscience
CD43	FITC	S7	BD Bioscience
CD43	Biotin	S7	BD Bioscience
Stv	APC	--	Invitrogen
CD24	PE Cy7	M1/69	BD Bioscience
BP-1	Biotin	6C3	eBioscience
AnnexinV	Alexa 647	--	BD Bioscience
Ig-kappa	FITC	187.1	BD Bioscience
DAPI	--	--	AnaSpec

7AAD	--	--	BD Bioscience
Lineage	PECy5		
B220		RA3-6B2	BD Bioscience
Mac1		M1/70	eBioscience
Gr1		RB6-8C5	eBioscience
CD3		145-2C11	eBioscience
Ter119		TER-119	eBioscience

Figure Legend

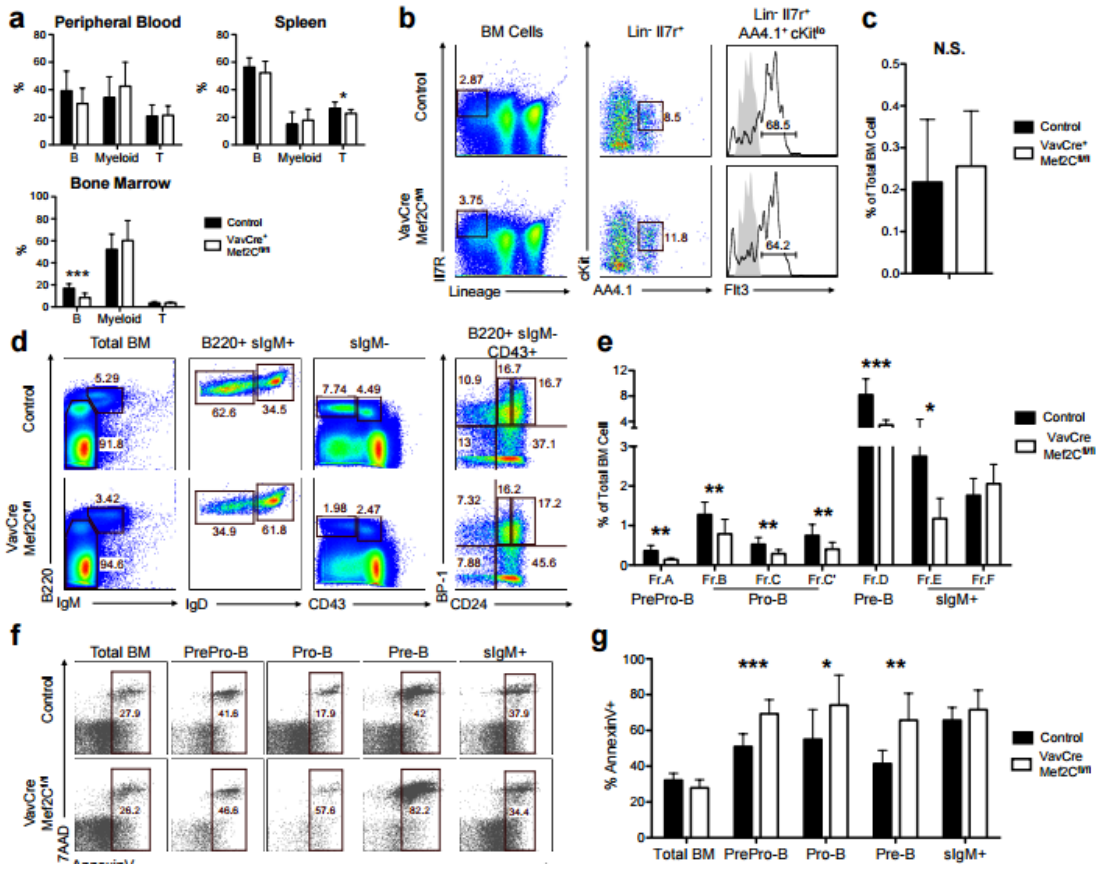

Figure 1. Mef2C maintains the integrity of B lymphoid compartment by promoting bone marrow B cell progenitor survival

(a) Deletion of Mef2C in hematopoietic cells in VavCre Mef2C$^{fl/fl}$ mice resulted in specific reduction of BM B cells (b,c) FACS analysis of BM suggested that loss of Mef2C does not affect the frequency of common lymphoid progenitors in the BM (n≥7). (d,e) FACS analysis of Hardy B lymphoid progenitor fractions in the BM revealed reduction of all B lymphoid progenitors in Mef2C deficient mice while the mature B cells in the BM (Fr.F) were not affected (n≥8). (f,g) FACS analysis of annexin V expression in B lymphoid progenitors documented increased cell death in Mef2C deficient B lymphoid progenitors while total BM was not affected (n≥7). All mice were analysed at 7-10 months of age. Data shown are the mean ± SD of three or more independent experiments. N.S. not significant, * P<0.05, ** P<0.01 and *** P<0.001.

progenitors without a major effect on sIgM+ B cells (n≥3). Data shown are the mean ± SD of two or more independent experiments. * P<0.05, ** P<0.01 and *** P<0.001.

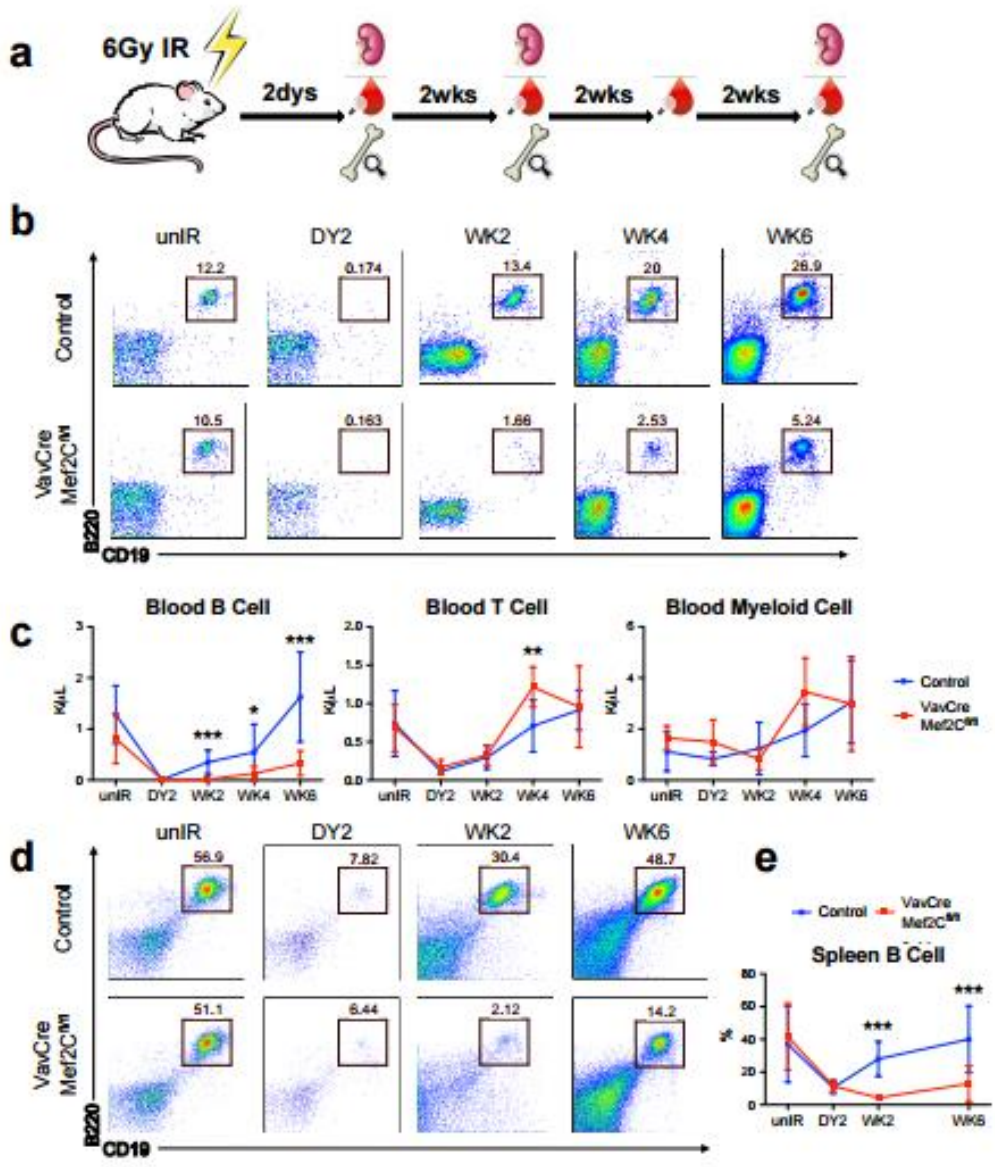

Figure 2. Mef2C is required for efficient peripheral B lymphoid recovery upon sub-lethal irradiation

(a) Experimental design of hematopoietic ablation by sub-lethal irradiation: mid-aged VavCre Mef2C$^{fl/fl}$ and control mice received 6Gy of total body irradiation. At day 2, week 2, 4 and 6, peripheral blood was collected for CBC and FACS analysis. At day 2, and week 2 and 6, spleen and bone marrow were analyzed by FACS. (b) Representative FACS analysis of peripheral blood B cells revealed defective B cell recovery in Mef2C deficient mice. (c) Quantification of peripheral blood lineage cell count (WBC count from CBC multiplied with lineage percentage from FACS) documents that loss of Mef2C compromised the recovery of B cells while T and myeloid cells were not affected. (d,e) FACS analysis of spleen B cells in both VavCre Mef2C$^{fl/fl}$

and control mice after irradiation revealed defective B cell recovery in Mef2C deficient mice. All mice were analysed at 9-11 months of age. Day 2: n=4, data shown are the mean ± SD of two independent experiments. Other time points: n≥5, data shown are the mean ± SD of three or more independent experiments. * P<0.05, ** P<0.01 and *** P<0.001.

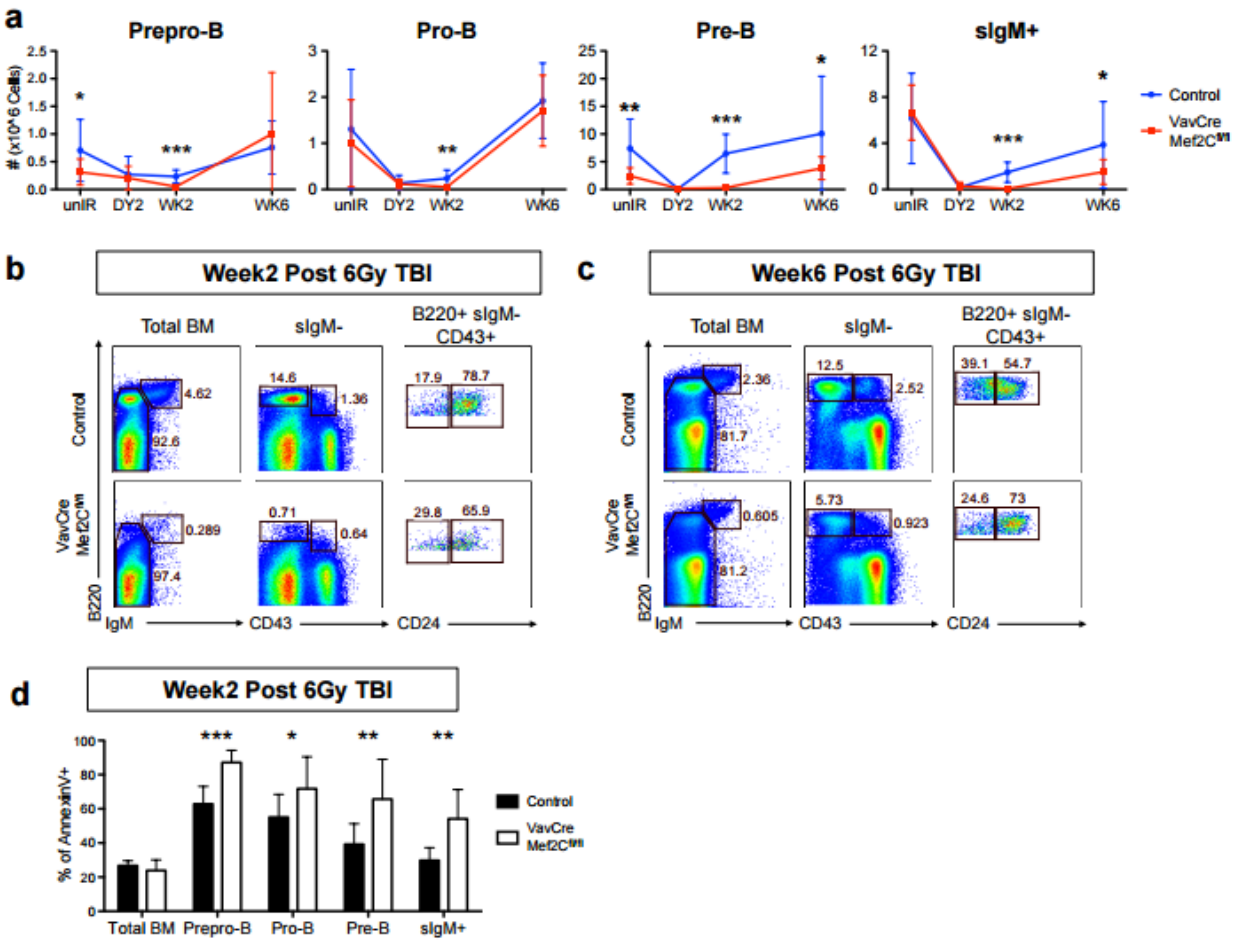

Figure 3. Pre-B cell stage becomes a major bottleneck for B lymphoid recovery in the absence of Mef2C

(a) Quantification of BM B lineage cell count (total BM cellularity multiplied with lineage percentage from FACS) shows that loss of Mef2C does not severely affect the recovery of early B lymphoid progenitors (prepro- & pro- B) while it compromises the recovery of pre-B cells and downstream sIgM+ BM B cells (Day2: n=4, other time points: n≥5). (b,c) Representative FACS analysis of BM B lymphoid progenitors at 2 and 6 weeks post 6Gy irradiation. (d) Quantification of annexin V expression revealed an exaggerated cell death in VavCre Mef2C$^{fl/fl}$ mice at 2 weeks post 6Gy TBI compared to un-irradiated ones (n≥9). All mice were analysed at 9-10 months of age. Day 2: data shown are the mean ± SD of two independent experiments. Other time points: data shown are the mean ± SD of three or more independent experiments. * P<0.05, ** P<0.01 and *** P<0.001.

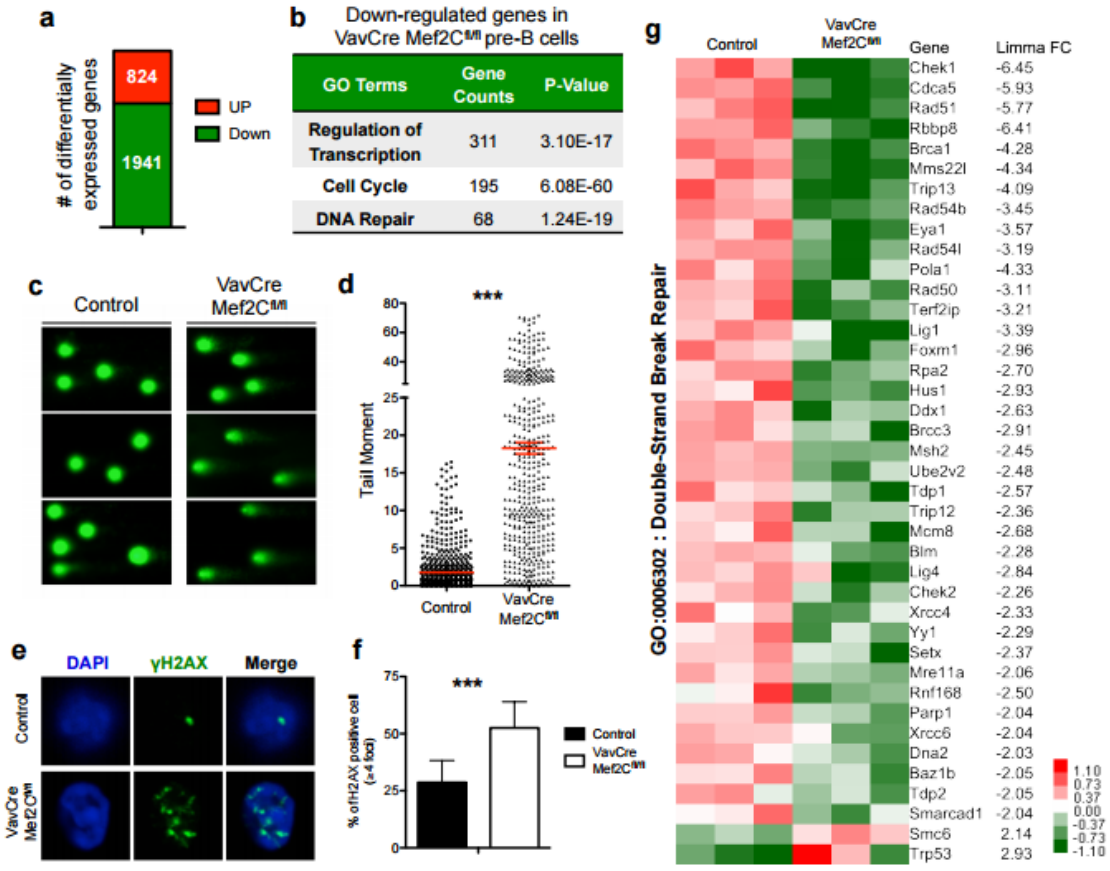

Figure 4. Mef2C regulates DNA double strand break (DSB) repair in pre-B cells

(a) Microarray analysis of pre-B cells from control & VavCre Mef2C$^{fl/fl}$ mice (9 mo) revealed 1941 significantly (|FC|≥2 and p≤0.05) down-regulated and 824 up-regulated genes in absence of Mef2C (n=3). (b) Regulation of transcription, cell cycle and DNA repair were among the top GO categories down-regulated in Mef2C deficient pre-B cells. (c,d) Representative figure and quantification of alkaline comets revealed increased DNA damage in Mef2C deficient pre-B cells (9-11 mo). Data shown are the mean ± SEM of three independent experiments, n≥6. 728 control pre-B cells and 450 Mef2C deficient pre-B cells.) (e,f) Representative IF analysis of γH2AX in pre-B cells (9-10 mo) revealed that Mef2C is required to promote proper DSB repair in pre-B cells. (n≥6, data shown are the mean ± SD of three independent experiments.). (g) DNA double-strand break repair genes that are significantly changed in Mef2C deficient pre-B cells are shown.

(*** P<0.001)

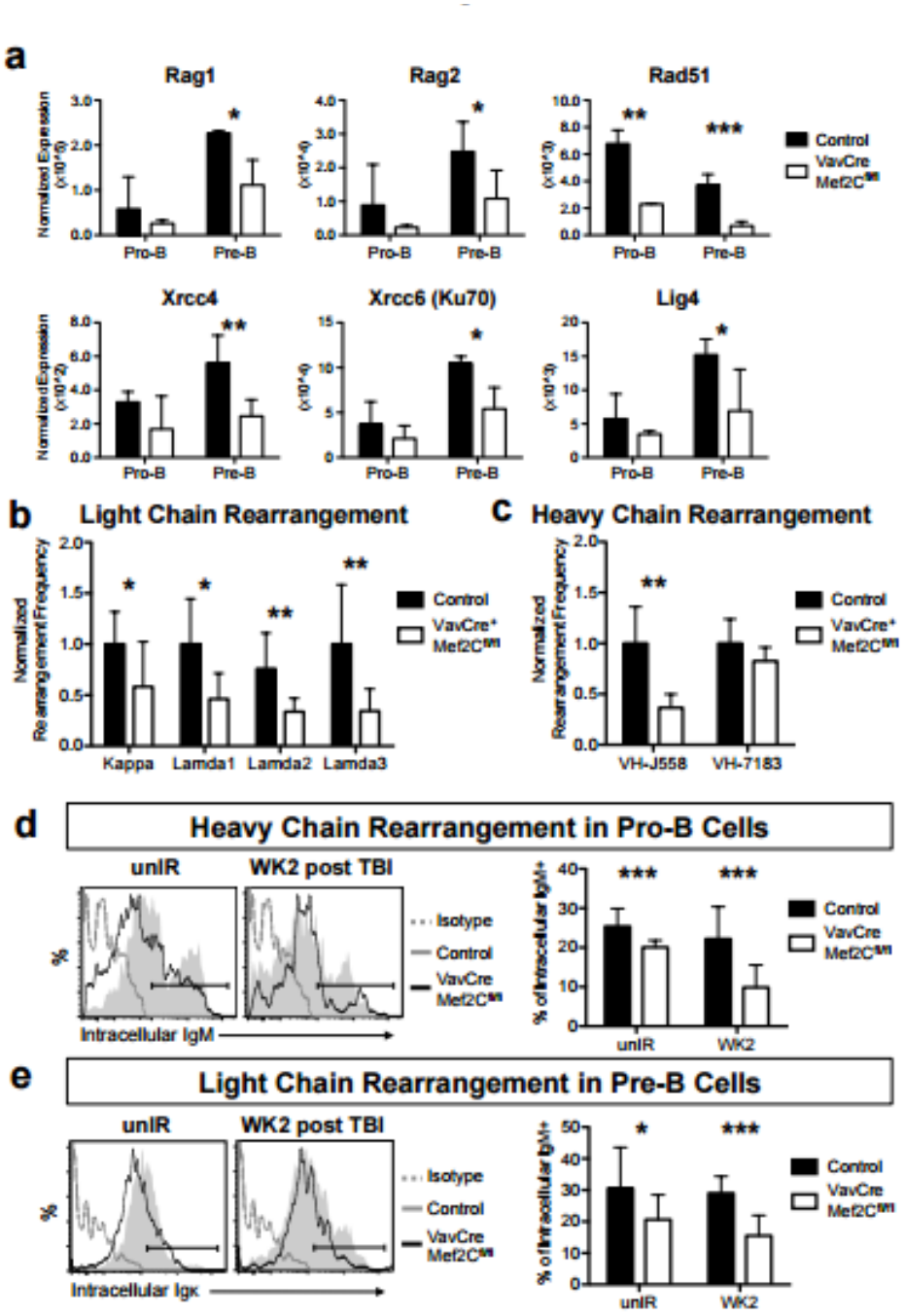

Figure 5. Mef2C regulates NHEJ repair and V(D)J rearrangement machinery to promote BCR rearrangement during B lymphoid development

(a) Expression of Rag 1&2, Xrcc 4&6 and Lig4 during pro-B to pre-B transition in both control & VavCre Mef2C$^{fl/fl}$ mice (9mo). Loss of Mef2C compromised the induction of all these factors

(n≥2). (b,c) Quantitative PCR analysis of κ, λ light chain rearrangement (n≥7) in BM sIgM+ cells and J558, 7183 heavy chain (n≥5) in pro-B cells (7-9 mo) revealed significantly reduced frequency of all light chain families and J558 heavy chain in absence of Mef2C. (d,e) Representative FACS plots and quantification of intracellular FACS analysis of μ heavy and κ light chain expression in BM pro-B and pre-B cells from mice without irradiation and 2 weeks post 6Gy total body irradiation (7-11mo, n≥10). Data shown are the mean ± SD of three or more independent experiments. * $P<0.05$, ** $P<0.01$ and *** $P<0.001$.

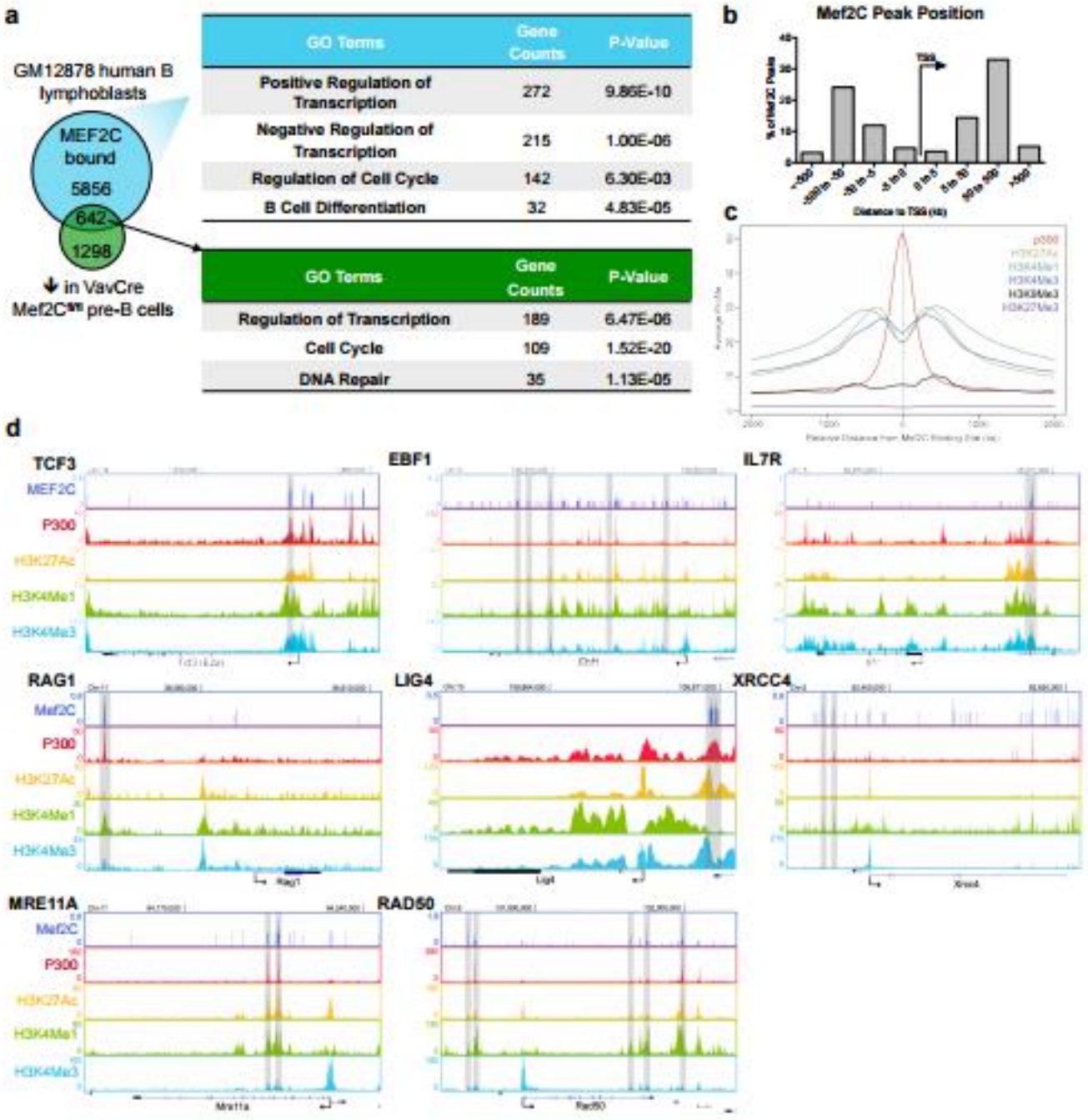

Figure 6. Mef2C regulates the expression of critical DNA repair and V(D)J genes through direct binding at promoters and enhancers

(a) Intersection of MEF2C bound genes in human B lymphoblasts and down-regulated genes in Mef2C deficient mouse pre-B cells identified DNA repair regulators as candidate direct target of Mef2C in pre-B cells. (b) GREAT analysis showed that MEF2C binding sites are located both around TSS and at distant regulatory elements. (c) Distribution of epigenetic marks around MEF2C binding sites shows correlation of Mef2C peaks with both enhancer and promoter marks. (d) MEF2C binding and epigenetic marking at genes encoding for key B cell regulator, DNA repair and V(D)J factors. MEF2C peaks defined by the ENCODE dataset are highlighted in grey.

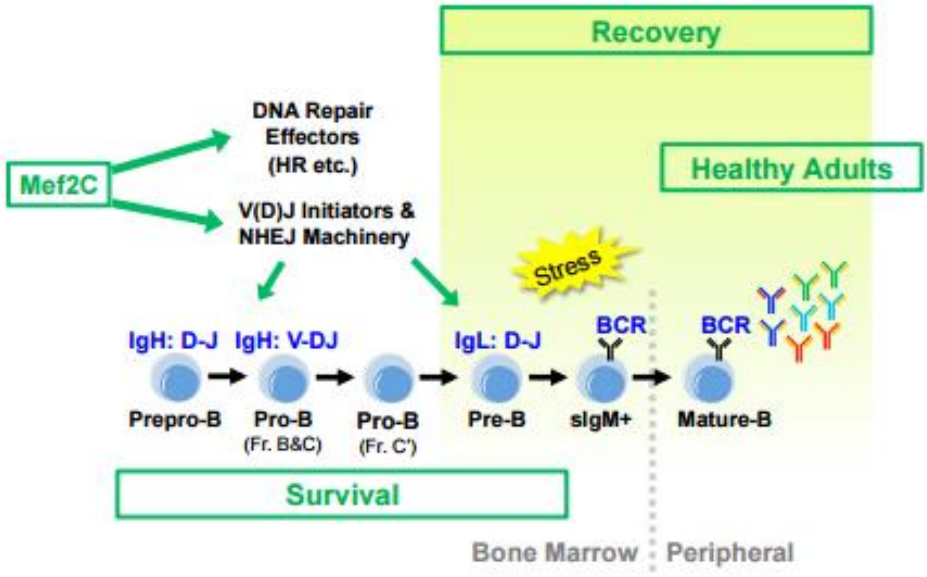

Figure 7. Mef2C protects BM B lymphopoiesis through the regulation of DNA repair machinery

Mef2C has a critical function in ensuring efficient BM lymphopoiesis during steady state and stress. At steady state, Mef2C enhances the expression of critical V(D)J initiators and DSB repair machinery to promote the rearrangement of both heavy and light chains, the success of which ensures the expression of wide spectrum of B cell receptor and survival of BM B cell progenitors. The requirement for Mef2C to promote V(D)J rearrangement is heightened after irradiation induced ablation when rapid production of B lymphoid cells is required to replenish the B lymphoid compartment. During recovery from irradiation, loss of Mef2C resulted in a temporal bottleneck in B lymphoid recovery at pre-B cell stage, which also led to a compromised recovery of downstream peripheral B lymphocytes.

References

[1] L. Lu and D. G. Osmond, "Apoptosis and its modulation during B lymphopoiesis in mouse bone marrow," *Immunol Rev*, vol. 175, pp. 158–174, 2000.

[2] I. Kirman, K. Zhao, Y. Wang, P. Szabo, W. Telford, and M. E. Weksler, "Increased apoptosis of bone marrow pre-B cells in old mice associated with their low number," *Int Immunol*, vol. 10, no. 9, pp. 1385–1392, 1998.

[3] Q. Lin, J. Schwarz, C. Bucana, and E. N. Olson, "Control of mouse cardiac morphogenesis and myogenesis by transcription factor MEF2C," *Science (80-.).*, vol. 276, no. 5317, pp. 1404–1407, 1997.

[4] D. Khiem, J. G. Cyster, J. J. Schwarz, and B. L. Black, "A p38 MAPK-MEF2C pathway regulates B-cell proliferation," *Proc Natl Acad Sci U S A*, vol. 105, no. 44, pp. 17067–17072, 2008.

[5] P. R. Wilker, M. Kohyama, M. M. Sandau, J. C. Albring, O. Nakagawa, J. J. Schwarz, and K. M. Murphy, "Transcription factor Mef2c is required for B cell proliferation and survival after antigen receptor stimulation," *Nat Immunol*, vol. 9, no. 6, pp. 603–612, 2008.

[6] S. F. Andrews, X. Dai, B. Y. Ryu, T. Gulick, B. Ramachandran, and D. J. Rawlings, "Developmentally regulated expression of MEF2C limits the response to BCR engagement in transitional B cells," *Eur J Immunol*, vol. 42, no. 5, pp. 1327–1336, 2012.

[7] S. Stehling-Sun, J. Dade, S. L. Nutt, R. P. DeKoter, and F. D. Camargo, "Regulation of lymphoid versus myeloid fate 'choice' by the transcription factor Mef2c," *Nat Immunol*, vol. 10, no. 3, pp. 289–296, 2009.

[8] C. Gekas, K. E. Rhodes, L. M. Gereige, H. Helgadottir, R. Ferrari, S. K. Kurdistani, E. Montecino-Rodriguez, R. Bassel-Duby, E. Olson, A. V Krivtsov, S. Armstrong, S. H. Orkin, M. Pellegrini, and H. K. Mikkola, "Mef2C is a lineage-restricted target of Scl/Tal1 and regulates megakaryopoiesis and B-cell homeostasis," *Blood*, vol. 113, no. 15, pp. 3461–3471, 2009.

[9] I. Debnath, K. M. Roundy, P. D. Pioli, J. J. Weis, and J. H. Weis, "Bone marrow-induced Mef2c deficiency delays B-cell development and alters the expression of key B-cell regulatory proteins," *Int Immunol*, vol. 25, no. 2, pp. 99–115, 2013.

[10] K. Nishii, D. L. Gibbons, I. Titley, D. Papworth, D. T. Goodhead, and M. Greaves, "Regulation of the apoptotic response to radiation damage in B cell development," *Cell Death Differ*, vol. 5, no. 1, pp. 77–86, 1998.

[11] U. Grawunder, T. M. Leu, D. G. Schatz, A. Werner, A. G. Rolink, F. Melchers, and T. H. Winkler, "Down-regulation of RAG1 and RAG2 gene expression in preB cells after functional immunoglobulin heavy chain rearrangement," *Immunity*, vol. 3, no. 5, pp. 601–608, 1995.

[12] M. Busslinger, "Transcriptional control of early B cell development," *Annu Rev Immunol*, vol. 22, pp. 55–79, 2004.

[13] T. S. Heng, M. W. Painter, and I. G. P. Consortium, "The Immunological Genome Project: networks of gene expression in immune cells," *Nat Immunol*, vol. 9, no. 10, pp. 1091–1094, 2008.

[14] E. ten Boekel, F. Melchers, and A. G. Rolink, "Changes in the V(H) gene repertoire of

developing precursor B lymphocytes in mouse bone marrow mediated by the pre-B cell receptor," *Immunity*, vol. 7, no. 3, pp. 357–368, 1997.
[15] H. D. Jeong and J. M. Teale, "Comparison of the fetal and adult functional B cell repertoires by analysis of VH gene family expression," *J Exp Med*, vol. 168, no. 2, pp. 589–603, 1988.
[16] E. P. Consortium, "The ENCODE (ENCyclopedia Of DNA Elements) Project," *Science (80-.).*, vol. 306, no. 5696, pp. 636–640, 2004.
[17] B. J. Swanson, H. M. Jäck, and G. E. Lyons, "Characterization of myocyte enhancer factor 2 (MEF2) expression in B and T cells: MEF2C is a B cell-restricted transcription factor in lymphocytes," *Mol Immunol*, vol. 35, no. 8, pp. 445–458, 1998.
[18] R. L. Riley, B. B. Blomberg, and D. Frasca, "B cells, E2A, and aging," *Immunol Rev*, vol. 205, pp. 30–47, 2005.
[19] D. Frasca, A. M. Landin, S. C. Lechner, J. G. Ryan, R. Schwartz, R. L. Riley, and B. B. Blomberg, "Aging down-regulates the transcription factor E2A, activation-induced cytidine deaminase, and Ig class switch in human B cells," *J Immunol*, vol. 180, no. 8, pp. 5283–5290, 2008.
[20] K. Ma, J. K. Chan, G. Zhu, and Z. Wu, "Myocyte enhancer factor 2 acetylation by p300 enhances its DNA binding activity, transcriptional activity, and myogenic differentiation," *Mol Cell Biol*, vol. 25, no. 9, pp. 3575–3582, 2005.
[21] K. Canté-Barrett, R. Pieters, and J. P. Meijerink, "Myocyte enhancer factor 2C in hematopoiesis and leukemia," *Oncogene*, 2013.
[22] A. V Krivtsov, D. Twomey, Z. Feng, M. C. Stubbs, Y. Wang, J. Faber, J. E. Levine, J. Wang, W. C. Hahn, D. G. Gilliland, T. R. Golub, and S. A. Armstrong, "Transformation from committed progenitor to leukaemia stem cell initiated by MLL-AF9," *Nature*, vol. 442, no. 7104, pp. 818–822, 2006.
[23] M. Schwieger, A. Schüler, M. Forster, A. Engelmann, M. A. Arnold, R. Delwel, P. J. Valk, J. Löhler, R. K. Slany, E. N. Olson, and C. Stocking, "Homing and invasiveness of MLL/ENL leukemic cells is regulated by MEF2C," *Blood*, vol. 114, no. 12, pp. 2476–2488, 2009.
[24] T. Helleday, E. Petermann, C. Lundin, B. Hodgson, and R. A. Sharma, "DNA repair pathways as targets for cancer therapy," *Nat Rev Cancer*, vol. 8, no. 3, pp. 193–204, 2008.
[25] K. Lukin, S. Fields, D. Lopez, M. Cherrier, K. Ternyak, J. Ramírez, A. J. Feeney, and J. Hagman, "Compound haploinsufficiencies of Ebf1 and Runx1 genes impede B cell lineage progression," *Proc Natl Acad Sci U S A*, vol. 107, no. 17, pp. 7869–7874, 2010.
[26] D. Han, M. Zhang, J. Ma, J. Hong, C. Chen, B. Zhang, L. Huang, W. Lv, L. Yin, A. Zhang, H. Zhang, Z. Zhang, S. Vidyasagar, P. Okunieff, and L. Zhang, "Transition pattern and mechanism of B-lymphocyte precursors in regenerated mouse bone marrow after subtotal body irradiation," *PLoS One*, vol. 7, no. 10, p. e46560, 2012.
[27] M. Mohrin, E. Bourke, D. Alexander, M. R. Warr, K. Barry-Holson, M. M. Le Beau, C. G. Morrison, and E. Passegué, "Hematopoietic stem cell quiescence promotes error-prone DNA repair and mutagenesis," *Cell Stem Cell*, vol. 7, no. 2, pp. 174–185, 2010.
[28] M. E. Johnson, S. Deliard, F. Zhu, Q. Xia, A. D. Wells, K. D. Hankenson, and S. F. Grant, "A ChIP-seq-Defined Genome-Wide Map of MEF2C Binding Reveals Inflammatory Pathways Associated with Its Role in Bone Density Determination," *Calcif Tissue Int*, vol. 94, no. 4, pp. 396–402, 2014.
[29] W. J. Kent, C. W. Sugnet, T. S. Furey, K. M. Roskin, T. H. Pringle, A. M. Zahler, and D.

Haussler, “The human genome browser at UCSC,” *Genome Res*, vol. 12, no. 6, pp. 996–1006, 2002.
[30] D. Blankenberg, G. Von Kuster, N. Coraor, G. Ananda, R. Lazarus, M. Mangan, A. Nekrutenko, and J. Taylor, “Galaxy: a web-based genome analysis tool for experimentalists,” *Curr Protoc Mol Biol*, vol. Chapter 19, p. Unit 19.10.1–21, 2010.
[31] C. Y. McLean, D. Bristor, M. Hiller, S. L. Clarke, B. T. Schaar, C. B. Lowe, A. M. Wenger, and G. Bejerano, “GREAT improves functional interpretation of cis-regulatory regions,” *Nat Biotechnol*, vol. 28, no. 5, pp. 495–501, 2010.

Chapter 5 Conditional inactivation of p53 in mature B cells Promotes generation of nongerminal center-derived B-cell lymphomas

Abstract

The p53 tumor suppressor is a transcription factor that regulates a large array of genes involved in control of cell cycle and apoptosis [1][2]. Transactivation-independent activities of p53 have also been described, ranging from transcriptional repression [3] to cytoplasmic and mitochondrial functions [2]. Levels of p53 protein are extremely low in normal conditions, but p53 becomes stabilized and activated by a variety of posttranslational modifications in cells subjected to different types of DNA damage as well as upon overexpression of oncogenes [1][2]. As a result of p53 activation, cells carrying potentially harmful lesions, such as DNA double-strand breaks (DSBs) or mutations that activate oncogenes, initiate cell cycle arrest to repair the lesion or undergo programmed cell death. Germ-line p53 mutations in humans cause Li-Fraumeni syndrome, a familial condition characterized by early onset of different tumors [4][5]. Moreover, the p53 gene is somatically mutated or deleted in a large number of human cancers, indicating that this tumor suppressor exerts its protective role against oncogenic transformation in multiple tissues [5]. Targeted disruption of the p53 gene in mice, however, results in a strong predisposition for early-onset thymic lymphomas [6]. A small percentage of germ-line p53-deficient mice succumb to B lineage lymphomas [7][8], but the short lifespan of these animal resulting from thymic lymphoma prevented more detailed studies of the effects of p53 deficiency in different stages of B-cell differentiation as well as in other tissues. By using the Cre/Lox approach in mice with p53-conditional alleles [6][9], several studies demonstrated that somatic inactivation of p53 is sufficient to promote tumor formation in some, but not all, tissues examined. Thus, for example, p53 deletion per se results in development of breast tumors [10]

and osteosarcomas [11][12], whereas development of ovarian or prostate cancers requires simultaneous deletion of other tumor suppressors [13][14].

Introduction

In humans, many B- and T-cell lymphomas are characterized by clonal translocations that usually juxtapose an oncogene to antigen receptor loci [15][16]. Translocations in progenitors of lymphoid tumors involve on one partner programmed DSBs that are generated in the context of *Ig* gene assembly in B cells, and T-cell receptor (*TCR*) assembly in T cells. This process, called V(D)J recombination, takes place in early stages of B- and T-cell differentiation and is initiated by the RAG endonuclease, formed by the products of recombination activating gene (RAG)-1 and -2. RAG introduces DSBs at target V, D, and J segments in the*Ig* and *TCR* loci, which are then joined by the classical nonhomologous DNA end-joining pathway (C-NHEJ) [16][17]. Upon antigen stimulation of mature B cells, the constant (C) region of the Ig heavy chain (*IgH*) molecule, which initially is encoded by the Cμ exons, can be exchanged to another heavy chain isotype, with different effector functions, by class switch recombination (CSR) [16][17]. CSR is initiated by activation-induced cytidine deaminase (AID) activity, which leads to DSBs within large repetitive sequences (S regions) that flank each set of *IgH* C region exons with the breaks subsequently being joined by C-NHEJ or alternative end-joining [16][17]. AID is also responsible for another Ig diversification process, somatic hypermutation (SHM), which introduces of mutations in the variable region exons, allowing the selection of B cells that produce Ig molecules with higher affinity for antigen [18][19]. SHM takes place in specialized structures, called germinal centers (GCs) that organize in peripheral lymphoid organ following antigen encounter, whereas CSR can also occur outside of the GC reaction [20].

Human B-cell lymphomas can originate at different stages of B-cell differentiation, as can be inferred by examining the pattern of *Ig* loci rearrangements. Many human B-cell lymphomas, such as follicular lymphomas or large B-cell lymphomas, are of GC or post-GC origin and accordingly carry switched and hypermutated *IgH* alleles [21]. These tumors routinely harbor translocations between *IgH* and oncogenes such as *c-myc* and *Bcl6*, with breakpoints that can be ascribed to aberrant CSR or SHM [16][17]. Although true pre-GC lymphomas, such as mantle cell lymphoma, are relatively rare, other cases, including splenic marginal zone lymphoma (MZL) and Waldenstrom macroglobulinemia, derive from B cells that may have undergone SHM but not CSR and usually do not harbor *IgH* translocations [22][23][24].

Despite the frequency of translocations involving antigen receptor loci in human lymphomas, T-cell tumors arising in germ-line p53-null animals harbor clonal translocations only in a minority of the cases. Moreover, the observed translocations are not recurrent and do not involve *TCR* loci [25]. When both p53 and C-NHEJ factors are deleted in the germ line or in B-lineage cells, mice invariably develop B-cell lymphomas with characteristic translocations between the *IgH* and the *c-myc* oncogene loci [16], and p53 deficiency allows accumulation of *IgH*/*c-myc* translocations in normal B cells stimulated to undergo CSR [26]. To better characterize the role of p53 in B-cell lymphoma formation, given that the onset of these tumors is masked by the fast appearance of thymic lymphomas in p53-null mice, we conditionally inactivated the p53 gene in mature B cells by mean of the Cre/Lox approach.

Results

Mice with Mature B Cell–Specific Inactivation of p53 Develop B-Cell Lymphomas.

To specifically delete the p53 gene in mature B cells, we bred a previously generated p53-floxed conditional allele ($p53^{F}$, Fig. 1*A*) [9] into the CD21-Cre background [27]. Cre recombinase expression from the CD21 promoter takes place during differentiation from immature transitional B cells to mature B cells; accordingly, efficient p53 deletion was observed by Southern blotting in peripheral B cells (Fig. 1*A*). CD21-Cre may become nonspecifically active in the germ line; therefore, we generated our experimental cohort by crossing CD21-Cre/$p53^{F/F}$ males to $p53^{F/F}$ females. CD21-Cre/$p53^{F/F}$ and CD21-Cre/$p53^{F/-}$ offspring (collectively referred to as "CP," with the latter deriving from nonspecific Cre-mediated deletion of one floxed p53 allele) was monitored for tumor development. Because deficiency of the histone variant H2AX does not confer tumor susceptibility [28][29], we similarly generated a cohort of CD21-Cre/$H2AX^{F/F}$ or CD21-Cre/$H2AX^{F/-}$ mice (referred to as "CH") as controls.

To promote immune responses, half of the mice in each cohort were immunized by injection of sheep RBCs, according to standard protocols [30]. No difference in overall survival and cause of death were observed between the nonimmunized and immunized groups (Table S1); therefore, results from the two groups are presented together. CP mice became moribund between 8 and 12 mo of age, whereas control CH mice usually lived up to 2 y of age (Fig. 1*B*). About 50% of CP mice succumbed to B-cell lymphomas, which likely originated in the spleen (affected in 10/10 mice and usually greatly enlarged, Fig. 1*C*). The tumor often involved peripheral lymph nodes (5/10 mice), and more rarely mesenteric lymph nodes (3/10 mice) and thymus (3/10 mice). Metastasis to the liver was observed in four animals. Development of B-cell lymphomas was more frequent in $p53^{F/F}$ than in $p53^{F/-}$ mice, because the latter were also susceptible to other types of cancers, likely from p53 heterozygosity (Table S1). Indeed, three CP mice of the $p53^{F/-}$ genotype developed thymic lymphomas and sarcomas, which are typical in p53 heterozygous

mice [31]. Mice 187 and 307 presented with normal spleens and tumor masses, which histologically were of mixed lymphoid and myeloid lineages; therefore, these two tumors were not analyzed further. In the CH cohort, only one mouse developed a B-cell lymphoma at 21 mo of age, and two mice died of ovarian tumors at more than 27 mo of age (Table S1).

CP B-Cell Lymphomas Are Surface IgM+ and of Pregerminal Center Origin.

Histopathologic studies of sections from CP tumor samples revealed a relatively complex picture. Tumor CP220 (Fig. 2*A*, *Upper Left*) was characterized by a nodular growth pattern and a mixed centrocytic/centroblastic population typical of murine follicular lymphomas [32]. Other cases (tumors CP245 and CP569; Fig. 2*A*, *Upper Right*) showed histologic and cytologic features characteristic of murine splenic MZL [33] and were remarkably similar to MZL previously identified in mice with a conventional knockout of p53 [8] or an altered p53 exon 1 [34]. Some cases had a more diffuse and aggressive phenotype, characterized by high mitotic rates (tumors CP239 and CP301; Fig. 2*A*, *Lower Left*), larger cells (tumor CP166), or anaplastic cells (tumor CP277; Fig. 2*A*,*Lower Right*). Analysis of surface marker expression by flow cytometry revealed that CP lymphomas were invariably B220+/IgM+, with most of the tumors also being Igκ+. Tumor CP301 was the only IgM+/Igλ+ case (Fig. 2*B*). These results suggest that CP B-cell lymphomas most likely originated from B cells that had not undergone CSR. Moreover, immunohistochemical analysis showed that a subset of the tumors were Bcl6-negative, consistent with a pre-GC origin (Table S2).

To further characterize these p53-deficient B-cell tumors, we analyzed rearrangements at the *IgH* and *Ig*κ loci in CP tumor DNA by Southern blotting. We first used probes hybridizing downstream of the J_H region ($JH_{4–3}$ probe; Fig. 3*A*, *Left*) and of the J_κ region (J_κ probe; Fig.

3*A*, *Right*), and found that all samples contained distinct, rearranged bands (Fig. 3*B*). These results indicated that the tumors are monoclonal with one or two non–germ-line bands (e.g., CP236, CP301) or oligoclonal with more than two non–germ-line bands (e.g., CP220, CP250) and usually originated from single cells that had undergone V(D)J recombination at both*IgH* and *Ig*κ loci. We next examined the status of the Sμ region by using an Iμ probe from the J_H to Cμ intron, which on an EcoRI digest recognizes a fragment that is not within the *IgH* V, D, or J segments and is not altered by V(D)J recombination (Fig. 3*A*, *Left*). Sμ is the donor switch region for the vast majority of *IgH*CSR events; therefore, detection of a rearrangement with this probe would indicate that the cell of origin of the tumor had undergone CSR. All but one (CP246) of the analyzed CP tumor samples carried germ-line, unrearranged Sμ bands (Fig. 3*C*), further confirming that they derive from cells that had not undergone CSR. We also analyzed SHM at the *IgH* locus by PCR amplification and sequencing of the region encompassing the intron between the intronic Eμ enhancer and the rearranged J_H segment (Fig. 3*D*). None of the lymphomas analyzed except CP246 had any mutations, consistent with the notion that they arose from naive pre-GC B cells (Fig. 3*D*).

B-cell lymphomas in humans and mice routinely harbor clonal translocations that involve *Ig* loci and different oncogenes, such as *c-myc*, *Bcl2*, or *Bcl6* [16]. To determine if this was also the case for CP lymphomas, we performed spectral karyotyping (SKY) on metaphase spreads from short-term tumor cell cultures. Most of the tumors showed variable degrees of aneuploidy, a characteristic associated with p53 deficiency [35]. All but one of the analyzed CP lymphomas carried multiple clonal translocations that were nonrecurrent, involving different chromosomes (chr) in each tumor analyzed (Fig. 4*A* and Table 1). Tumor CP569 harbored reciprocal T(14;2) and T(2;14) translocations; tumor CP239 harbored T(3;1), T(4;3), and T(17;2); and tumor CP166

carried reciprocal T(1;15) and T(15;1) plus T(13;10) and T(10;9). Two tumors also harbored complex translocations: tumor CP220 had a complex translocation involving chr 8, 14, and 12 in addition to a T(2;5) and a T(17;4), whereas tumor CP277 had a complex T(5;3;5) translocation in addition to clonal T(6;19), T(4;6) and frequent T(17;10), and T(X;3). Another tumor generated outside of the experimental cohort, tumor CP752, similarly carried multiple clonal translocations including T(10;6), T(9;1), T(15;16), T(14;1), and T(11;14). Only tumor CP246 lacked any translocations that could be identified by SKY. This was also the only tumor exhibiting SHM and it developed with a shorter latency than any of the other tumors (Table S1), suggesting it may represent a different tumor type than other CP tumors.

Mouse models deficient for p53 and C-NHEJ or DSB-response factors usually carry translocations involving*Ig* loci [16]. The *IgH* locus lies on the telomeric portion of chr 12, whereas the *Ig*κ and *Ig*λ loci lie on chr 6 and 16, respectively. Tumor CP220 has a complex T(8;14;12) translocation. However, the chr 12 breakpoint did not involve the *IgH* locus, as demonstrated by FISH analysis with *IgH*-flanking probes (Fig. 4*B*, *Left*, and Fig. S1*A*). Surprisingly, FISH analyses with probes flanking the TRCα/δ locus on chr 14 showed that the complex translocation in this B-cell tumor splits the 5′ and 3′ ends of the *TCR*α/δ locus, which normally rearranges during V(D)J recombination in pro-T cells. However, other translocations involving chr 14 in tumors CP569 and CP752 did not involve *TCR*α/δ (Fig. S1 *C* and *D*). Tumors CP277 and CP752 had translocations involving chr 6 and tumor CP752 also had a chr 16 translocation. FISH analysis with probes flanking *Ig*κ and *Ig*λ showed that these loci were not involved in the translocations (Fig. 4*B* and Fig. S1 *B*and *D*). Chr 6 also carries the *TCR*β locus, which was not translocated in tumor CP752 but was partially duplicated in tumor CP277 (Fig.

4*B* and Fig. S1 *B* and *D*). Together, these analyses indicated that CP tumors do not carry translocations involving *Ig* loci.

Mouse B-cell lymphomas often rearrange or amplify the *c-myc* oncogene, resulting in high levels of *c-myc*expression that contribute to transformation [36][37][38]. This seems not to be the case for CP lymphomas because only one tumor, CP166, had a translocation involving chr 15 that bears the *c-myc* locus. To confirm that *c-myc* overexpression was not a key factor during lymphomagenesis in CP mice, we performed Northern blotting on RNA from selected CP tumors. High levels of *c-myc* transcripts were not detected (Fig. 4*C*), indicating that other, unknown mechanisms promote transformation of CP B cells.

Discussion

Here we show that specific inactivation of the p53 tumor suppressor gene in mature B cells is sufficient to promote oncogenic transformation and results in the development of splenic mature B-cell lymphomas. By histopathologic criteria, several CP B-cell tumors resemble murine splenic marginal zone lymphomas (SMZL), with some cases showing a more aggressive phenotype consistent with diffuse large B-cell lymphomas characteristic of high-grade MZL in mouse [33]. Indeed, a previous study identified the prevalent B-cell tumor in germ-line p53 knockout mice as SMZL and found progression from marginal zone hyperplasia to invasive lymphomas composed of more pleomorphic cells [8]. More recently, it was found that mice with an altered first exon resulting in B cell–specific deletion of p53 also developed SMZL [34]. These studies, however, were limited to histological analyses and did not examine cytological abnormalities nor determine the cellular origin of the tumors. Nonetheless, the combined results

of these studies clearly indicate that, at least in mice, splenic marginal zone B cells are uniquely sensitive to the transforming effects of p53 deficiency.

We found that all CP B-cell tumors were IgM^+ and that only one exhibited somatic hypermutation, indicating that their cell of origin was a mature B cell that had not passaged the germinal center or undergone CSR. Accordingly, CP tumors lacked clonal translocations involving *Ig* loci or the *c-myc* oncogene, which are believed to originate from mistakes in rejoining DSBs generated during CSR and SHM [16][17]. These results are in keeping with the fact that splenic marginal zone B cells are almost universally IgM-positive with BCRs enriched for germ-line sequences [39].

Given that half of the CP mice analyzed had been immunized to stimulate T cell–dependent immune responses, our results suggest that naive B cells are better targets for transformation induced by p53 deficiency in the absence of other deficiencies, such as C-NHEJ deficiency. Because p53-dependent responses have been shown to be reduced during the GC reaction by BCL6 [40], it is possible that other p53-independent mechanisms are operational in cells undergoing CSR and SHM to safeguard genomic stability. A previous study used mb1-Cre to delete p53 from early developing B cells and showed that this resulted in generation of tumors from multiple stages of B-cell differentiation including pro-B cells and mature B cells [41]. In contrast to our results, a subset of mice from this earlier study developed IgM-negative B-cell lymphomas with S region rearrangements and T(12;15) translocations. Given that mb1-Cre–mediated deletion of p53 takes place at the progenitor B-cell stage, the precise origin of these tumors remains unclear. Moreover, the exact nature of T(12;15) translocations in tumors that derived from mb1-Cre deletion of p53 were not determined, and it is possible that they originated

from V(D)J recombination breaks at the *IgH* locus that persisted from the pro-B-cell stage. Alternatively, lack of p53 from early B-cell development could have favored accumulation of other mutations, which in turn allowed survival of cells carrying *IgH/c-myc*translocations. It is also possible that development of mb1-Cre–deleted p53-deficient tumors that appear to derive from B cells undergoing CSR was influenced by other factors, including differences in the housing conditions of the experimental animals, resulting in exposure to different types of antigens, and potential differences between the genetic backgrounds of the experimental animals.

Clonal translocations, even those not involving *Ig* loci, were present in all but one of the CP tumors as well as in many of the IgM^+ tumors from mb1-Cre–deleted p53-deficient mice [41]. These translocations were not recurrent and involved different chromosomes in each tumor. Moreover, most of the tumors carried multiple, sometimes complex translocations, which that made it most unlikely that any single oncogenic event was responsible for transformation of CP B cells. Such high frequency of translocations in CP B-cell tumors may reflect a propensity of B cells to tolerate high levels of DSBs. Indeed, recent work from our laboratory suggests that translocations in activated cycling B cells are more frequent than in G1-arrested pro-B-cell lines [42][43]. However, metaphases from p53-deficient splenic B cells stimulated in vitro to undergo CSR do not show high levels of chromosomal breaks and translocations, suggesting the activity of other checkpoint mechanisms [44][45]. It is possible that splenic B cells activated in vitro are not representative of the population of B cells from which CP tumors arise in vivo. An alternative, nonexclusive explanation is that p53 deficiency in B cells allows accumulation of oncogenic translocations that occur at very low levels because of a defective apoptotic response. Indeed, a specific increase in oncogenic *IgH/c-myc* translocations can be detected in p53-deficient cultured splenic B cells [26]. Moreover, evidence suggests that the proapoptotic

functions of p53 are responsible for protecting against B-cell lymphoma development, whereas its cell-cycle arrest functions are more important for suppression of T-cell lymphomas, which lack clonal translocations [6].

Given that organization and function of primary and secondary lymphoid organs are significantly different between mice and humans, it is often difficult to compare B-cell malignancies in these species [32]. Indeed, only few CP tumors closely resemble human MZL by histopathologic criteria, with most of them showing a more diffuse pattern. However, for several characteristics, CP tumors might represent a model for human SMZL or other IgM-positive human malignancies, such as Waldenstrom macroglobulinemia. First, somatic p53 inactivation is found in about 20–30% of human SMZL. Moreover, although translocations between oncogenes and *Ig* loci are present in most human B-cell lymphomas, splenic MZL or Waldenstrom macroglobulinemia most often lack these characteristic aberrations [22][23][24]. These tumors usually also carry evidence of SHM [22][23][46], but mouse SMZLs are not hypermutated [33], again indicating an intrinsic difference between mouse and human B-cell biology. Finally, similarly to human MZL and Waldenstrom macroglobulinemia, which are slowly progressing diseases, CP tumors arise with long latencies, suggesting they may initially develop as indolent disease and become more aggressive after accumulation of additional mutations.

Materials and methods

Generation of CP and CH Mice.

CD21-Cre, $H2AX^{F/F}$, and $p53^{F/F}$ mice have been previously described [9][27][47]. Because the CD21-Cre transgene deletes nonspecifically more in the female than in the male germ line,

CD21-Cre/H2AX$^{F/F}$ or CD21-Cre/p53$^{F/F}$ males were crossed with H2AX$^{F/F}$ and p53$^{F/F}$females, respectively, to generate the experimental cohorts. Mice were maintained in a pathogen-free environment. For immunization, 1×10^8 sheep RBCs resuspended in 100 μL of PBS were injected intraperitoneally; booster injections were performed every 2 wk. Induction of a robust GC reaction 10 d after immunization was confirmed in selected mice by histological examination of the spleen and by an increase in PNA^{hi} splenic B cells according to published protocols [30]. Experimental animals were monitored for tumor formation and killed for analysis when clear signs of disease appeared.

All animal experiments were performed under protocols approved by the institutional Animal Care and Use Committee of Boston Children's Hospital (Protocol 11-11-2074R).

FACS Analysis.

Single-cell suspensions from tumor masses and control organs were stained with CyChrome (CyC)-labeled anti-mouse B220 (eBiosciences), FITC-labeled anti-mouse CD43 (BD Biosciences), and RPE-labeled anti-mouse IgM (Southern Biotech) antibodies or with CyC-labeled anti-mouse B220 (eBiosciences), FITC-labeled anti-mouse Igκ (BD Biosciences), and PE-labeled anti-mouse Igλ (BD Biosciences).

Data acquisition was performed on a FACSCalibur flow cytometer equipped with CellQuest software (Becton Dickinson). Analysis was performed with FlowJo software (Tree Star).

Histological Analysis.

Tumor tissues were fixed in 10% (vol/vol) buffered formalin and stored in 70% (vol/vol) ethanol. Paraffin-embedded tissues were sectioned and stained with H&E. Histologic diagnoses were made on the basis of established criteria [32].

Southern Blotting.

Genomic DNA isolated from tumor masses or normal control tissues were separated on 0.8% agarose gel and transferred to Zeta-Probe GT (Biorad) nylon membrane. Hybridization was performed in 50% (vol/vol) formamide/SScPE at 42 °C. The 5′ p53 probe was a 600-bp XbaI fragment upstream of p53 gene exon1 and has been described previously. The JH_{4-3} probe was a 1.6-kb HindIII/EcoRI fragment downstream of JH_4; the J_κ probe was a 1-kb fragment downstream of $J\kappa_5$; and the Iμ probe was a 1.2-kb XbaI/PstI fragment encompassing part of the Iμ promoter. The *c-myc* probe used for Northern blot was generated by PCR-amplifying *c-myc* exon2.

Somatic Hypermutation Analysis.

The genomic region encompassing J_{H1} to J_{H4} and part of the intron downstream of J_{H4} was PCR-amplified from tumor DNA using degenerate oligonucleotides corresponding to the different V_H families [48] as forward primers and oligonucleotides downstream of J_{H4}(5′AGGCTCTGAGATCCCTAGACAG3′ or 5′CCTCTCCAGTTTCGGCTGATCC3′) as reverse primers. Proofreading polymerase (iProof High-Fidelity DNA Polymerase, Biorad) was used for amplification and PCR conditions were as previously published [48]. Amplification products were purified from agarose gel and submitted to sequencing. Sequences were compared with the published 129/Sv and C57/B6 sequences (accession

nos. NT_114985.2 and NT_166318.1, respectively). PCR amplification and sequencing was repeated two or three times for each sample.

Metaphase Preparation, SKY, and FISH.

Tumor cell suspensions were cultured for overnight and Colcemid (KaryoMAX Colcemid Solution; GIBCO) was added at the final concentration of 50 ng/mL for 3–5 h. Metaphase spreads were prepared according to standard protocols [44]. Spectral karyotyping was performed with a mouse SKY paint kit (Applied Spectral Imaging) following manufacturer's indications. Images were acquired with BX61 Microscope (Olympus) equipped with a motorized automatic stage, a cooled-CCD camera, and an interferometer (Applied Spectral Imaging). A 63× objective was used. Analysis was performed with the HiSKY software (Applied Spectral Imaging). At least 15 metaphases per each sample were analyzed.

Acknowledgements

We thank Roberto Chiarle for helpful suggestions. This work was supported by National Institutes of Health Grants 5P01CA92625 and CA098285 and a Leukemia and Lymphoma Society of America (LLS) Specialized Center of Research grant (to F.W.A.). This work was supported in part by the Intramural Research Program of the National Institutes of Health, National Institute of Allergy and Infectious Diseases (to H.C.M.). M.G. was an LLS senior fellow. C.H.B. is an LLS Scholar. F.W.A. is an investigator of the Howard Hughes Medical Institute.

This article contains supporting information online atwww.pnas.org/lookup/suppl/doi:10.1073/pnas.1222570110/-/DCSupplemental.

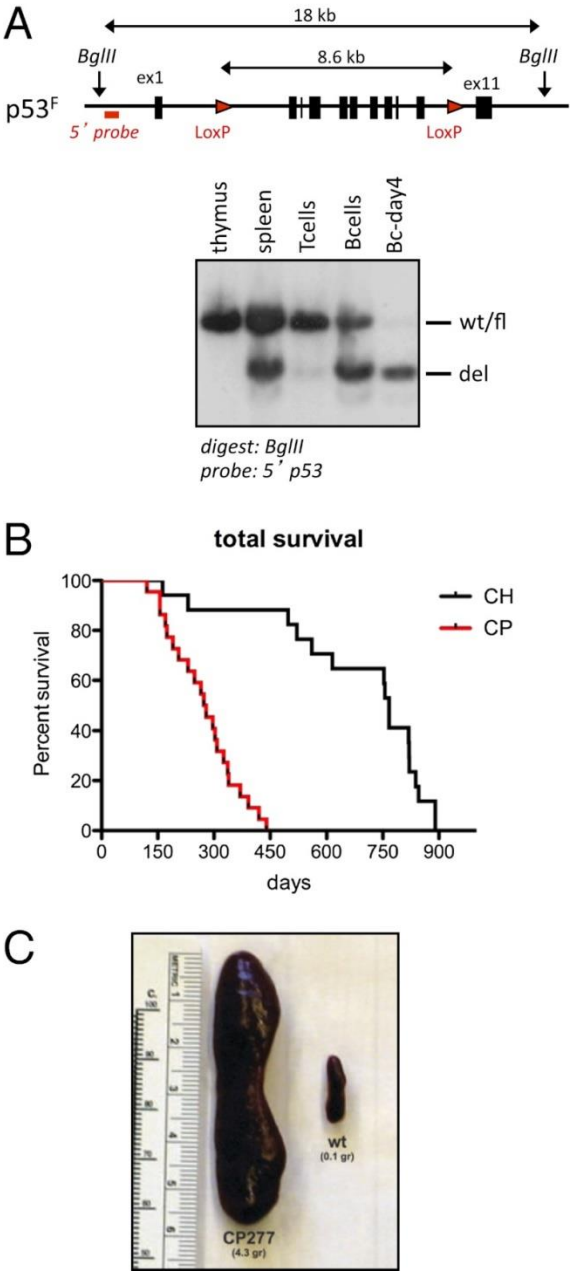

Figure 1

CP mice develop B-cell lymphomas. (*A*) Southern blot analysis demonstrating deletion of p53 gene in mature B cells. A schematic map with the position of relevant restriction sites and probes used is shown at top. Position of the bands corresponding to the wild-type (wt), floxed (fl), and deleted (del) p53 alleles is indicated. Bc-day4, purified splenic B cells cultured for 4 d with anti-CD40/IL4; Bcells, purified splenic B cells; Tcells, purified splenic T cells. (*B*) Kaplan-Meier curve of the CP (n = 22) and control CH (n = 17) cohorts. Curves represent total survival. (*C*)

(*Left*) Example of enlarged spleen frequently observed in CP mice succumbing to B-cell lymphomas; (*Right*) normal control spleen.

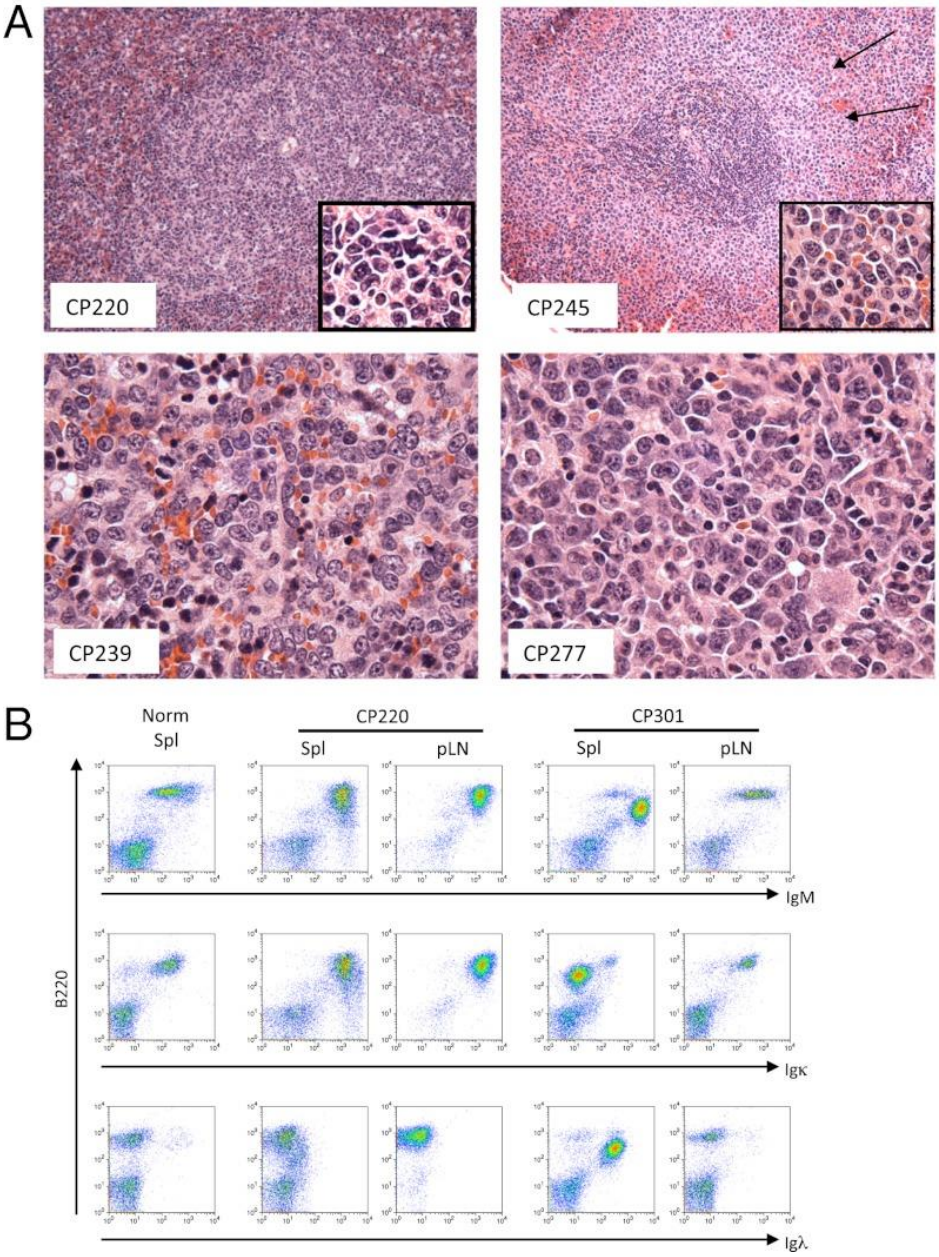

Figure 2.

CP B-cell lymphomas are IgM+ and show features of MZL. (*A*) Representative histologic sections from indicated CP tumors, stained with H&E. (*B*) Representative FACS analysis on CP220 and CP301 tumors, using antibodies against B220 and IgM, Igκ, or Igλ, as indicated. (*Left*) Normal spleen sample. pLN, peripheral lymph nodes; Spl, total spleen.

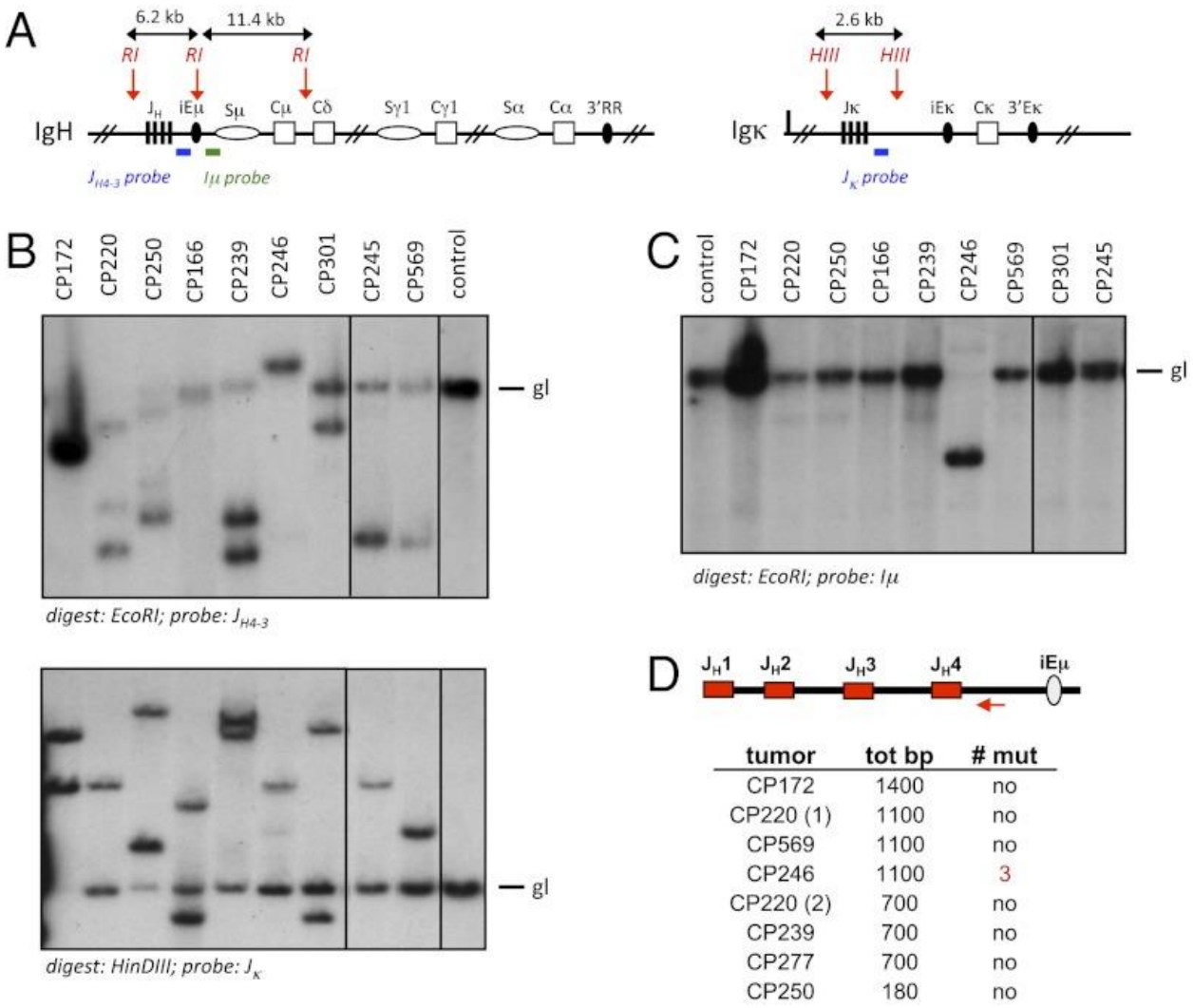

tumor	tot bp	# mut
CP172	1400	no
CP220 (1)	1100	no
CP569	1100	no
CP246	1100	3
CP220 (2)	700	no
CP239	700	no
CP277	700	no
CP250	180	no

Figure 3

CP B-cell tumors harbor clonal *IgH* and *Igκ* loci rearrangements, but are not somatically hypermutated. (*A*) Schematic of the *IgH* and *Igκ* loci showing restriction sites and probes used for Southern blot analyses. *RI*, EcoRI; *HIII*, HinDIII. (*B*) Southern blot analysis of DNA from CP tumors indicated on top demonstrating clonal rearrangements in the J_H (*Upper*) and Jκ (*Lower*) regions. (*C*) Southern blot analysis of DNA from indicated CP tumors with the Iμ probe, which detects rearrangements in the Sμ region. (B and C), probes and restriction enzyme used are indicated at the bottom of each panel. Position of the germ-line bands (gl) is shown. DNA from normal spleen was used as control. (*D*) Table summarizing the results of experiments to verify levels of SHM in DNA from CP tumors. The diagram on the top shows the region of the *IgH*locus used for PCR amplification and sequencing.CP B-Cell Lymphomas Harbor Clonal Nonrecurrent Translocations.

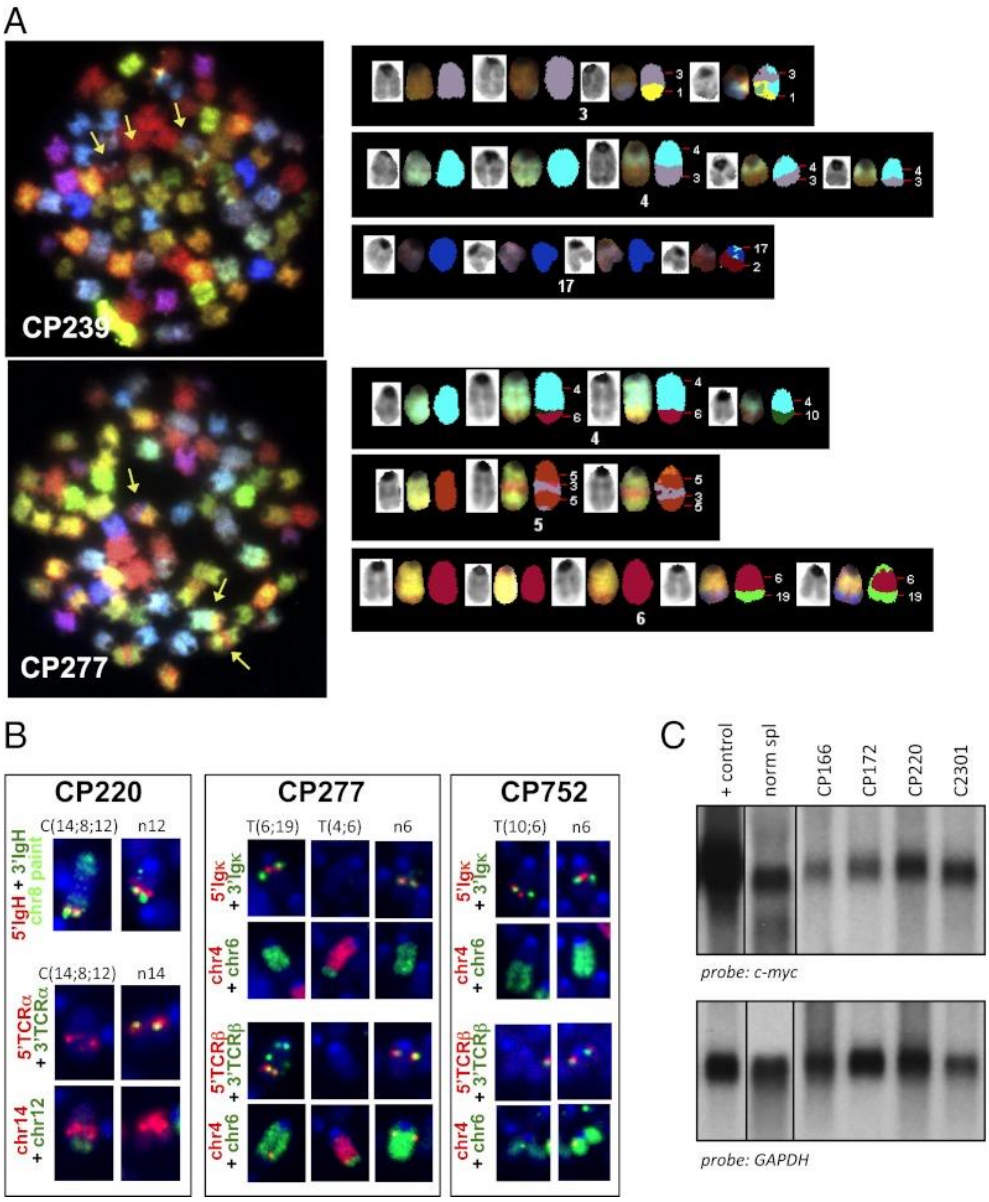

Figure 4

CP B-cell tumors harbor clonal, nonrecurrent translocations that do not involve *Ig* loci and *c-myc*. (*A*) SKY analysis of selected CP tumors. One representative metaphase is shown. The arrows indicate chromosomes involved in clonal translocations. Detailed view of these chromosomes is presented in the panels at the side, showing DAPI, spectral, and computer-classified staining for each chromosome. (*B*) FISH and chromosome paint analyses on CP tumors carrying chr 12 and chr 6 translocations. Sequential hybridization with the set of probes indicated on the left was performed. Only chromosomes involved in translocations are shown, with corresponding normal (n) counterparts. The whole metaphases are presented in Fig. S1. (*C*) Northern blot analysis on RNA from indicated CP tumors with probes specific for *c-myc*(*Upper*)

or GAPDH (*Lower*) as loading control. RNA from normal spleen (norm spl) and from a pro-B-cell tumor with *c-myc* overexpression (+ control) is included for comparison.

Table 1.

SKY and FISH analysis of CP tumors

	SKY		FISH				
Tumor no.	Clonal tr.	Nonclonal tr.	IgH	Igκ	Igλ	TCRα/δ	TCRβ
220	T(2;5), T(17;4), C(8;14;12)		Normal	ND	ND	C(14;8;12)	ND
277	T(4;6), T(6;19), C(5;3;5)	T(17;10, TX;3)	ND	Normal	ND	ND	Duplicated
166	T(15;1), T(10;9), T(13;10)	T(1;15), T(10;13)					
239	T(3;1), T(4;3), T(17;2)						
246	No translocations						
569	T(10;5), T(14;10)		ND	ND	ND	Normal	ND
752	T(10;6), T(9;1), T(15;16), T(14;1), T(11;14)		ND	Normal	Normal	Normal	Normal

At least 10 metaphases were analyzed per each sample. Clonal translocations (tr.) are present in more than 50% of metaphases analyzed; nonclonal translocation are present in less than 50% of metaphases analyzed. ND, not done.

Table 1

SKY and FISH analysis of CP tumors

At least 10 metaphases were analyzed per each sample. Clonal translocations (tr.) are present in more than 50% of metaphases analyzed; nonclonal translocation are present in less than 50% of metaphases analyzed. ND, not done.

Chapter 6 Conclusions to the Dissertation

These studies describe the levels of DNA damage and mutation generated by over-expression or deletion of particular genes that are required to carry out principal functions in healthy lymphocytes. The findings highlight the influence of these genes on the development and repair of DNA damage and mutation. IL-13 and AID play a role either indirectly or directly in generating DNA breaks while Mef2c and p53 are important in regulating DNA break repair to prevent malignancies.

IL-13 and AID which indirectly generate DNA breaks cannot have reduced activity without sacrificing immune function and therefore proper regulation of these genes is critical to the health of an organism. With regard to its role in immune function, IL-13 is essential in facilitating the elimination of parasites. However, we found that an increase in IL-13 levels has the capacity to initiate genotoxicity in the lungs as well as in peripheral blood cells of mice. AID's function involves inducing mutations that are necessary for producing antibody diversity, but we found that the presence of AID also induces translocations involving a number of genes including those which are implicated in leukemia and lymphomas. Augmented levels and/or mutation of IL-13 and the IL-13 receptors [1] [2] as well as AID [3][4][5] are implicated in several cancers. Our research emphasizes the importance of regulating gene expression so that appropriate levels of these proteins can maintain optimum health. Correspondingly, Mef2c and p53, both transcriptional activators which regulate DNA break repair, must also be meticulously regulated for optimal expression. Atypical regulation of DNA break repair pathways increases the likelihood of generating mutations and consequently oncogenic transformation. Studies have shown a relationship between aberrant Mef2c expression and oncogenic transformation [6][7][8]. In B cells we found that Mef2c deficiency results in high levels of double strand breaks due to the cell's reduced ability to repair V(D)J-recombination associated breaks via activation of DNA

repair genes. Deficiency of p53 which causes a reduction in the apoptotic response and allows DNA damage and mutations to persist will result in tumorigenesis. We found that p53 deficiency induced clonal B cell tumors which likely developed due to the absence of p53's pro-apoptotic function which normally prevents oncogenic transformation. These findings, like those in our reports on IL-13 and AID, also highlight the importance of tightly regulating these transcription factors.

We found that in addition to exhibiting the histological phenotype of asthma, IL-13 induces a global inflammatory response. We found that IL-13 initiated oxidative stress leading to assorted types of genotoxicity with increased levels of gamma-H2AX and 8-oxoguanine in the lungs as well as peripheral blood cells. We also found micronucleus formation in erythrocytes. Our study implicates IL-13 as having a role in the induction of genotoxicity. The mechanism by which IL-13 induces systemic genotoxicity is unknown. Westbrook et al. [9] found that inflammation of the gut also leads to systemic genotoxicity. Local organ inflammation may activate innate immune cell-mediated release of reactive species that injure circulating blood cells. Alternatively, but not exclusively, cytokine receptor-mediated production of free radicals may damage remote blood cells in the periphery. This study provides a basis for the possible use of IL-13 as a therapeutic target for asthma and potentially other pulmonary diseases. The induction of DNA damage through increased levels of IL-13 may provide insight for studies which describe cancer progression induced by the cytokine and its receptors [10][11][12]. It is possible that the increase in DNA damage, likely due to the effector function of receptors with affinity to IL-13 plays a part in the development and progression of these malignancies. Future studies should focus on identifying cell type-specific DNA damage to better understand the implications of IL-13 induced damage.

In the genome-wide translocation sequencing study we found that most translocations joined sequences of the same chromosome proximal to the targeted break. However, AID induced double strand breaks resulted in translocations preferentially occurring among several genes across the genome at transcription start sites of actively transcribed genes. AID's programmed function is to induce mutations which mediate the double strand breaks on the immunoglobulin heavy chain locus. This process required for recombination and accordingly antibody diversity. The results show that AID also induces breaks at other genes during active transcription and leads to translocations involving these genes. These findings are in accord with studies showing that AID promotes cellular transformation [4][5]. Utilizing this high throughput technique in other cells types could facilitate differentiating the importance of site specificity versus transcriptional activity with regard to the AID dependent translocations. An enhanced level of AID is associated with several cancers. This system could also potentially discover targets of AID which lead to oncogenic transformation. One of the AID dependent translocations occurring frequently was the Il4ra gene which encodes a subunit of an IL-13 binding receptor. The receptor's activity plays a potential role in the progression of cancers [11][13]. The genotoxic effects of IL-13 overexpression may be related to the Il4ra effector function. Mef2c was another gene hotspot. Given that the hotspots were associated with high levels of transcription, this result could indicate that Mef2c has a function downstream of recombination. Indeed we found that Mef2c enhances transcription of NHEJ factors.

We showed the importance of Mef2c, a MADS box transcription factor on maintaining B cell homeostasis through DNA repair among bone marrow B cell progenitors. We found that Mef2c deficient preB cells have reduced efficiency of lymphopoiesis and that Mef2c is essential in the recovery of irradiated B cells as it is an enhancer of DNA repair machinery. Studies have

implicated overexpression and mutated Mef2c with leukemic progression [8][7]. Our results give light to the possibility that Mef2c's role in leukemia involves the dysregulation of repair factors resulting in oncogenic translocations. Since Mef2c appeared as a hotspot in the high throughput study, future experiments looking into the role of Mef2c during class switch recombination through inactivation of Mef2c in mature B cells may indicate that DNA double strand breaks are increased in activated cells. Our study shows that the B cell compartment was not reduced in mature B cells; however these B cells were not stimulated to undergo class switch recombination.

The importance of controlling p53 levels and the role of p53 deficiency in the development of many cancers due to the loss of DNA damage regulation are both well-established [14]. In the presence of DNA damage, p53 is stabilized by phosphorylation and activates expression of p21 which blocks cyclin dependent kinase 2. This in turn inhibits cell cycle progression from G1 to S phase [15] and the result is cell cycle arrest, allowing DNA repair. P53 also activates genes which trigger caspase 9 mediated cell apoptosis [16]. Therefore tumor suppression is reduced when p53 is mutated or deficient. p53 inactivation in mature B cells led to polyclonal mature B-cell lymphomas with non-recurring translocations. P53 deletion in mature B cells led to tumors which overall did not undergo class switch recombination or somatic hypermutation even when immunized with sheep red blood cells. These mice may provide a model for human splenic marginal zone lymphomas which share some of the tumor characteristics in these mice such as the absence of translocations involving the immunoglobulin loci.

Here we distinguished the characterization of DNA damage and mutation through abnormal expression of IL-13, AID, Mef2c, and p53. These studies help to better understand the

mechanistic role of DNA damage during the development of diseases associated with abnormal expression of these genes.

References:

[1] T. Fujisawa, B. H. Joshi, and R. K. Puri, “IL-13 regulates cancer invasion and metastasis through IL-13Rα2 via ERK/AP-1 pathway in mouse model of human ovarian cancer,” *Int. J. Cancer*, vol. 131, no. 2, pp. 344–356, Jul. 2012.

[2] A. Walczak, K. Przybyłowska, R. Trzciński, A. Sygut, L. Dziki, A. Dziki, and I. Majsterek, “Association of -1112 c/t promoter region polymorphism of the interleukin 13 gene with occurrence of colorectal cancer.,” *Pol. Przegl. Chir.*, vol. 83, no. 1, pp. 27–31, Jan. 2011.

[3] H. Marusawa, “Aberrant AID expression and human cancer development.,” *Int. J. Biochem. Cell Biol.*, vol. 40, no. 8, pp. 1399–402, 2008.

[4] A. Takai, T. Toyoshima, M. Uemura, Y. Kitawaki, H. Marusawa, H. Hiai, S. Yamada, I. M. Okazaki, T. Honjo, T. Chiba, and K. Kinoshita, “A novel mouse model of hepatocarcinogenesis triggered by AID causing deleterious p53 mutations.,” *Oncogene*, vol. 28, no. 4, pp. 469–78, Jan. 2009.

[5] I. Okazaki, H. Hiai, N. Kakazu, S. Yamada, M. Muramatsu, K. Kinoshita, and T. Honjo, “Constitutive expression of AID leads to tumorigenesis.,” *J. Exp. Med.*, vol. 197, no. 9, pp. 1173–81, May 2003.

[6] I. Homminga, R. Pieters, A. W. Langerak, J. J. de Rooi, A. Stubbs, M. Verstegen, M. Vuerhard, J. Buijs-Gladdines, C. Kooi, P. Klous, P. van Vlierberghe, A. A. Ferrando, J. M. Cayuela, B. Verhaaf, H. B. Beverloo, M. Horstmann, V. de Haas, A.-S. Wiekmeijer, K. Pike-Overzet, F. J. T. Staal, W. de Laat, J. Soulier, F. Sigaux, and J. P. P. Meijerink, “Integrated transcript and genome analyses reveal NKX2-1 and MEF2C as potential oncogenes in T cell acute lymphoblastic leukemia.,” *Cancer Cell*, vol. 19, no. 4, pp. 484–97, Apr. 2011.

[7] Y. Du, S. E. Spence, N. A. Jenkins, and N. G. Copeland, “Cooperating cancer-gene identification through oncogenic-retrovirus-induced insertional mutagenesis.,” *Blood*, vol. 106, no. 7, pp. 2498–505, Oct. 2005.

[8] M. Schwieger, A. Schüler, M. Forster, A. Engelmann, M. A. Arnold, R. Delwel, P. J. Valk, J. Löhler, R. K. Slany, E. N. Olson, and C. Stocking, “Homing and invasiveness of MLL/ENL leukemic cells is regulated by MEF2C,” *Blood*, vol. 114, no. 12, pp. 2476–2488, 2009.

[9] A. M. Westbrook, B. Wei, J. Braun, and R. H. Schiestl, “Intestinal Mucosal Inflammation Leads to Systemic Genotoxicity in Mice,” *Cancer Res.*, vol. 69, no. 11, pp. 4827–4834, 2009.

[10] D. Gurusamy, J. Shoe, J. Hocker, and A. Hurwitz, “A role for IL-13 in the progression of

prostate tumors (TUM10P.1046)," *J. Immunol.*, vol. 194, no. 1 Supplement, pp. 211.27–211.27, 2015.

[11] K. T. Venmar, K. J. Carter, D. G. Hwang, E. A. Dozier, and B. Fingleton, "Molecular and Cellular Pathobiology IL4 Receptor ILR4a Regulates Metastatic Colonization by Mammary Tumors through Multiple Signaling Pathways."

[12] K. T. Venmar and B. Fingleton, "Lessons from immunology: IL4R directly promotes mammary tumor metastasis."

[13] F. Roth, A. C. De, L. Fuente, J. L. Vella, A. Zoso, L. Inverardi, and P. Serafini, "Aptamer-Mediated Blockade of Il4ra Triggers Apoptosis of MDSCs and Limits Tumor Progression."

[14] J. T. Zilfou and S. W. Lowe, "Tumor suppressive functions of p53.," *Cold Spring Harb. Perspect. Biol.*, vol. 1, no. 5, p. a001883, Nov. 2009.

[15] J. Wade Harper, G. R. Adami, N. Wei, K. Keyomarsi, and S. J. Elledge, "The p21 Cdk-interacting protein Cip1 is a potent inhibitor of G1 cyclin-dependent kinases," *Cell*, vol. 75, no. 4, pp. 805–816, Nov. 1993.

[16] M. Schuler, E. Bossy-Wetzel, J. C. Goldstein, P. Fitzgerald, and D. R. Green, "p53 Induces Apoptosis by Caspase Activation through Mitochondrial Cytochrome c Release," *J. Biol. Chem.*, vol. 275, no. 10, pp. 7337–7342, Mar. 2000.